The Pennsylvania State University

The Graduate School

College of Earth and Mineral Sciences

TOWARD MULTI-PROXY RECONSTRUCTIONS OF HYDROCLIMATE OVER THE CONTIGUOUS UNITED STATES FROM A.D. 500 TO PRESENT

A Thesis in

Meteorology

by

Daniel J. Brouillette

Submitted in Partial Fulfillment
of the Requirements
for the Degree of

Master of Science

August 2015

The thesis of Daniel J. Brouillette was reviewed and approved* by the following:

Michael E. Mann
Distinguished Professor of Meteorology
Thesis Advisor

Jenni L. Evans
Professor of Meteorology

Raymond G. Najjar
Professor of Oceanography

Johannes Verlinde
Professor of Meteorology
Associate Head of the Department of Meteorology

*Signatures are on file in the Graduate School.

ABSTRACT

For the reconstruction of two targets, summer drought (by way of the Palmer Drought Severity Index (PDSI)) and winter precipitation, gridded instrumental data were calibrated with differing combinations of proxy data that comprised a network. This proxy network consisted of 797 records derived from multiple indicators intended to represent both high- and low-frequency variability (time-scales of less than and greater than 20 years, respectively). Three experiments, performed for both targets, modified the Regularized Expectation Maximization (RegEM) algorithm to yield high-skill reconstructions that depict low-frequency variability going back farther in time. Experiment 1 involved the RegEM algorithm regularized by ridge regression and using in the calibration only tree-ring records, which represented a much expanded data-set compared to previous studies. Experiment 2 introduced a new hybrid RegEM method in which the same tree-ring-only proxy data-set as in Experiment 1 was used in the calibration for two sub-reconstructions -- one regularized using ridge regression and the other regularized using truncated total least-squares (TTLS) regression – that were added together to make a total reconstruction. Experiment 3 used the same new hybrid method but introduced the low-frequency part of the proxy network to the calibration for the TTLS sub-reconstruction. Experiment 4 used a new regionalized version of the Experiment 3 hybrid method. It was found that, back to 1700, reconstructions arising from the RegEM-ridge (Exp. 1) method exhibited the greatest and most widespread skill for summer PDSI while also minimizing variance loss and was, thus, preferred. However, for reconstructions of that same target that extended farther back in time, the regionalized hybrid RegEM method in which low-frequency records are additionally used in the calibration (Exp. 4) was preferred because it produced reconstructions that depicted low-frequency variability going back in time with moderate to high cross-validation skill though not as high as that realized in some previous work. For winter precipitation, reconstructive skill was much more limited, restricted to the western part of the reconstruction domain. In that part of the domain, a hybrid method was preferred for similar reasons as it was for the longer reconstructions of summer PDSI.

Table of Contents

List of Figures

Figure 4.5 – This series of eight plots ((a) – (h)) shows graphs of the each of the eight regional areal-mean summer PDSI reconstruction series made using the RegEM-ridge method with the expanded tree-ring proxy network (Exp. 1) (and their $\pm 2\sigma$ uncertainty bounds). Noted for each figure are the RE and CE scores for the corresponding reconstruction. All RE and CE P-values are less than 0.05. The reconstructions are shown as far back as a high level of skill remained as explained in more detail in the text. A legend of graph line colors is given in (a).

Figure 4.6 – Contour map of the difference in RE scores between those calculated for a 1700-1927 reconstruction of summer PDSI using the hybrid RegEM method with only the tree-ring part of the proxy network (Exp. 2) and those calculated for a reconstruction of the same target using the RegEM-ridge method with expanded tree-ring network (Exp. 2). Scores were calculated for each of 155 grid points and then interpolated. Difference values greater than zero indicate that the hybrid RegEM method had greater reconstructive skill than the RegEM-ridge method – both using the same proxy network.

Figure 4.7 – Contour map of RE scores, as calculated for each of 155 grid points and then interpolated, for the 1700-1927 reconstruction of summer PDSI using the hybrid RegEM-ridge method with only the tree-ring part of the proxy network (Exp. 2). Warmer colors indicate greater values of RE score, and cooler colors indicate lesser values. The map of CE scores is qualitatively similar.

Figure 4.8 – This series of eight plots ((a) – (h)) shows graphs of the each of the eight regional areal-mean reconstruction series made using the hybrid RegEM method with only the tree-ring part of the proxy network (Exp. 2)(and their $\pm 2\sigma$ uncertainty bounds), the RegEM-ridge method with expanded tree-ring proxy network, the Zhang et al. (2004) method, and the Cook et al. (1999) method as well as the eight regional areal-mean instrumental series. A legend of graph line colors is given in (a). The full reconstruction period was 1700-1927, but series are shown over the only 1895-1927 validation period.

Figure 4.9 – This plot shows the graph (in red) of the Region 5 regional areal-mean 1200-1927 summer PDSI reconstruction series (and its $\pm 2\sigma$ uncertainty bounds), made using the hybrid RegEM method with only the tree-ring part of the proxy network (Exp. 2), that exhibited a moderate or high level of skill as explained in more detail in the text. Noted are the RE and CE scores for the reconstruction and their P-values. Also shown is the graph (in black) of the Region 5 1895-1995 instrumental series.

Figure 4.10 – Contour map of RE scores, as calculated for each of 155 grid points and then interpolated, for the 1700-1927 reconstruction of summer PDSI using the hybrid RegEM method with only the tree-ring part of the proxy network used in the ridge sub-reconstruction and the full proxy network used in the TTLS sub-reconstruction (Exp. 3). Warmer colors indicate greater values of RE, and cooler colors indicate lower values of CE. The map of CE scores is qualitatively similar.

Figure 4.11 -- This series of eight plots ((a) – (h)) shows graphs of the each of the eight regional areal-mean summer PDSI reconstruction series made using the hybrid RegEM method with only the tree-ring part of the network used in the ridge sub-reconstruction and the full proxy network used in the TTLS sub-reconstruction (Exp. 3) (and their $\pm 2\sigma$ uncertainty bounds), the RegEM-ridge method with expanded tree-ring proxy network (Exp. 1), the Zhang et al. (2004) method, and the Cook et al. (1999) method as well as the eight regional areal-mean instrumental series. A legend of graph line colors is given in (a). The full reconstruction period was 1700-1927, but series are shown over the only 1895-1927 validation period.

Figure 4.12 – This series of eight plots ((a) – (h)) shows graphs of the eight regional areal-mean 500-1927 (top panel) and 1000-1927 (bottom panel) summer PDSI reconstruction series (and their $\pm 2\sigma$ uncertainty bounds) made using the hybrid RegEM method with only the tree-ring part of the proxy network in the ridge sub-reconstruction and the full proxy network in the TTLS sub-reconstruction (Exp. 3). In black are the instrumental series from 1895-1995. Noted for each figure are the RE and CE scores for the corresponding reconstruction. The P-values for all RE and CE scores are 0 to three decimal places.

Figure 4.13 – This series of eight plots ((a) – (h)) shows graphs of the eight regional areal-mean 500-1927 (top panel) and 1000-1927 (bottom panel) summer PDSI reconstruction series (and their $\pm 2\sigma$ uncertainty bounds) made using the regionalized hybrid RegEM method (Exp. 4). In black are the instrumental series from 1895-1995. Noted for each figure are the RE and CE scores for the corresponding reconstruction. The P-values for all RE and CE scores are 0 to three decimal places.

Figure 4.14 – This series of eight plots ((a) – (h)) shows graphs of the eight regional areal-mean 500-1927 (top panel) and 1000-1927 (bottom panel) summer PDSI reconstruction series (and their $\pm 2\sigma$ uncertainty bounds) made using the hybrid RegEM method with only the tree-ring part of the proxy network in the ridge sub-reconstruction and the full proxy network in the TTLS sub-reconstruction (Exp. 3). In black are the instrumental series from 1895-1995. Noted for each figure are the RE and CE scores for the corresponding reconstruction. The P-values for all RE and CE scores are 0 to three decimal places.

Figure 4.15 – Contour map of RE scores, as calculated for each of 6373 grid points and then interpolated, for the 1700-1930 reconstruction of winter precipitation using the hybrid method in which only the tree-ring part of the proxy network was used in the ridge sub-reconstruction and the entire proxy network was used in the TTLS sub-reconstruction (Exp. 3). Warmer colors indicate greater values of RE, and cooler colors indicate lesser values of RE. Only the areas shaded in red or dark red exhibit skill ($RE \geq 0$). The map of CE scores is qualitatively similar.

Figure 4.16 – This series of two plots ((a) – (b)) shows graphs of the validation-period portion (1902-1930) of two regional areal-mean 1700-1930 winter precipitation reconstruction series (and their $\pm 2\sigma$ uncertainty bounds) made using the hybrid RegEM method with only the tree-ring part of the proxy network in the ridge sub-reconstruction and the full proxy network in the TTLS sub-reconstruction (Exp. 3). In black are the

instrumental series from 1895-1995. Noted for each figure are the RE and CE scores for the corresponding reconstruction. These two regions were chosen for reasons described in the text.

Figure 4.17 – This series of two plots ((a) – (b)) shows graphs of the 500-1930 (top panel) and 1000-1930 (bottom panel) areal-mean winter precipitation reconstructions (in red; lighter red are their $\pm 2\sigma$ uncertainties) for Regions 1 and 5 that were made using the hybrid RegEM method in which only the tree-ring part of the proxy network was used in the ridge sub-reconstruction and the entire proxy network was used in the TTLS sub-reconstruction (Exp. 3). In black are the areal-mean 1902-2000 instrumental series. RE and CE scores for each reconstruction are also given.

List of Tables

Acknowledgments

I would be remiss not to make several acknowledgments concerning this thesis.

I begin with professional acknowledgments. I thank Mike Mann for his advisement and supervision during the past two-and-a-half years as well as Jenni Evans and Ray Najjar, the two other committee members, who provided valuable feedback on this work. I make prominent note of the very patient guidance that Scott Rutherford (collaborator at Roger Williams University) gave me regarding methodology and the often messy and disorganized legacy RegEM scripts and associated files that were the basis of this project. I acknowledge the help of Byron Steinman (formerly a Mann Research Group member, now a faculty member at the University of Minnesota at Duluth) in rounding up the proxy data records that were instrumental to this study. I am grateful for the technical support of Sonya Miller. I cannot forget that my undergraduate advisor Dave Changnon (faculty member at Northern Illinois University) suggested in my first advising meeting in October 2009, in the middle of my first semester at NIU, that I think about graduate school as I went forward in my undergraduate studies. I did, and here we are.

I gratefully acknowledge the financial support that the American Meteorological Society, the National Oceanic and Atmospheric Administration, and The Pennsylvania State University have provided me in my work toward the master's degree.

I thank my friends; they know who they are. Not only have these individuals provided social camaraderie, but they have also kept me grounded in reality in my moments of unmerited optimism and abject pessimism.

‘The farther backward you can look, the farther forward you will likely see’.

--Sir Winston Churchill

Chapter 1
Introduction

Owing to anthropogenically driven increases in atmospheric greenhouse-gas concentrations (e.g., Ruddiman 2001), the temperature of the Earth in the late 20th century and early 21st century, at least at hemispheric scales, is at its highest level in at least the past 2000 years (Mann 2007). As temperature is tied to precipitation and other elements of the hydrologic cycle and system, changes in temperature are tied to changes in the hydrologic cycle.

The hydrologic cycle governs water, which is an essential component of life on Earth: not only are its abundance and delivery needed to meet societal and ecological demands, it influences the intensity of climate variability and change and serves as a key feature of extreme events such as droughts and floods (e.g., Neukom et al. 2010). Hence, it is of interest to understand ongoing and future changes hydroclimate. Gaining such an understanding can be achieved by studying its past variability. As climate exhibits variability on all resolvable time-scales (from inter-annual to geologic) (Mann 2007), it behooves scientists to reconstruct, or infer, climatic variables, such as precipitation or indices derived from climatic variables, like drought, as far into the past as possible to enhance this understanding of present and potential future states of climate. The past approximately 1500 years provide a prudent time-frame in which to examine past climate to determine the envelope of natural climate variability, as the basic boundary conditions of Earth's climate (e.g., the continental arrangement, orography, Earth-orbital parameters, and the spatial extent of continental ice sheets) have remained stable during that period (Mann 2007).

Scientists can get a very good idea of the variability in precipitation climate over broad regions during the past 100 to 150 years, especially in the mid-latitude regions of the Northern Hemisphere, by examining the instrumental record. However, because the instrumental record extends back only 100 to 150 years, other observational evidence is required to reconstruct hydroclimatic variables farther back beyond the scope of the instrumental record and to identify modes of climate variability that operate at very low frequency (period of a century or more).

An important line of such long-term observational evidence is found in paleontological proxy records, or climate proxies. A climate proxy is defined as an observable quantity thought to vary in a consistent manner with a climate variable of interest (which, in the present study, is precipitation). Though the paleontological climate record is sparse, noisy, and cumbersome, use of high-resolution proxy types (e.g., tree rings, lake and marine sediments, speleothems) and application of careful calibration and cross-validation procedures can bear useful information about past climate (e.g., Jones et al. 2009).

Any one proxy chronology record answers to past climate for only a particular location or perhaps a small region. Using one proxy chronology record, a climatic time series for that location or small region can be inferred. However, if multiple such records are assembled to form a proxy network, a mean climatic time series can be calculated for a region that spans the area covered by the records. The methods that are used for calculating such areal mean series are known as composite-plus-scale (CPS) methods. Jones and Mann (2004) provide an extensive review of CPS methods.

Even though an areal mean series provides certain information, and does so in a concise way, it does not provide any information about the spatial variability of a climatic variable. Because there is much to be learned from examining dynamic modes of climate variability, which can be inferred from spatial patterns of climatic variables, it is preferable to reconstruct spatial patterns of a climate variable rather than just a single areal mean series (e.g., Rutherford et al. 2005; Mann 2007; Mann et al. 2007(a); Jones et al. 2009). The primary approach to reconstructing past spatial patterns of climate is known as the climate-field reconstruction (CFR) approach. A rather extensive review of CFR approaches is provided by Jones et al. (2009). Most recently, the Regularized Expectation Maximization (RegEM) algorithm of Schneider (2001) has been adapted into a proxy-based CFR method that has been used for temperature reconstructions (Mann and Rutherford 2002; Rutherford et al. 2003; Mann et al. 2005; Mann et al. 2007(a); Mann et al. 2007(b); Mann et al. 2008; Mann et al. 2009; Rutherford et al. 2010), a drought reconstruction for the United States (Zhang et al. 2004), and, very recently, a precipitation reconstruction for a portion of Asia (Feng et al. 2013). An important strength of the RegEM is that it takes advantage of non-local relationships between predictand (i.e., climatic variable, precipitation here) and predictor (i.e., proxies). A summary of the details of the RegEM as it applies to this study is given in the Methods chapter (Chapter 3).

Although CFR approaches, such as the RegEM, appeal to the dictate to reconstruct spatial fields of the climatic variable in question, they do not necessarily appeal to the desire to reconstruct low-frequency variability or seasonality in a climatic variable faithfully. The goals of reconstructing both low-frequency variability and seasonality in

precipitation translate to a choice about what proxies should be included in the network to be used for the reconstruction and about what methods support that choice of proxies.

Many existing reconstructions rely upon tree-ring proxies to the exclusion of other types of proxies from the proxy network. One reason for this reliance on tree-ring records is their relatively widespread spatial distribution. A second reason for this reliance is the relative strengths of tree-ring records. In particular, they are continuous, defined precisely with annual or finer resolution, dated accurately on a calendar time-scale, and calibrated rigorously against observed climate data (e.g., Fritts 1976; Jones et al. 2009). However, tree-ring records suffer from a host of limitations, which are discussed and referenced in more detail in the Data chapter (Chapter 2). The sum of these limitations is that tree-ring records fail to capture adequately the low-frequency variability and seasonality in precipitation (e.g., Esper et al. 2002). Besides the disadvantages of tree-ring records specifically, no one proxy type alone is adequate for reconstructing large-scale patterns of climate (Jones et al. 2009).

As using only one proxy type to the exclusion of other types is considered inadequate for large-scale reconstructions, a multi-proxy reconstruction approach, wherein multiple different types of proxy record are employed as predictor data, is favored and employed in the present study. Other types of proxy record include, among others, those derived from lake sediments, marine sediments, and speleothems. Information from multi-proxy networks is often complementary, which lends to a more robust climate reconstruction (Mann et al. 1998; Mann 2002; Mann et al. 2008, 2009; Jones et al. 2009). The key consequence of this complementarity is that different types of proxy record resolve different levels of temporal variability and patterns of seasonality in the climatic variable

(e.g., Jones et al. 2009). The RegEM algorithm can be hybridized, as discussed in the Methods chapter (Chapter 3), to handle multiple types of proxy record.

Given multiple types of proxy data and a CFR method, namely the RegEM algorithm, a large-scale spatial reconstruction of a hydroclimatic variable that infers conditions on the centennial or millennial scale and can distinguish among seasons can be produced. Not only can such a reconstruction yield information about precipitation climate at fine temporal resolution, it can yield information about precipitation climate during specific periods of interest. Two periods of climatic interest during the past ~1500 years are the Medieval Climate Anomaly (900 to 1250, per Mann et al. (2009)) and the Little Ice Age (1400 to 1700, per Mann et al. (2009)). Both these periods were characterized by a range of temperature, hydroclimate, and marine changes that were manifested in distinct regional and seasonal expressions (e.g., Bradley 2003; Mann et al. 2009). Generally, the Medieval Climate Anomaly (MCA) was characterized in the Northern Hemisphere by higher temperatures relative to a 1961-1990 climate-normal period, and, by contrast, the Little Ice Age (LIA) was characterized by lower temperatures. Although much is known about temperature patterns at temporal resolutions as fine as decadal during both these periods of interest, the dynamical origins of this observed climate during these periods is less clear (Mann et al. 2009). Knowledge of large-scale patterns of precipitation, paired with the knowledge of the temperature patterns, is considered a void toward understanding the dynamical origins of the climate.

Some attempts to reconstruct large-scale spatial patterns of summer drought, by way of PDSI, have been made (e.g., Cook et al. 1999; Zhang et al. 2004). On the other hand, no large-scale, multi-proxy reconstruction of precipitation for mid-latitude North

America has been attempted, and no attempt has been made to distinguish between cold-season and warm-season precipitation at a large spatial scale. However, numerous efforts have been undertaken to reconstruct precipitation for small regions. These smaller-scale reconstructions have led to certain ideas about precipitation climate, and its link to large-scale dynamical processes, during the last 1500 years, especially the MCA and LIA periods.

Arid conditions were commonplace in the western and likely central portions of the U.S. from 400 to 1300, which partially overlaps the MCA. The dominance of aridity over much of the western U.S. is supported by a wide range of proxy and archaeological records (e.g., Muhs 1985; Mehringer and Wigand 1990; Swetnam 1993; Stine 1994; Hughes and Funkhouser 1998; Kennett and Kennett 2000; Cook et al. 1994; Jones and Schwaitalla 2008).

Some questions have arisen recently about the magnitude, seasonality, spatial coherence, and causes of droughts and pluvials at the multi-decadal and centennial scales during this period (e.g., Steinman et al. 2014). Particularly, some disagreement has arisen concerning conditions in the Pacific Northwest region of the U.S. and adjacent parts of Canada. Using tree-ring-based evidence, Cook et al. (2014) concluded that mega-droughts are absent in the last 1500 years in the Pacific Northwest and that there was little change in drought variability in the MCA-to-LIA and LIA-to-modern period transitions. This conclusion is in stark contrast to those made by Steinman et al. (2014), who, using lake-sediment records, concluded that wetter conditions prevailed during the MCA and drier ones prevailed during the LIA; they also concluded that the LIA dry anomalies were smaller inland from the coast of the Pacific Ocean. An additional theme in hydroclimate

in the western United States is that the sign in precipitation anomaly tends to differ in the Pacific Northwest compared to the Southwest (McCabe et al. 2004, 2008; Steinman et al. 2012).

A link has been shown to exist between hydroclimate in western U.S. and mechanisms rooted in the tropical Pacific Ocean and the North Atlantic Ocean. The El Niño-Southern Oscillation (ENSO) and the Pacific Decadal Oscillation (PDO) influence the Aleutian Low and North Pacific high-pressure systems, which influence westerlies in the Pacific Northwest. That is, wet periods in the Pacific Northwest tend to coincide with La Niña periods, in which the Aleutian Low weakens and shifts west, which is communicated as a strengthening of westerlies in the region. The sum of these dynamical relationships suggests that the MCA was dominated by the negative phases of the PDO and ENSO and that the LIA was dominated by the positive phases of the PDO and ENSO. This relationship between hydroclimate in the western United States and ENSO and PDO dynamics is well supported by previous proxy and instrumental-record evidence and studies (e.g., Kennett and Kennett 2000; McCabe et al. 2004; Graham et al. 2007; McCabe et al. 2008; Graham et al. 2011). Dynamics in the North Atlantic Ocean also appear to influence North America hydroclimate. There is a substantial line of proxy evidence in support of a consistently positive phase of the North Atlantic Oscillation (NAO) during the MCA. It has also been noted that the timing of climatic changes in western North America between the MCA and LIA was similar to the timing of changes in conditions in Europe, the North Atlantic, and the tropical Pacific. Such an inter-hemispheric symmetry of multi-centennial hydroclimatic signals bolsters the idea that tropical sea-surface temperatures

(SSTs) have a important, if not direct causal, influence on westerlies in the Northern Hemisphere and hence on hydroclimate in North America (Graham et al. 2007, 2011).

At the same time, despite this understanding of dynamics in both the Pacific and North Atlantic during the MCA and LIA, the understanding of the relative importance of dynamics in each of these areas is more limited (e.g., McCabe et al. 2004). Booth et al. (2006) noted that more limited knowledge of hydroclimate in the central and eastern portions of the United States is a major void toward this understanding. This lack of spatiotemporal coherence hampers efforts to gain understanding of underlying dynamics.

As such, gaps in the understanding of the aforementioned dynamic mechanisms greatly motivate an effort to improve a basic understanding of long-term hydroclimate in the contiguous United States over the last 1500 years in a spatially coherent fashion and in a fashion that distinguishes between cold and warm season. Thus, the prime objective of the study to be described in this thesis was to develop a method to assemble reconstructions of summer (June-July-August) drought and winter (December-January-February) precipitation that are characterized by high skill and faithful depiction of low-frequency variability. The summer target was chosen because a number of summer drought reconstructions, by way of PDSI, had been undertaken in the past (e.g., Cook et al. 1999, Zhang et al. 2004), and an ability to compare reconstructions made using the methods of this study to those past reconstructions was considered desirable. The winter target was chosen because, in the colder part of the year, because temperatures are lower, drought is a less relevant metric for assessing relative wetness and dryness. Total precipitation is a more direct metric of hydroclimate during the cold season.

The balance of this thesis is organized by chapter. Chapter 2 specifies the instrumental and proxy data-sets that were used in the calibration for the reconstructions. Chapter 3 motivates and describes the RegEM algorithm, the experiments that were performed to modify the RegEM algorithm, and the cross-validation scheme that was used to estimate reconstructive skill. Chapter 4 reports and discusses the results of the experiments. Chapter 5 offers conclusions and ideas for follow-up work.

Chapter 2
Data

The data used to make a paleoclimatic reconstruction can be divided into two basic categories. One of the basic categories is paleontological climate records (or, proxies), and the other is the instrumental data with which the proxy data are calibrated. In this study, instrumental data for the precipitation reconstructions were provided by a gridded product from the Global Precipitation Climatology Centre (GPCC), and instrumental data for the drought reconstructions were provided by a gridded PDSI data-set developed by Zhang et al. (2004) after a product developed by Cook et al. (1999). Proxy data were records from multiple types of indicator, including tree rings, lake sediments, marine sediments, and speleothems. This chapter motivates and describes each data-set used.

2.1 – Instrumental Data

2.1.1 – Winter Precipitation

The GPCC Full Data Reanalysis: Monthly Land-Surface Precipitation, version 6.0, 0.5^o x 0.5^o resolution (Schneider et al. 2011) was the instrumental data-set used for the reconstructions of winter precipitation. This so-called reanalysis product can be viewed as a gridded instrumental product. It is noted that 1.0^o and 2.5^o resolution data-sets are also available; the 0.5^o data-set was chosen because it offers sufficiently fine resolution and follows the use of 0.5^o data in a successful similar precipitation reconstruction study by Feng et al. (2013). The data-set covers the global land surface and includes monthly values for 110 years starting with January 1901 and ending with December 2010 (Becker et al.

2013). Further information about how the data-set was developed is found in Becker et al. (2013) and Schneider et al. (2014).

As the GPCC re-analysis set is global and covers a time period longer than the calibration period selected, it was necessary to obtain a subset of the product that corresponds to the reconstruction domain. The subset obtained is given by a latitude-longitude rectangle bounded on the south by the grid-box centered on 26.75^{o}N, the north by 48.75^{o}N, the east by 68.25^{o}W, and the west by 121.25^{o}W. For the purpose of the reconstructions, as each of them contains missing-value flags for all months, all grid-boxes lying in the ocean within this subset were discarded. Also, all grid-boxes otherwise lying mainly outside the contiguous United States were discarded.

In addition to the fine resolution of the grid, use of this product over others was motivated by the rigorous quality-control procedures applied to the data. Schneider et al. (2014) claim that the quality-control measures used for similar gridded data-sets are too rudimentary given the frequent errors of various types that tend to be present in the raw station data from which the gridded data-sets are derived. The quality-control measures used for the GPCC re-analysis set are aimed at improving upon this shortcoming. At the basis of these quality-control measures is a segregation of station records by their source or observing system in the database in which the records are aggregated, allowing for a cross-comparison of stations at a common location. Such segregation avoids duplication of stations in the set of raw stations and ensures that records are assigned to the correct station in the database. The remaining quality-control measures are semi-automatic in that both objective procedures and human intervention are involved. These measures include a statistical check for outliers, a visual check for spatial consistency, and a further check

for temporal homogeneity. A full description of the quality-control measures is given in Schneider et al. (2014).

2.1.2 – Summer Drought

For the reconstructions of summer drought, summer values of the Palmer Drought Severity Index (PDSI) were used as a target. PDSI is an index of meteorological drought that is calculated from temperature, precipitation, and the local available water content of the soil (Palmer 1965). Although there exist other indices of drought, PDSI provides a societally relevant notion of drought and is, as such, the most widely used. Because of its popularity, it has been used in other drought reconstruction studies (e.g., Cook et al. 1999, 2004, 2007; Zhang et al. 2004). The strengths of PDSI in comparison to other drought indices are that it provides a measurement of the abnormality of recent hydroclimatic conditions, an opportunity to place current conditions in an historical perspective, and spatial and temporal representations of historical droughts (Alley 1984). However, PDSI suffers from certain drawbacks related to how it handles soil type and behavior and groundwater runoff as well as how it treats the lag between when precipitation falls and the start and end of drought periods (Alley 1984; Karl and Knight 1985).

The instrument-based gridded summer PDSI data-set used in this study was that developed for and used by Zhang et al. (2004) in their study and is based on that used by Cook et al. (1999) in their study. Cook et al. (1999) developed a 155-point instrumental gridded PDSI data-set that covered the contiguous United States. Its resolution is 2^{o} in latitude and 3^{o} in longitude. At that resolution, the points of the data-set correspond to a rectangle bounded by 25^{o}N latitude on the south side, 49^{o}N on the north side, 121^{o}W longitude on the west side, and 68^{o}W on the east side. Points that reside primarily outside

the land-mass of the contiguous United States are excluded, leaving a total of 155 points instead of 228. The data-set was developed from 1036 single-station monthly PDSI records estimated from the Historical Climatology Network (Karl et al. 1990) and modified according to Guttman (1991). Those 1036 monthly records were interpolated to the 155 points following the inverse-distance weighting method of Meko et al. (1993) and Cook et al. (1996). Not all 155 resulting records began in the same year though all records began no later than 1913. Zhang et al. (2004) modified the Cook et al. (1999) data-set so that the records of all 155 points began in 1895.

2.2 – Proxy Data

2.2.1 – Tree-Ring Records

Tree-ring data were obtained from the International Tree-Ring Data Bank (ITRDB). Tree-ring chronologies submitted by contributors to the ITRDB must satisfy certain requirements, aimed at maintaining quality, before they can be assimilated into the holdings. More information about the ITRDB can be found in Grissino-Mayer and Fritts (1997) and at National Climatic Data Center (2008).

Chronology records available from the ITRDB were acquired. A chronology record corresponds to a single proxy record and is a time series of index values, where index values are a stand-in for ring width. A search feature is available on a NCDC Paleoclimatology tree-ring data Web site (http://hurricane.ncdc.noaa.gov/pls/paleox/f?p=514:1:0). A subset of 'advanced search' features is also available. These advanced-search features were set such that all chronology records available in the latitude-longitude region bounded on the east by 51°W, the west

by 134°W, the south by 20°N, and the north by 55°N were obtained. This latitude-longitude region corresponds roughly to the portion of North America that has a mid-latitude climate regime.

These relatively raw search criteria returned chronology records of a variety of types. A full description of the types, as well as the format of the data, is available at National Climatic Data Center (2008). For the records of the several types available, only those tree-ring width records of the 'standard' type were retained. The standard record type is processed by fitting a curve to the ring-width series and then dividing each ring-width value by the corresponding curve value to generate a series of growth indices. Chronology records of the 'ARSTAN' and 'residual' types were also available and included in this first batch of records but were discarded for two reasons. One reason was that ARSTAN records are processed in a manner such that they may not be appropriate for reconstructions (cf. Cook 1985) and residual records would have required extensive processing for use in the reconstructions. The second reason was that ARSTAN and residual records from a given location are generally associated with a standard record for that same location, providing largely redundant information. The overall goal of this initial selection of records was to obtain a liberally large number of records to bolster the overall density of proxy records in the study domain.

Searching in this manner yielded a collection of records that were downloaded from the NCDC Web site. Each of the records in that collection was then processed using a FORTRAN script called 'Ind2Col' so that data appeared in columns and could then be analyzed. The 'Ind2Col' script is available for download from the Web site of the Lamont-

Doherty Earth Observatory at <http://www.ldeo.columbia.edu/res/fac/trl/public/ftp/Public/Software/>.

A three-criteria quality-control procedure was applied to the initial set of standard-type chronology records. The criteria that were assessed are analogous to those used in Mann et al. (2008). Criterion 1 concerns length of time series. Specifically, if the earliest series year of a chronology was after 1800 or the most recent series year was before 1970, or both, the record was removed from the set. This criterion ensures a sufficient overlap of the time span of a record's time series with the time span of the re-analysis product and allows for proper implementation of the RegEM procedure. Criterion 2 concerns number of samples used to construct the chronology record. For each year in a record's chronology series, a number of tree-core samples was used to arrive at that year's time-series value. Greater faith can be had in a time-series value that was derived from a larger number of samples. Thus, it was required that eight samples were used to arrive at each year's series value during the 1901-2000 period, which corresponds to the calibration period for the winter precipitation reconstructions. Criterion 3 concerns high correlation of the series with the local instrumental record. Some records share a common location with another record (or several records). 'Common location' was defined as common latitude-longitude coordinates at a precision of two decimal places. The time series of these same-location records should have high correlation, as too low correlation suggests that these records may not offer much information about the climate at that location. Over the 1800-1970 period, it was required that time-series values of each of the records from a common location have a Pearson moment (or, ordinary) correlation coefficient value (e.g., Wilks 2011) of greater than 0.50 with the values of each of the other records from that location.

After subjecting the records to the three quality-control criteria, 787 records remained in the quality-controlled tree-ring set and were ultimately added to the proxy network. For both the pre-quality control and post-quality control sets, all records began in or before 1800. It was noted that there is essentially no difference in the fraction of records beginning at or before any 50-year cut-off between the post- and pre-quality control data-set. Indeed, approximately 50% of the records begin in or before 1600, and approximately 10% of them begin in or before 1200 (Figure 2.1). It was also noted from inspection that the geographic distribution of the records is unchanged by the quality control.

The tree-ring records in the network arose from a geographical distribution that spans the contiguous United States and immediately adjacent parts of Canada and Mexico. The records are most dense in the western United States and in portions of the eastern third of the United States. They are least dense in the center of the reconstruction domain because of the prevalence of plains that lack trees (Figure 2.2). Metadata about each of the 787 tree-ring records in the network appear in Table A.1 of the Appendix.

2.2.2 – Non-Dendrochronological Records

Certain non-dendrochronological (i.e., non-tree-ring) records were included in the network for their depiction of low-frequency variability. Low- (high-)frequency variability is here defined as that corresponding to time-scales longer (shorter) than 20 years. A more subjective approach was taken to identifying non-tree-ring records to include in the proxy network. In general, it was required that, for a record to be included, it had to exhibit substantial sensitivity to precipitation or temperature at the location or in the region from which it was derived. It was also required that a record be free of odd or spurious trends

or distributions. The proxy network used in Mann et al. (2008) was used as a basis for identifying these additional records, and other more recently assembled records were considered and added, as well. First, the sources from which the proxies are derived are explained; in this study, the sources included lake sediment, marine sediment, and speleothem.

One source for proxy records is lake sediment. Lake bottoms accumulate sediments from the surrounding environment of the lake, so cores of lake sediments can provide a record of changes in that surrounding environment. As the rate of sediment accumulation in lakes is high, but provided that their records can be adequately dated, lake sediments offer the potential to provide high-resolution records of past climate.

Organic and inorganic materials reside in these sediments. These materials contain stable isotopes of oxygen, ^{18}O and ^{16}O. The ratio of ^{18}O to ^{16}O, or $\delta^{18}O$, is a proxy indicator of local evaporation and water input. That is, because rain water is enriched with ^{16}O, lower values of $\delta^{18}O$ indicate pluvials, whereas higher values of $\delta^{18}O$ indicate drier conditions. The relative amounts of the stable isotopes at a given time can be inferred using radiometric-dating techniques (Bradley 1999). Additionally, these materials contain stable isotopes of carbon, ^{13}C and ^{12}C. The ratio of ^{13}C to ^{12}C, or $\delta^{13}C$, is also a proxy indicator of local evaporation and water input. Higher values of $\delta^{13}C$ indicate higher productivity in plants due to more ^{12}C being locked up in plants. Thus, higher values of $\delta^{13}C$ indicate drier conditions, and lower values indicate wetter conditions. Similar to isotopic oxygen, radiometric-dating techniques form the basis of dating (Leavitt and Long 1989; Bradley 1999).

In a similar fashion to lake sediments, marine sediments provide an archive of climatic conditions near the ocean surface or on the adjacent continents.

Marine sediments are composed of both biogenic and terrigenous materials. Biogenic materials are remains of organisms. They provide a record of past climate and oceanic circulation in terms of surface water temperature and salinity, dissolved oxygen in deep water, nutrient/trace-element concentrations, etc. On the other hand, terrigenous materials originate on land. These materials mainly provide a record of humidity-aridity variations on the continents, the intensity and direction of winds blowing from land areas to the oceans, and other modes of sediment transport to and within the oceans (Bradley 1999).

In the marine-sediment record employed, assembled by Cronin et al. (2003), the ratio of magnesium to calcium (hereinafter, Mg/Ca ratio) in ostracod shells contained in sediment from the Chesapeake Bay (hereinafter, CB) is the proxy indicator (cf. Chivas et al. 1986). The Mg/Ca ratio in ostracod shells is influenced by the temperature of the water in which the shell was secreted and by the Mg/Ca ratio of the water itself. Because the Mg/Ca of the water in the CB varies little, Mg/Ca variability in fossil shells from the CB can be attributed to changes in water temperature, which means that the Mg/Ca ratio in the fossil shells is a paleoclimate proxy for SST. Because of possible teleconnections to the North Atlantic Oscillation (NAO) pattern (e.g., Ning and Bradley 2014), variability in sea-surface temperature (SST) in the CB may provide information about hydroclimatic variability in the northeastern United States and southeastern Canada. SSTs in the CB generally reflect regional SST patterns in the adjacent North Atlantic Ocean over monthly and inter-annual time-scales (Cronin et al. 2003).

Still another source for proxy records is speleothem deposits. Speleothems are drip stones that form in caves as a part of the meteoric water cycle (Lauritzen and Lundberg 1999). Cessation of speleothem growth over a large geographical area is more likely due to a climatic factor than anything else. Thus, dating periods of speleothem growth can provide useful paleoclimatic information (Harmon et al. 1977; Bradley 1999). Because speleothems form as part of the meteoric water cycle, variations in their growth rate and composition reflect environmental changes on the land surface above the cave. Cave drip waters can be seen as an integration of rainfall over time, which implies that speleothems are excellent hydroclimatic archives. As such, slow drip rates or long transport routes can yield dripwater compositions that are representative of mean annual rainfall. A caveat to this representativeness of mean annual rainfall is that there can be a bias toward representation of winter rainfall in areas where summer evaporation is high or toward summer rainfall where the ground freezes in winter. In addition to their laminations, deposits of minor and trace elements, and crystallography, radiometric dating of their oxygen and carbon isotopes can be used to derive a proxy indicator of precipitation and drought (Lauritzen and Lundberg 1999), as was used for the two speleothem-derived records used in this study.

Metadata for each of the 10 non-dendrochronological records that were ultimately included in the proxy network are found in Table 2.1.

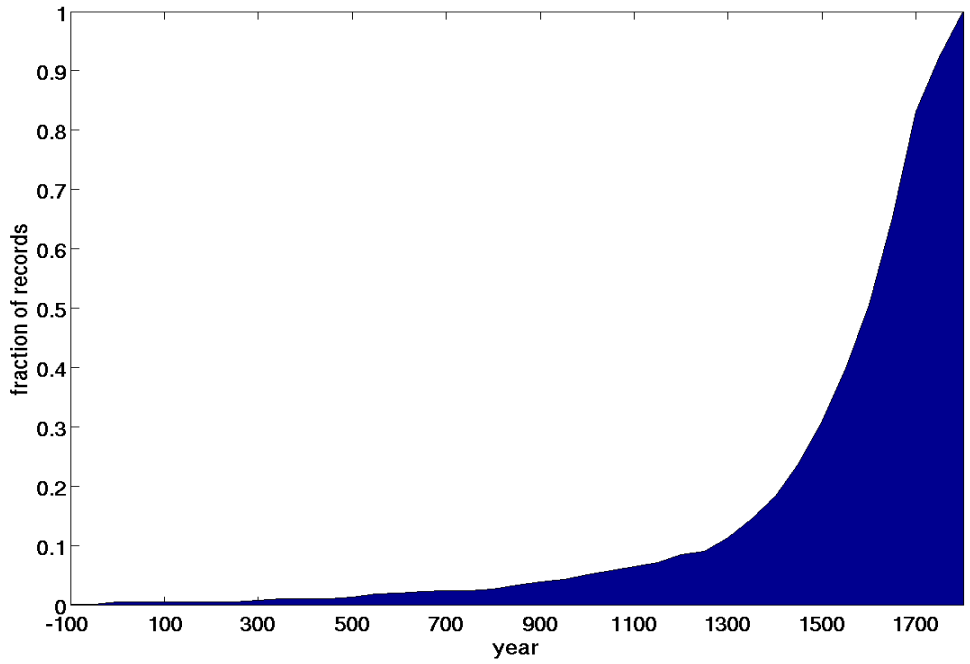

Figure 2.1 – Plotted is the fraction of the 787 tree-ring records included in the proxy network whose chronology series began in or before a certain year. For example, 100 percent of the series began in or before 1800, and approximately 50 percent began in or before 1600. Fractions were calculated at 50-year increments (i.e., in 1800, 1750, 1700, etc.) and interpolated for the other years.

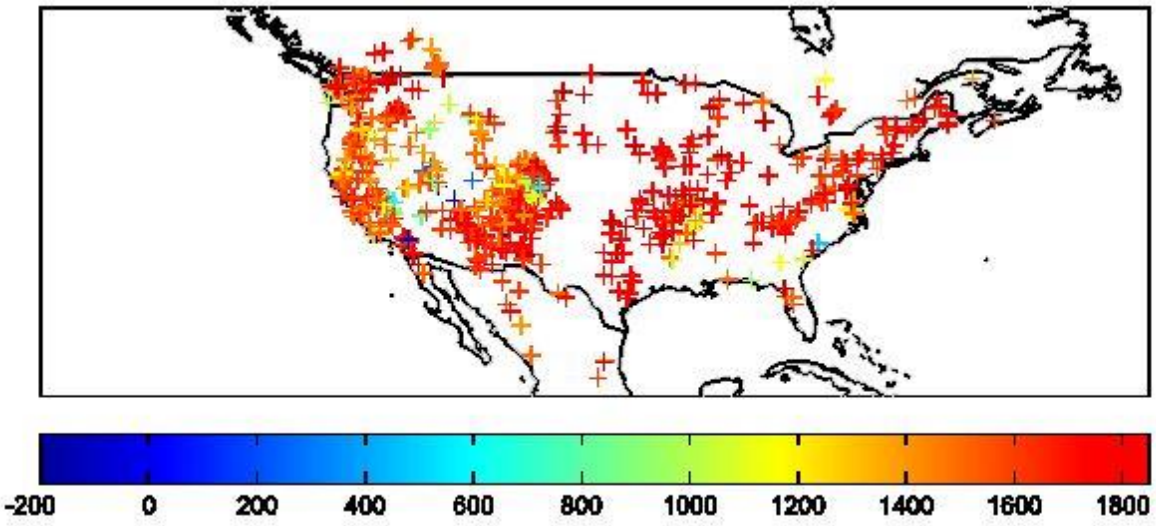

Figure 2.2 – This map displays the location of each of the 787 tree-ring records included in the proxy network. Each cross corresponds to a record, and its color corresponds to the year in which the record's chronology series began, where warmer colors correspond to later beginning years (AD) and cooler colors correspond to earlier beginning years.

Table 2.1 – This table displays various metadata for the 10 non-dendrochronological records included in the full proxy network for the reconstructions.

Record Description	Latitude-Longitude Coordinates	Period of Record (AD)	Average resolution (years)	Type of Record	Reference
Yellow Lake, Colorado, lake sediment	39.7°N, 107.3°W	1 - 2006	26	$\delta^{18}O$	Anderson (2011)
Mono Lake, California, lake sediment	38.0°N, 119.0°W	1698 - 1999	5	$\delta^{18}O$	Benson et al. (2003)
Cleland Lake, British Columbia, lake sediment	50.8°N, 116.3°W	-5611 - 2009	3	$\delta^{18}O$	Pompeani et al. (2013)
Renner Lake, Washington, lake sediment	48.8°N, 117.2°W	-682 - 2008	10	$\delta^{18}O$	Steinman et al. (2012)
Castor Lake, Washington, lake sediment	48.5°N, 119.6°W	-1 - 1998	12	$\delta^{18}O$	Steinman et al. (2012)
Crevice Lake, Montana, lake sediment	45.0°N, 110.6°W	587 - 1993	10	$\delta^{18}O$	Stevens and Dean (2008)
Foy Lake, Montana, lake sediment	48.2°N, 114.4°W	-1162 - 1992	9	$\delta^{18}O$	Stevens et al. (2006)
Chesapeake Bay marine sediment	38°N, 76°W	-183 - 1998	10	Mg/Ca ratio	Cronin et al. (2003)
Bat Cave, New Mexico, speleothem	32.2°N, 104.4°W	541 – 2004	10	$\delta^{13}C$	Asmerom et al. (2013)
Bat Cave, New Mexico, speleothem	32.2°N, 104.4°W	541 - 2004	10	$\delta^{18}O$	Asmerom et al. (2013)

Chapter 3
Methods

This chapter discusses the methods used in the study. First, the Regularized Expectation Maximization (RegEM) algorithm is explained, which is the general framework used for reconstructions, including its assumptions and a new hybrid modification to it. As well, the experimental set-up to arrive at a preferred RegEM framework is described. The cross-validation scheme as well as the estimation of reconstruction skill, uncertainty, and statistical significance is discussed next. Lastly, a mode of analysis of past hydroclimate from the summer drought and winter precipitation reconstructions made in this study is laid out.

3.1 -- Introduction and Motivation for Climate-Field Reconstructions

Mann et al. (2007a) define climate reconstruction as the estimation of the missing values of the rows of a data matrix, in which the missing values correspond to an instrumental series and occur prior to the modern period for which instrumental data are available.

Paleoclimatic reconstruction is often envisioned in terms of a data matrix. Suppose, for example, that a reconstruction of a climate field over the last 2000 years is desired. The data matrix, then, contains 2000 rows, or records, that correspond to time in years and columns, or variables, that correspond to locations in space as grid-boxes. Suppose further that instrumental data are available for the last 100 of the 2000 years. Then, initially, the last 100 rows, which correspond to those last 100 years, contain the instrumental data, whereas the other 1900 rows contain missing values. At the same time, there are proxy

records from a variety of locations inside (or even outside) the geographical domain of the desired reconstruction that span variously from the 2000th year to a time in the pre-instrumental period. The period of overlap for with both proxy values and instrumental values exist is known as the calibration period. It is this overlap in time of between proxy and instrumental data that serves as the basis for extending the climate record back in time to the pre-instrumental era, and statistical methods can foster this task. Figure 3.1 provides a schematic of the data matrix.

There are two general methods of statistical paleoclimatic reconstruction: composite-plus-scale (CPS) methods and climate-field reconstruction (CFR) methods. In the CPS methods, proxy data that are considered sensitive to past variations in a climatic field of interest are standardized and centered and then composited to form a series. That series is then regressed or scaled against a target instrumental series to yield a reconstruction of the climate field for a particular region (e.g., an entire hemisphere, a continent). Reconstructions made using CPS methods can only take the form of simple mean series and provide no spatial information. By contrast, CFR methods yield reconstructions of the underlying spatial climate patterns. Knowledge of such spatial climate patterns can be the impetus for insights into underlying climate dynamics. Spatial reconstructions formed in this way can be averaged to form mean series like the ones derived from CPS methods. Many CFR methods also offer the advantage of making use of non-local relationships between predictors (proxy data) and predictands (spatial field targeted for reconstruction). Such CFR methods represent a delicate compromise between the incorporation of potentially physical and potentially spurious distant statistical relationships into the calibration process. Although CFR methods offer a wealth of

information that CPS methods do not, CFR methods rely more heavily on assumptions about the stationarity of relationships between proxy indicators and climate patterns than do CPS methods (e.g., Zhang et al. 2004; Mann et al. 2007a). The Regularized Expectation Maximization (RegEM) algorithm of Schneider (2001) is an example of a CFR method.

3.2 – Description of the Regularized Expectation Maximization (RegEM) algorithm and its modifications

Use of the RegEM algorithm is motivated by the existence of an incomplete data matrix containing unknown, missing values that is paired with a lack of estimates of the mean vector and co-variance matrix (hereinafter, 'mean' and 'co-variance') for that data matrix. The problem, then, is that the calculation of the mean and co-variance requires knowledge of the unknown, missing values yet that estimation of those unknown, missing values requires knowledge of the unknown statistics of the data-set, which include the mean and co-variance. Hence, the imputation of missing values in data-set is a non-linear problem that must be solved iteratively (Schneider 2001). Developing the RegEM algorithm requires that the Expectation Maximization (EM) algorithm first be developed.

3.2.1 – The Expectation Maximization (EM) algorithm

The Expectation Maximization (EM) algorithm provides the basis for this iterative solution, wherein maximum-likelihood estimates of the parameters of any probability distribution can be computed from incomplete data (Dempster et al. 1977; Little and Rubin 1987; Schneider 2001). This algorithm begins, for Gaussian data, with initial guesses for the mean and co-variance and cycles through the alternating steps of imputing missing values and re-estimating the mean and co-variance using the completed data-set and an

estimate of the co-variance of the imputation error. Iterations of this cycle continue until the algorithm reaches a point of convergence. Convergence implies that mean and co-variance estimate and imputed values cease changing appreciably from iteration to iteration. This stagnation tolerance value is set by the user. As it converges linearly, meaning that the rate of convergence depends on the fraction of values missing in the data-set, the algorithm may require many iterations to converge. Schneider (2001) provides a full, mathematical review of the EM algorithm.

3.2.2 – The EM algorithm with regularization: the RegEM algorithm

To be applied to typical climate data, the EM algorithm requires modification. In particular, the EM algorithm for Gaussian data is based on iterated linear-regression analyses (e.g., Little and Rubin 1987). However, iterated linear-regression analysis requires that the data matrix be full-rank, and that requirement is problematic for typical climate data-sets, which contain thousands of variables and perhaps as many as a few hundred records (i.e., a matrix with many more columns than rows). That is, the number of variables in a record that have available values is greater than the number of degrees of freedom available for the estimation of the co-variance matrix. Hence, the statistics that provide estimates of the parameters of the regression models in the EM algorithm, as well as the conditional expectations of the missing values given the available values, are under-determined.

A modification that resolves this under-determination, or ill-posedness, and provides other valuable statistical properties is the imposition of a regularization method on the EM algorithm. Regularization renders the solution unique by the imposition of additional constraints (Schneider 2001). The resulting RegEM algorithm diminishes the

contributions of higher-order patterns, which are retained under this methodological framework, and that, in turn, effectively smooths out increasingly heterogeneous co-variance structures. Although regularization introduces a bias in estimated missing values, a price for reduced variance, it is a necessary trade-off with respect to the ill-posedness problem, and it endows the iteration algorithm with the important feature of providing for variance estimates in addition to the expected values (Mann et al. 2007a). Two methods of regularization, both used in this study, arise from ridge regression and truncated total least-squares regression. Both these methods of regularization offer an implicit accounting of errors in both the predictor and response variables. Brief descriptions of both ridge regression and truncated total least-squares regression follow, and Schneider (2001) provides a more comprehensive review.

3.2.2.1 – Regularization by ridge regression

In ridge regression, first presented by Tikhonov and Aresenin (1977), the ridge parameter h specifies the degree of inflation $(1 + h^2)$ of the main diagonal of the co-variance matrix. This ridge parameter, in effect, determines the degree of smoothness of the estimated missing values. It has been shown that the value of h chosen should be the minimizer of the generalized cross-validation function (Golub et al. 1979).

3.2.2.2 – Regularization by truncated total least-squares (TTLS) regression

In truncated total least-squares (TTLS) regression, which was developed by Fierro et al. (1997), regression coefficients are computed in a truncated basis of principal components of the overall co-variance matrix $\boldsymbol{\Sigma}$, and regularization is accomplished through a choice of truncation parameter K. In choosing a value for K, a conservative choice that has been found to work well in practice in past reconstructions of temperature

field is to estimate K as corresponding to the number of leading eigenvalues of the calibration-period data matrix that lie above the estimated noise continuum. The noise continuum is estimated by a linear fit to the logarithmic eigenvalue spectrum. However, in the low-frequency band, in practice, it has been found that retaining the first K eigenvalues that resolve 33% of the data variance works well (Mann et al. 2007a; Rutherford et al. 2010). Mann et al. (2007a) note that TTLS might be considered the preferred method of regularization because it is more robust compared to ridge regression and also that it is more parsimonious in terms of the number of parameters that need to be estimated, as TTLS requires one truncation parameter per iteration compared to the one ridge parameter per record required in ridge regression.

3.2.3 – Assumptions for the RegEM algorithm

A couple of assumptions must be made to use the RegEM algorithm. First, it is assumed that data are missing at random, which implies that the fact that a value is missing does not depend on the magnitude of the missing data values (Schneider 2001; Mann et al. 2007a). It is noted that, in this study (and other ones that deal with climate reconstruction), instrumental data are selectively missing during the pre-calibration interval, which challenges this assumption. However, Rutherford et al. (2003) and Mann et al. (2005) show that, in practice, reconstructions are insensitive to this non-randomness of data.

The second assumption is that the data have common dimensions and have homogeneous errors (Schneider 2001; Mann et al. 2007a). However, in this study, the instrumental precipitation data had units of millimeters, the instrumental PDSI data were standardized anomalies, and the proxy data had arbitrary units. Thus, to satisfy this assumption, it was necessary to standardize by mean centering all proxy records over some

common period. The choice of period over which the standardization is performed is an important decision, particularly if ridge regression is used as the regularization method (Mann et al. 2007a,b). In this study, standardization was done over the calibration period.

3.2.4 – Modification to the RegEM algorithm: Hybridization

A modification that was made to the RegEM algorithm in select experiments in this study was a hybridization of the reconstructions by frequency band. This hybridization involves using the RegEM to make two different sub-reconstructions of the climate field in question. One sub-reconstruction is made using the RegEM that is regularized by ridge regression. The other sub-reconstruction is made using the RegEM that is regularized by TTLS regression. Then, a low-pass filter is applied to both the ridge sub-reconstruction and the TTLS sub-reconstruction. For this filtering, $f = 0.05$ cpy, which corresponds to a period of 20 y, as past work has shown this frequency-split point to be suitable for hybridization in climate reconstructions. Extracting only two bands is a necessary trade-off between discerning distinct patterns of variability with respect to time-scale and keeping a sufficiently high number of statistical degrees of freedom to characterize and calibrate both bands of variability (Rutherford et al. 2005). For the ridge sub-reconstruction, the high-frequency part of the sub-reconstruction (period less than 20 y) is retained; for the TTLS reconstruction, the low-frequency part of the sub-reconstruction (period greater than 20 y) is retained. Ultimately, the high-frequency part of the ridge sub-reconstruction is added to the low-frequency part of the TTLS sub-reconstruction, yielding a total, hybrid reconstruction.

There are several motivations for making a hybrid modification to the RegEM algorithm. One motivation is that it must be made when, as in some reconstructions in this

study, decadally resolved and annually resolved proxy records are used. An additional motivation is that different types exhibit fundamentally different frequency-domain characteristics (Rutherford et al. 2005; Jones et al. 2009). A third motivation is that some proxies may respond differently to climate at low and high frequencies (La Marche 1974; Osborn and Briffa 2000; Hughes and Funkhouser 2003). A further motivation is the suggestion by Rutherford et al. (2010) that the hybrid modification can help to compensate for a sub-optimal calibration period (too short) and stagnation-tolerance setting (too high).

3.2.5 – Modification to the RegEM algorithm: Pre-whitening of data

An additional modification to this study's application of the RegEM algorithm involved the pre-whitening of the instrumental and proxy data that are inputted into any ridge reconstruction (whether as a full, ridge-only reconstruction or a sub-reconstruction of a hybrid reconstruction). Pre-whitening requires first that the original data series spanning T time elements, which is given by y_t, where $t = 1, 2, \ldots, N$, be modelled as

$$y_t = \rho y_{t-1} + w_t, \tag{3.10}$$

where ρ is the lag-1 auto-correlation of the series and w_t is the innovation term at t. By design, w_t has zero auto-correlation. Then, w_t can be calculated from y_t, forming the sequence

$$w_t = y_t - \rho y_{t-1}, \tag{3.11}$$

starting with the final data point in the series $y_{t=N}$ and working successively backward. The pre-whitened sequence w_t, along with the similarly constructed sequences for the other instrumental and proxy series, is used in the RegEM with ridge regularization. The RegEM

produces a proxy-reconstructed version of each w_t. To determine the full series y_t (i.e., to 're-redden' the data), the following equations are applied:

$$y_1 = w_1 \qquad t = 1 \tag{3.12}$$

$$y_t = \rho y_{t-1} + w_t \qquad t > 1 \tag{3.13}$$

This pre-whitening of the data is motivated by the greater serial persistence present in PDSI (and, to a lesser extent, precipitation) time series compared to time series of other climatic variables such as surface air temperature or sea-level pressure. Pre-whitening removes this serial correlation, whose extent may vary between the instrumental data and the proxy data (which exhibit temporal auto-correlation), during the calibration process. Re-reddening the final reconstructions restores this serial correlation to the final reconstructions (e.g., Cook et al. 1999; Zhang et al. 2004).

3.3 – Description of reconstruction experiments and their evaluation

3.3.1 – Objectives of the reconstruction experiments

A couple of key, related objectives were established. To help facilitate evaluation of these objectives, the contiguous United States was divided into eight regions (Figure 3.2). These eight regions, which collectively represent homogeneous regions of drought, were the same ones defined by Zhang et al. (2004) by performing a cluster analysis of the 1895-1978 part of their gridded PDSI data-set. Each reconstruction made was evaluated in terms of these eight regions. That is, for a given region, the grid-boxes corresponding to that region were identified, and the series of reconstructed values for those grid-boxes were averaged together to form a regional areal-mean reconstruction series. Evaluating the reconstructions in terms of these areal-mean series allowed for convenient comparison of

results obtained from different experiments. As well, it allowed for convenient objective, skill-based comparison of results from experiments from this study to results from past studies.

The first objective was to produce high-skill regional reconstructions of summer PDSI and winter precipitation. To quantify skill in an objective manner, skill scores, described later, were calculated for all reconstructions in a cross-validation scheme. The calculation of these skill scores is discussed later in this chapter. The second objective was to produce reconstructions that extend as far into the past as possible while also maintaining skill and faithful depiction of variability, especially at low frequency. Skill in these longer reconstructions was defined by meeting a skill-score threshold for a given regional areal-mean reconstruction. Evaluation of the depiction of variability was by visual inspection.

3.3.2 – RegEM algorithm settings

Values of various parameters of the RegEM algorithm can be specified by the user. Most of these settings were held constant in all the experiments (Table 3.1).

3.3.3 – Experiments and their justification

For both the summer PDSI and winter precipitation targets, a set of experiments was undertaken. The experiments involved modifying the RegEM algorithm toward meeting the aforementioned objectives: increasing the skill of the reconstructions and extending the reconstructions back in time while depicting low-frequency variability faithfully.

In each experiment, the reconstructions were made back only to 1700. The year 1700 was chosen because the skill of the PDSI reconstructions was compared to the skill of the PDSI reconstructions produced by Cook et al. (1999) and Zhang et al. (2004). Cook

et al. (1999) (hereinafter, C99) used a proxy network comprising 425 tree-ring chronology records and the point-by-point regression (PPR) method to reconstruct summer PDSI in the contiguous United States back to 1700. As used in that study, PPR is the sequential, automated fitting of single-point principal-components regression models of tree rings to a grid of climate variables, and the method is based on the premise that only those tree-ring chronologies proximal to a given PDSI grid-point are likely to be true predictors of drought at that location. The PPR premise is in stark contrast to a major premise of the RegEM algorithm, as discussed earlier in this chapter, which is that non-local relationships among predictors are important. Zhang et al. (2004) (hereinafter, Z04) used a proxy network comprising 483 tree-ring chronology records (the 425 records used by C99 plus 58 others) and the RegEM algorithm regularized by ridge regression to reconstruction summer PDSI in the contiguous United States back to 1700. For a regional areal-mean reconstruction produced in some experiment to be considered a 'success', it had to beat the skill of the same regional areal-mean reconstruction made using the data and method of both C99 and Z04. Data to make the C99 regional areal-mean reconstructions were obtained from a Web site of the National Climatic Data Center (http://www.ncdc.noaa.gov/paleo/usclient2.html), and the Z04 regional areal-mean reconstructions were made using data that were available from the Holocene archives of the research group (and that are also available from the NCDC Paleoclimatology Web site). Then, reconstructions were made back in time as long as skill remained. For these longer reconstructions, not only was skill evaluated, but also the faithfulness of their depiction of variability, especially low-frequency variability, was assessed. Although there were no

large-scale precipitation reconstructions for comparison, the same procedure was followed for the winter precipitation reconstructions.

Following this basic evaluation framework, the first experiment in the set (Experiment 1) involved making a reconstruction using the method of Z04 in which the global set of predictors was calibrated against the global predictand in a ridge-only RegEM set-up. This global-global calibration used all proxy records (all of which were tree-ring chronology records) from across the reconstruction domain (all 483 of them) and the full 155-point summer PDSI grid. Analogously, in this study, all 787 tree-ring chronology records in the full proxy network (i.e., the tree-ring part of the network) were calibrated against the full summer PDSI and winter precipitation grids in a ridge-only RegEM set-up. The 787-record tree-ring data-set represented a substantial increase in number of records over the Z04 data-set, and the sensitivity of the resulting regional areal-mean reconstructions to this data change was assessed.

The next experiment in the set (Experiment 2) involved the hybrid RegEM method. In both the ridge and TTLS sub-reconstructions, only the tree-ring part of the proxy network was used in the calibration against the full summer PDSI and winter precipitation grids. Hybridization of the RegEM is necessary if low-frequency proxy records are to be used. It was hypothesized that addition of the low-frequency records to the proxy network would improve the depiction of the low-frequency variability in the reconstruction target, especially farther back in time. A hybrid experiment in which only tree-ring records were used was a means toward assessing this hypothesis.

Experiment 3 involved applying the hybrid RegEM method but also using the full proxy network (797 records), which included both high-frequency tree-ring records (787

records) and low-frequency records (10 records) based on lake and marine sediments and speleothem (i.e., the low-frequency part of the proxy network). One version of the experiment involved using the tree-ring part of the proxy network for the ridge sub-reconstruction and the low-frequency part of the proxy network for the TTLS sub-reconstruction. A second version of the experiment involved using the tree-ring part for the ridge sub-reconstruction and the full network for the TTLS sub-reconstruction.

The final experiment, Experiment 4, involved the regionalization of the second version of the hybrid method used in Experiment 3. Regionalization meant making eight different reconstructions, one for each of the eight Z04 regions, in which the full, domain-wide proxy network was calibrated with an instrumental field specific to that region. This approach was preferred and found to perform best by Z04 on the premise that it makes use of large-scale, teleconnection-driven co-variance structures in the relatively long-term proxy data whereas it does not make use of the large-scale co-variance structures of the relatively short instrumental record.

3.3.4 – Evaluation of reconstructions

The skill, statistical significance, and uncertainty of the regional areal-mean reconstructions were estimated. To develop the methods of this evaluation, it is useful to consider the composition of the reconstructions. Reconstructions made using the RegEM algorithm can be thought to contain three components, which, according to Rutherford et al. (2003), are (1) the mean of the reconstruction period relative to the calibration period, (2) the trend of the reconstruction period, and (3) the inter-annual or –decadal variability. Additionally, such estimation should be objective and quantitative.

The basis of these evaluation methods is cross-validation. Cross-validation requires first that a calibration period and a validation period be designated. The RegEM algorithm, strictly speaking, does not specify the conventional calibration period or validation period that is associated with many methods of standard multi-variate regression. However, the calibration period can be defined as that period that is distinctly data-rich and the one used to estimate the co-variance between predictor and predictand. The validation period, by contrast, can be defined as that distinctly data-sparse period during which imputed values are compared with withheld data to assess reconstructive skill. In the context of this study, the validation period is a sub-set of the calibration period. The validation period preferentially used was 1895 to 1927 for the summer PDSI reconstructions and 1902 to 1930 for the winter precipitation reconstructions. That is, data from the 1895-1927 (summer PDSI) or 1902-1930 (winter precipitation) period were withheld, and the imputed values for that period were compared with the withheld data. This early, rather than late, validation period was preferred because, as mentioned by Mann et al. (2009), when a late validation period is chosen for the cross-validation of climate-field reconstructions, an instrumental field that is likely based on sparser data is used in the calibration, which can introduce bias.

In this study, reconstructions were made for a number of separate reconstruction periods. For example, a 1700-1927 summer PDSI reconstruction corresponds to a 1700-1927 reconstruction period; the last 33 years of that reconstruction period correspond also to the validation period, and 1928-1995 is the calibration period. On the other hand, a 1000-1927 reconstruction corresponds to a 1000-1927 reconstruction period and is made from a separate application of the RegEM algorithm for that particular reconstruction

period; the validation period and calibration period are the same as for the 1700-1927 reconstruction, and, thus, skill-score calculations, which are described in the next paragraph, remain the same. The difference between these two reconstructions is proxy data availability in the early part of their respective reconstruction periods. Proxy data generally become more sparse in the early part of the reconstruction period as the beginning of the reconstruction period is moved farther back in time. Therefore, proxy data are more sparse in the early part of a 1000-1927 reconstruction (~7% of proxy records available) than in the early part of a 1700-1927 one (~70% availability) (Figure 2.1, Table 2.1). Generally, because of more sparse data availability farther back in time, the skill of a longer (e.g., 1000-1927) reconstruction will be less than that of a shorter (e.g., 1700-1927) reconstruction on the basis of the cross-validation method used in this study.

Two quantitative diagnostics of skill were calculated: reduction of error (RE) (Lorenz 1956; Fritts 1976) and coefficient of efficiency (CE) (Nash and Sutcliffe 1971; Briffa et al. 1988; Cook et al. 1994). We let $\overline{x_c}$ denote the mean of the calibration-period instrumental values, $\overline{x_v}$ denote the mean of the validation-period instrumental values, $\hat{x}_i$ denote a reconstructed value at a time i during the validation period, and x_i denote an actual, instrumental value at time i during the validation period. Then, RE is defined as

$$RE \equiv 1 - \frac{\sum(x_i - \hat{x}_i)^2}{\sum(x_i - \overline{x_c})^2}. \tag{3.14}$$

CE is defined as

$$CE \equiv 1 - \frac{\sum(x_i - \hat{x}_i)^2}{\sum(x_i - \overline{x_v})^2}. \tag{3.15}$$

The range of both the RE and CE score values is given by $(-\infty, 1)$. For both RE and CE, a reconstruction whose score is -1 is characterized as a random guess. Scores residing in the range (-1, 0) designate reconstructions that are better than a random guess but that offer no skill. An RE score of identically zero designates a reconstruction that is the mean of the calibration period and that offers no skill, and a CE score of identically zero designates a reconstruction that is the mean of the validation period and that offers no skill. Scores increasingly greater than zero are indicative of increasingly more skillful reconstructions, and a score of unity indicates a perfect reconstruction. A skillful reconstruction on the basis of CE (i.e., $CE \geq 0$) is more challenging to achieve because, unlike RE, CE does not reward the reconstruction for an observed change in mean relative to the calibration period (e.g., Rutherford et al. 2005).

For regional areal-mean reconstructions that were said to have sufficient skill based on their RE and CE score values, their statistical significance was estimated using RE and CE as test statistics. Null distributions of RE and CE were formed by Monte Carlo simulation under the null hypothesis of first-order auto-regressive red noise. That is, for each actual reconstruction series, 1000 surrogate random reconstructions (or, realizations) were generated that have the same lag-1 auto-correlation structure, variance, and mean as the corresponding instrumental series over the calibration period. For each realization, an AR(1) noise process was projected back in time over the validation period, starting from the first year of the calibration period. From the RE and CE null distributions that were formed, the 95^{th}-percentile values of those distributions were calculated. The 95^{th}-percentile value of such distributions delineates the threshold for statistical significance at the 95% level. Therefore, if both the RE and CE scores of an actual reconstruction series

were equal to or greater than the 95th-percentile values of their respective null distribution, the actual reconstruction series was said to be statistically significant at the 95% level (hereinafter, simply 'statistically significant'). Those reconstruction series that were not statistically significant at the 95% level were discarded (e.g., Mann et al. 2005). The P-values of both RE and CE (i.e., their percentile value, divided by 100, in their respective null distribution) were also estimated.

The uncertainty of the statistically significant reconstructions was estimated using a 2σ (two-sigma) confidence interval, where σ gives the standard error. An estimate of 2σ can be found by calculating

$$2\sigma = 2\sqrt{(1 - RE)\sigma_{cal}^2}, \tag{3.16}$$

where RE is the reduction-of-error score for the reconstruction and σ_{cal}^2 is the variance of the calibration-period instrumental values. The upper bounds of the confidence intervals were formed by adding 2σ to each reconstructed value, and the lower bounds were formed by subtracting 2σ from each reconstructed value (e.g., Mann et al. 2005). An interpretation of the two-sigma confidence interval is that, if the actual reconstructed value is taken to be the mean value of a null distribution of possible realizations of the target value, there is a 95.4% probability that the value lies between the upper bound and the lower bound of the confidence interval (e.g., Wilks 2011).

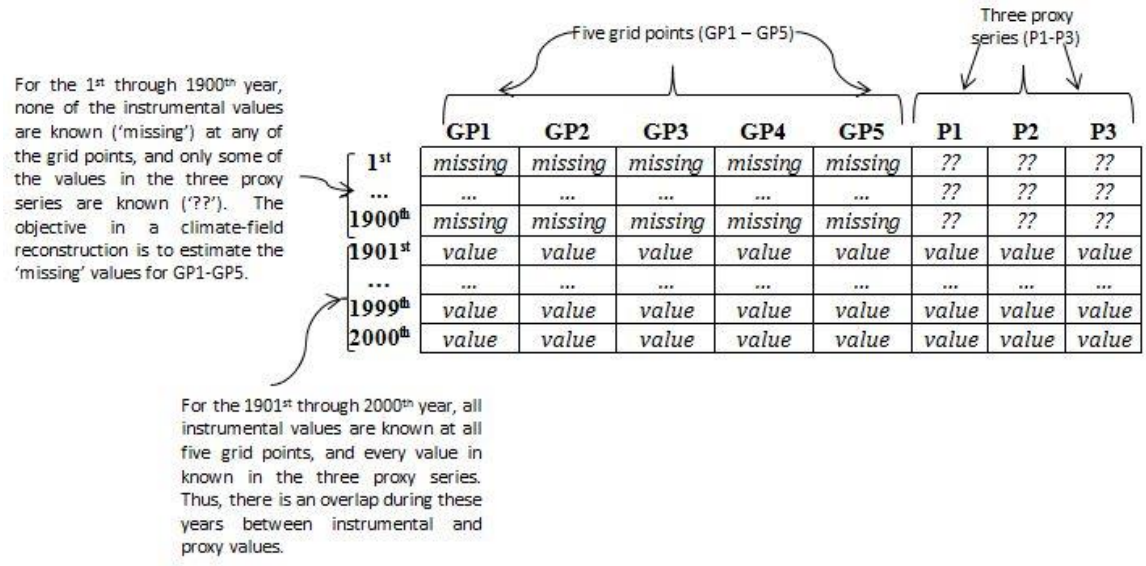

Figure 3.1 – Schematic of a data matrix for a climate reconstruction. It answers to a hypothetical situation in which three annual-resolution proxy chronology records are calibrated against a gridded field of a climate variable consisting of five points.

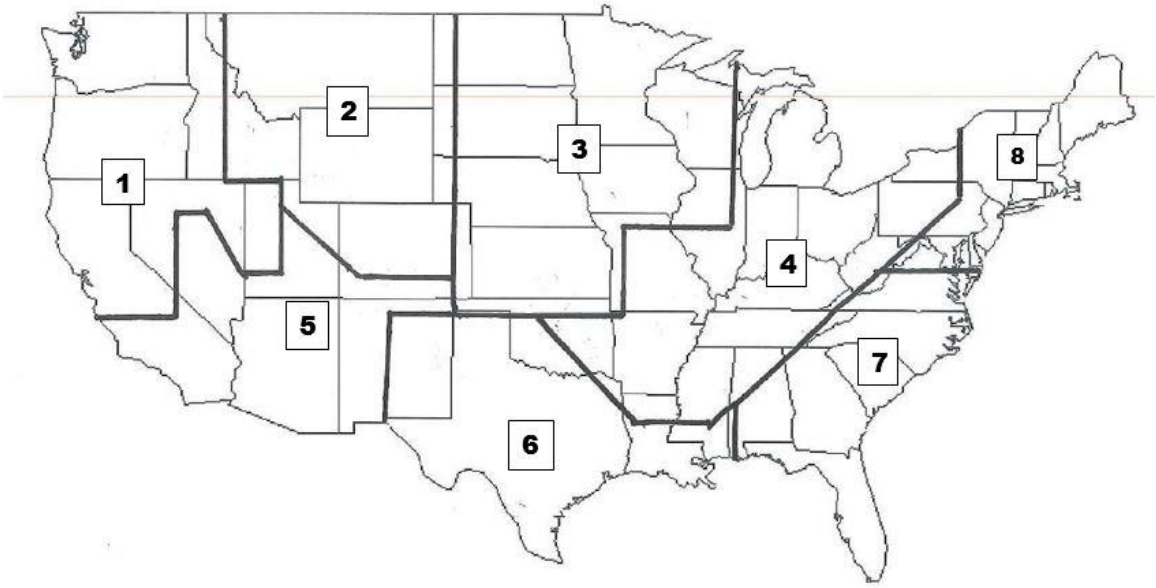

Figure 3.2 – Map showing the contiguous United States divided into the eight regions designated by Zhang et al. (2004).

Table 3.1 – Displays information about the various parameters set by the user for the RegEM. The values used for 'stagtol', 'maxit', 'inflation, 'relvar_res', and 'minvarfrac' were those used in the Zhang et al. (2004) global-global reconstruction.

Parameter Name	Description	Parameter Value
Regularization Method ('regress')	Specifies the regression procedure to be used for regularization. Can be set to multiple ridge regression ('mridge'), individual ridge regression ('iridge'), or truncated total least-squares regression ('ttls').	'mridge' for ridge-only reconstructions; 'mridge' and 'ttls' for hybrid reconstructions
Regularization Parameter ('regpar')	Specifies the regularization parameter. For ridge regression, if left unset, generalized cross-validation (GCV) function selects parameter value. For TTLS regression, it must be set and is fixed.	Not set (default) for ridge-only reconstructions; not set for ridge part of hybrid reconstruction and 3 for the TTLS part
Stagnation Tolerance ('stagtol')	Specifies that the EM algorithm stops iterating when consecutive iterates of the missing values are so close that $\|\|X_{mis}(it) - X_{mis}(it-1)\|\| \leq stagtol * \|\|X_{mis}(it-1)\||$, where $X_{mis}(it)$ is the matrix of imputed values at the it^{th} iteration and $stagtol$ is the value set for stagnation tolerance.	5×10^{-6}
Maximum Number of EM Iterations ('maxit')	Specifies the maximum number of iterations of the EM algorithm. Algorithm will stop iterating after this number of iterations regardless of whether the stagnation-tolerance condition has been met.	30 (default)
Inflation Factor for the Residual Covariance Matrix ('inflation')	Regularization results in the residual covariance matrix underestimating the conditional covariance matrix of the imputation error. Specifying a value greater than 1 for this parameter corrects this underestimation.	1 (default)
Minimum Relative Variance of Residuals ('relvar_res')	Specifies a lower bound for the regularization parameter to prevent the GCV from erroneously choosing too small a regularization parameter	5×10^{-2} (default)
Minimum Fraction of Total Variation in Standardized Variables	Specifies an approximate upper bound for the regularization parameter. Default value is 0, which corresponds to	0.7

Retained in Regularization (‘minvarfrac’)	no upper bound for the regularization parameter.	
Initial Imputed Values (‘Xmis0’)	Specifies a matrix of the same size as the input data-set that contains initial guesses in place of the missing values in the input data-set.	Not set (default)
Initial Estimate of Co-variance Matrix (‘C0’)	Specifies initial estimate of co-variance matrix. If no initial co-variance matrix is given but initial imputed values are specified, the sample co-variance matrix of the data-set completed with initial imputed values is taken as an initial estimate of the co-variance matrix.	Not set (default)
Number of eigenvalue-eigenvector pairs to be computed for TTLS regression (‘neigs’)	Specifying this number accelerates the computations can be accelerated, which results in the residual co-variance matrices being inaccurate. Default is to compute all non-zero eigenvalues and corresponding eigenvectors.	Not set (default)

Chapter 4
Results and Discussion

In this chapter, results of the RegEM method experiments are presented and discussed. The methods evaluated are the RegEM method in which ridge regression is used for regularization and the expanded tree-ring-only proxy data-set (i.e., the tree-ring part of the proxy network) used in the calibration (referred to as Experiment 1), the hybrid RegEM method in which only the tree-ring records are used in the calibrations for both the ridge and TTLS sub-reconstructions (Experiment 2), the hybrid RegEM method in which only tree-ring records are used in the calibration for the ridge sub-reconstruction and the full proxy network (including both tree-ring and low-frequency records) is used in the calibration for the TTLS sub-reconstruction (Experiment 3), and a regionalized hybrid RegEM method (Experiment 4). Summer PDSI and winter precipitation are considered separately in this presentation and discussion of the method evaluation, with more detail given for summer PDSI and the conclusions made for summer PDSI applied to winter precipitation. Additionally, one of the methods is named the preferred method, which is used to make regional areal-mean reconstruction series. Using these areal-mean series, past drought and precipitation are examined.

4.1 – Evaluation of RegEM methods: Summer PDSI

4.1.1 – Experiment 1: RegEM-ridge with expanded tree-ring proxy data-set

Regional areal-mean reconstruction series of 1700-1927 summer PDSI were assembled. RE and CE scores were calculated (Tables 4.1 and 4.2, respectively). These scores indicate that reconstructive skill is moderate to high in all regions – lowest near the

East Coast and in the Southern Plains and western and central Gulf Coast (Regions 6-8; Figure 3.2 for map of regions). Additionally, the P-values of the RE and CE scores for all regional areal-mean series are zero at three decimal places, which is much less than $\alpha = 0.05$ and is, thus, indicative of statistically significant reconstructions at the 95% level.

Because a reconstruction series was calculated for each of the 155 grid points in the domain, RE scores can be calculated for the all those reconstructions, interpolated in space, and then mapped (Figure 4.1). Considering skill in this way reveals that it is generally greatest in the southern part of the domain, especially in portions of the Southwest centered on southern Nevada and on west Texas and in the middle Mississippi, lower Ohio, and Tennessee river valleys. Skill is least in northern New England and the far northern Great Plains.

In Tables 4.1 and 4.2, the RE and CE scores are compared to those realized from the Z04 method and the C99 method. Based on this comparison, the skill of the reconstruction made using the Exp. 1 method is higher than that of the reconstruction made using the Z04 method in all regions except Regions 1 and 2. However, the skill of the Exp. 1 reconstruction beats that of the C99 reconstruction only in Regions 1, 4, and 5. On the other hand, the skill of the Z04 reconstruction beats that of the C99 reconstruction in those same regions. Therefore, differing from the Z04 method only by using more tree-ring records in the calibration, the Exp. 1 method yields a higher-skill reconstruction in most regions than that derived from the Z04 method. However, the expanded data-set used in the Exp. 1 reconstruction is not sufficient to beat the skill of the C99 reconstruction in a widespread fashion. In confirmation, from a contour map of difference in RE between that calculated for the Exp. 1 grid-point reconstructions and that calculated for the C99 grid-

point reconstructions (Figure 4.2), there are only a few pockets in which Exp. 1 skill is higher than C99 skill (portions of the northern Great Basin – corresponding to Region 1, much of the Great Lakes – corresponding to Region 4, and an area centered on southern Nevada – corresponding to Region 5). As a follow-up investigation, there may be some value in examining the sensitivity of reconstructive skill for a given location to the addition of the proxy records in the vicinity of that location, as it is unclear whether there is a pattern though Exp. 1 skill is lower in the Great Plains from where few records were obtained (Figure 4.3).

Plots of the Exp. 1 regional areal-mean reconstruction series were constructed for a period spanning only the validation period (1895-1927) to examine how they behave compared to the Z04 and C99 areal-mean series and the instrumental series (Figure 4.4a-h). With the notable exception of Region 2, the C99 series generally reside within the 2σ uncertainty intervals of the Exp. 1 areal-mean series. There is also generally very close agreement between the Exp. 1 and Z04 areal-mean series, which indicates that the RegEM algorithm is robust to varying data-sets. Some indication exists that the Exp. 1 (and Z04) areal-mean series reproduce the bigger peaks and valleys (bigger droughts and pluvials) present in the instrumental series more faithfully than the C99 series do, whereas the C99 series depict the mean behavior of the instrumental series more faithfully.

Reconstructions farther back in time were also made. For each region, an areal-mean series was calculated as far back in time as high skill remained (defined as RE and CE both being greater than 0.5). That is, in 100-year increments (back to 1700, back to 1600, etc.), a reconstruction was separately made, mean series calculated, and then the skill scores estimated. Thus, in Region 8, a reconstruction was made that extended back to

1400; in Regions 4 and 5, to 1200; and, in Regions 1-3, to 1000. In Regions 6 and 7, in no reconstruction were RE and CE both greater than or equal to 0.5, so those areal-mean series were calculated from a reconstruction made back only to 1700. All these regional areal-mean series are plotted in Figure 4.5a-h. A troublesome feature emerges in the early part of the longer series (e.g., Figures 4.5a-c), however. The series, as they proceed backward in time, exhibit substantial variance loss despite retaining skill based on cross-validation. This variance loss particularly affects the depiction of low-frequency variability, which is a feature of particular interest. Thus, hybridization of the RegEM method by frequency band was pursued for longer reconstructions.

4.1.2 – Experiment 2: Hybrid RegEM using only tree-ring records

The hybrid RegEM method was applied to the same data-set as used in Exp. 1 as a potential means of reducing the loss of variance over time in reconstructions that extend farther back in time and improving the depiction of low-frequency variability. RE and CE scores (Tables. 4.1 and 4.2) for the resulting regional areal-mean 1700-1927 series show that they had the same but mostly lower skill than the series derived from the reconstruction made using the Exp. 1 ridge-only method. In almost all areas, skill was the same or lower than that realized from the Exp. 1 reconstructions over the domain (Figure 4.6). Indeed, only in Regions 6 and 7 was the skill from the Exp. 2 reconstructions greater than that of the corresponding Z04 areal-mean series, and only in Region 4 was the skill greater than that of the corresponding C99 areal-mean series. From a contour map of RE score, skill was, as in the Exp. 1 reconstructions, greatest in the southern part of the domain, especially, again, in the middle and lower Mississippi river valley (Figure 4.7).

Plots of the regional areal-mean 1700-1927 reconstruction series over the 1895-1927 validation period (Figure 4.8a-h) illustrate that the Exp. 2 reconstruction series are similar to the corresponding Exp. 1 and Z04 (RegEM-based) reconstruction series in that they faithfully depict the relative patterns of drought and pluvial with respect to the instrumental series. However, the Exp. 2 series values tend to deviate more from the instrumental series values than the Exp. 1 and Z04 series values in terms of specific values, which explains their decreased skill.

The skill of most the regional areal-mean series decreased considerably when the reconstruction length was increased even just 100 years to 1600. Notably, however, skill remained relatively great in Region 5 areal-mean series from reconstructions made as far back as 1200. From the plot of this series (Figure 4.9), it is noted that the variance loss going back in time seen in the Exp. 1 reconstruction series is not present; low-frequency variability appears to be depicted.

Hybridization was seen to offer promise toward depicting low-frequency variability going back farther in time. However, the loss in skill compared to the Exp. 1 reconstructions was something that needed to be addressed. Hence, Exp. 3 was pursued.

4.1.3 – Experiment 3: Hybrid RegEM using tree-ring and low-frequency records

In an attempt to retain and enhance the hybrid RegEM method's advantage of depiction of low-frequency variability but also to increase the skill of the reconstructions derived from this method, records from the low-frequency part of the proxy network were also used in the calibration in the TTLS sub-reconstruction.

As the first part of this experiment, a 1700-1927 reconstruction was made in which only the tree-ring part of the proxy network was used in the calibration for the ridge sub-

reconstruction and only the low-frequency part of the proxy network was used in the calibration for the TTLS sub-reconstruction. Regional areal-mean reconstruction series were assembled, and their skill was evaluated by way of RE and CE scores (Tables 4.1 and 4.2). In most regions, except Regions 4 and 5, these scores show skill to be very low or non-existent.

The subsequent part of this experiment involved making a 1700-1927 reconstruction in which only tree-ring records were used in the ridge sub-reconstruction calibration and all records in the proxy network were used in the TTLS sub-reconstruction calibration. The RE and CE scores of the resulting regional areal-mean reconstruction series is displayed in Tables 4.8 and 4.9. Reconstructive skill is greater in all regions, except Region 5, than that realized when only the low-frequency records were used in the TTLS sub-reconstruction. Perhaps more importantly, moderate to high skill is widespread across the regions compared to the reconstructions arising from the Exp. 2 method in which only tree-ring records were used in both sub-reconstruction calibrations, and that skill is statistically significant at $\alpha = 0.05$ (i.e., P-values for RE and CE scores are less than 0.05). As in the reconstructions resulting from the other experiments, skill is generally higher in the southern part of the domain compared to the northern part, with enhanced skill in portions of the middle and lower Mississippi river valley (Figure 4.10).

The regional areal-mean reconstruction series were plotted (Figure 4.11a-h). In general, the Exp. 3 series resemble the other RegEM-based reconstruction series, indicating a robust result. Reconstructions that extended back to 1000 and 500 were made and regional areal-mean series assembled again from each of those two reconstructions (Figure 4.12a-h). Low-frequency variability is depicted by these reconstruction series, but it

appears that it may be enhanced artificially farther back in time. This possible artificial enhancement of low-frequency variability may stem from the choice of low-frequency proxy records that were used in the calibration and requires further investigation. Another interesting feature of several of the 500-1927 areal-mean series (Regions 1, 2, 3, 4, and 8 -- the northern part of the domain) is that, prior to approximately 1000, PDSI values are generally much lower than those in the series after that time. Especially as the skill of the 500-1927 reconstructions is lower than the 1000-1927 reconstructions, and thus the uncertainty greater, it is unclear whether that is a real feature of hydroclimate in those regions. Nonetheless, superimposed on that apparent dry regime before 1000 is decadal variability – that is, there were relatively drier and wetter periods that each spanned several decades.

For the period from 1700 to the beginning of the instrumental record (1895), the Exp. 1 method, though it produces regional areal-mean reconstructions lower in skill than those made using the C99 method, offers a reasonably viable methodological framework for reconstructing PDSI in the contiguous United States. However, for the more distant period from 500 to 1700, with some caveats, including that it yields reconstructive skill lower than that yielded by the C99 method, the hybrid RegEM method in which low-frequency records are included in the TTLS sub-reconstruction calibration is the methodological framework that is required to depict low-frequency variability in a faithful fashion.

4.1.4 – Experiment 4: Regionalized Hybrid RegEM

To implement a more physically defensible method and to improve reconstructive skill, the same hybrid RegEM method used in Exp. 3 was used but was regionalized. That

is, for each region, the hybrid RegEM method was implemented in a fashion in which the domain-wide set of proxy records was calibrated with the instrumental PDSI field corresponding to that region.

As in the other three experiments, a 1700-1927 reconstruction was made to evaluate skill compared to other reconstruction efforts. The regional areal mean series arising from this reconstruction are plotted in Figure 4.13a-h, and RE and CE scores were calculated (Table 4.1). Reconstructive skill under this regionalized method is at least somewhat improved compared to the Exp. 3 method in Regions 1, 2, 3, and 4, approximately the same in Region 5, and degraded in Regions 6, 7, and 8 (along the Gulf and East Coasts). Because the regionalization puts more stock in the use of teleconnection relationships to infer drought, this pattern of coherence in the improvement and degradation of skill continues to suggest the notion that teleconnection relationships are inappropriately communicated for the far southern and eastern U.S., which is a point also made by Z04.

A reconstruction that extends back to 1000 and another that extends back to 500 were made and regional areal mean series calculated and plotted (Figure 4.14a-h). These series generally exhibit the same features as those present in the series derived from the Exp. 3 reconstruction.

4.2 – Evaluation of RegEM methods: winter precipitation

A similar set of experiments was performed for the winter precipitation reconstruction target as was performed for the summer PDSI target. In all regions, regardless of method, the skill of the reconstructions of winter precipitation was much lower than of summer PDSI. Because skill in Regions 1 and 5 was marginally moderate

and because the two regions are adjacent to each other in the western part of the domain, an area of particular interest, focus was limited to those two regions. The problems of variance loss in the early part of the reconstructions (Exp. 1) and skill degradation in a tree-ring-only application of the hybrid RegEM method (Exp. 2) arose again, so it was decided that the Exp. 3 method (hybrid RegEM method with the tree-ring part of the proxy network used in the ridge sub-reconstruction and the full proxy network used in the TTLS sub-reconstruction) would be applied to winter precipitation, as well.

Regional areal-mean 1700-1930 reconstruction series for Regions 1 and 5 were assembled and their skill, and its statistical significance, evaluated by way of RE and CE scores (Tables 4.3 and 4.4). The skill of the series for Regions 1 and 5 is statistically significant at $\alpha = 0.05$. A contour map of RE confirms that skill is nearly non-existent outside the western part of the domain (Figure 4.15). Plots of the Regions 1 and 5 areal-mean reconstruction series over the validation period (1902-1930) shows that these two reconstructions tend to depict times of higher and lower precipitation in relative terms but that they struggle in depicting the specific values relative to the instrumental series.

Reconstructions that extend back to 1000 and 500 were made, and Region 1 and 5 areal-mean reconstruction series were assembled (Figure 4.16). The skill of the areal-mean series back to 500 is substantially less than that of ones back to 1000 to the extent that the 500-1930 areal-mean series for Region 5 might be characterized as having low skill.

These low-skill results are disappointing but must be considered in light of the fact that no published comprehensive spatial reconstruction of precipitation exists for the contiguous United States. Nonetheless, it would be a worthy effort going forward to develop an infrastructure, data-set and method, that allows the skillful long-term spatial

reconstruction of precipitation. Skillful precipitation reconstructions would allow for the independent consideration of temperature and precipitation, which may be critical to a comprehensive understanding of the underlying climate-system dynamics.

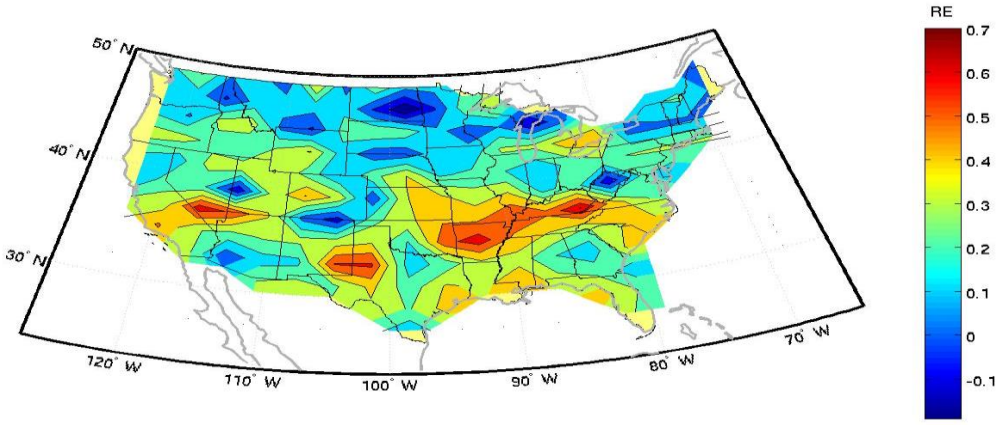

Figure 4.1 – Contour map of RE scores, as calculated for each of 155 grid points and then interpolated, for the 1700-1927 reconstruction of summer PDSI using the RegEM-ridge (Exp. 1) method with the expanded tree-ring proxy network. The contour map of CE scores is qualitatively similar.

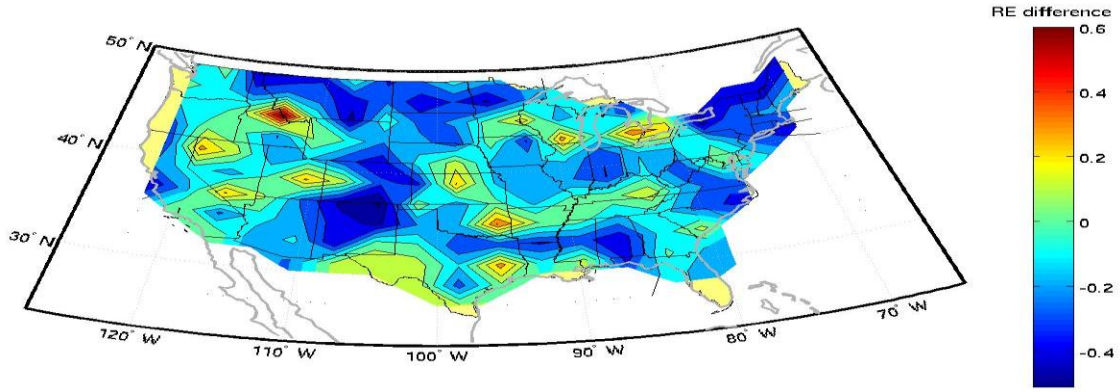

Figure 4.2 – Contour map of the difference in RE scores between those calculated for a 1700-1927 reconstruction of summer PDSI using RegEM-ridge using the expanded tree-ring proxy network (Exp. 1) and those calculated for a reconstruction of the same target using the method of Cook et al. (1999). Scores were calculated for each of 155 grid points and then interpolated. Differences values greater than zero indicate that the RegEM-ridge-expanded method had greater reconstructive skill than the Cook et al. (1999) method. The contour map of CE score differences is qualitatively similar.

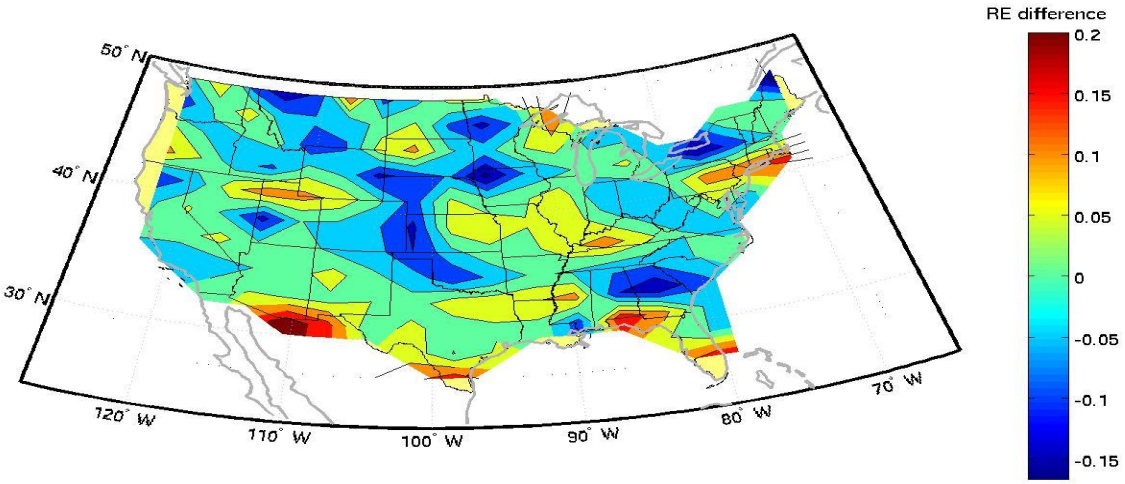

Figure 4.3 – Similar to Figure 4.2 but showing RE differences between 1700-1927 reconstructions made using RegEM-ridge-expanded (Exp. 1) method and the Zhang et al. (2004) method and proxy network. The contour map of CE score differences is qualitatively similar.

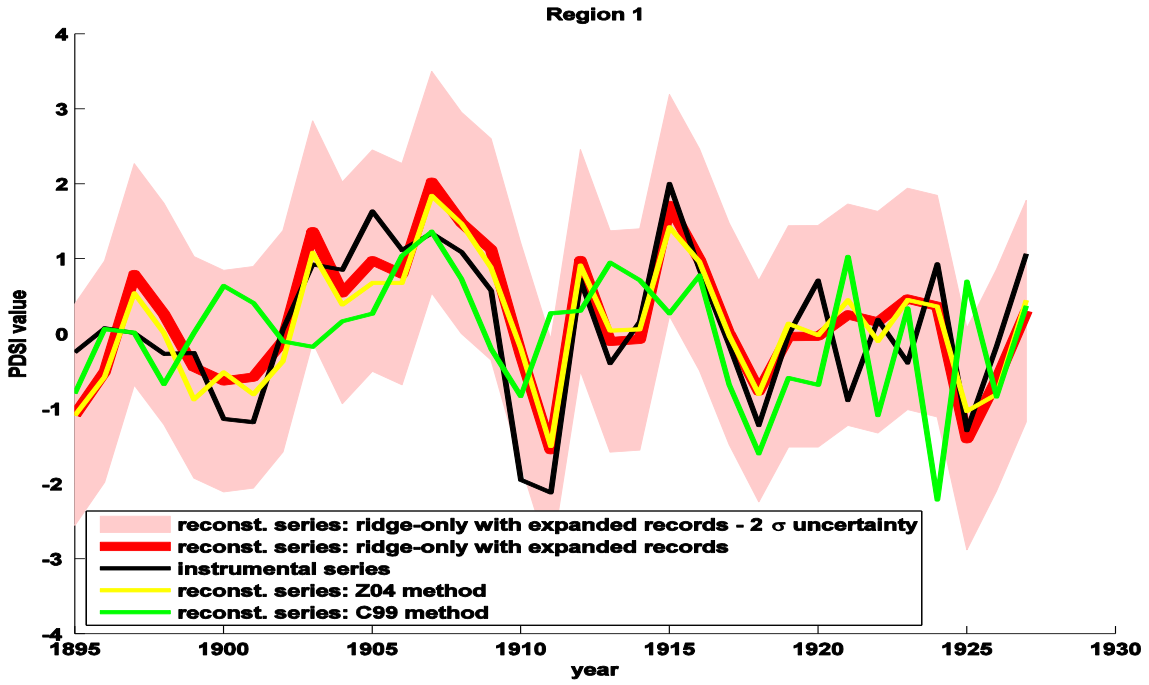
Region 1
PDSI value
year
reconst. series: ridge-only with expanded records - 2 σ uncertainty
reconst. series: ridge-only with expanded records
instrumental series
reconst. series: Z04 method
reconst. series: C99 method

(a)

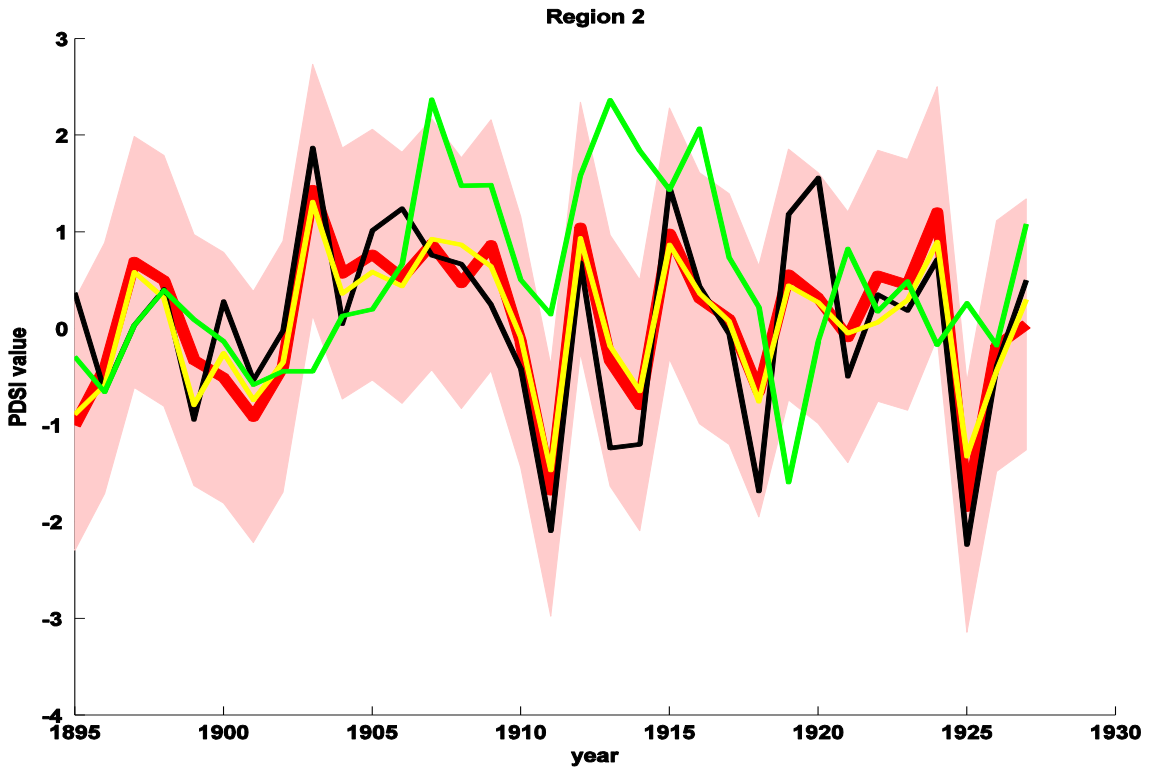
Region 2
PDSI value
year

(b)

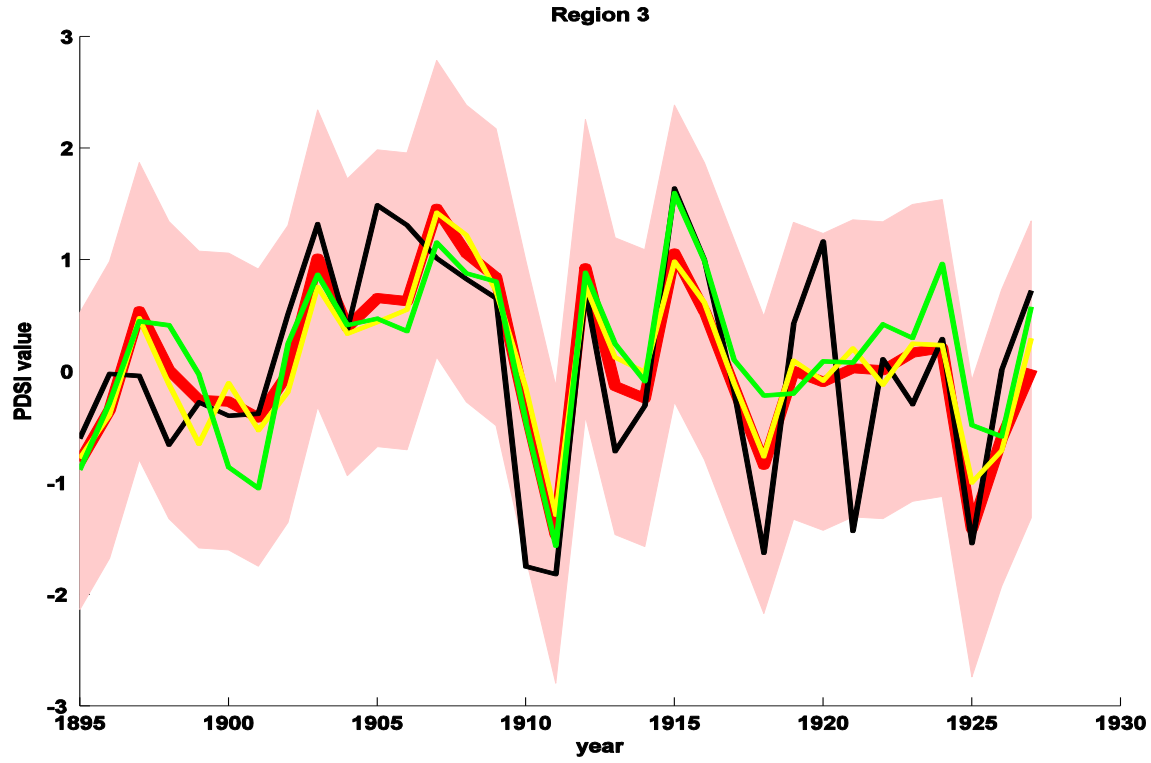
Region 3
PDSI value
year
3
2
1
0
-1
-2
-3
1895
1900
1905
1910
1915
1920
1925
1930

(c)

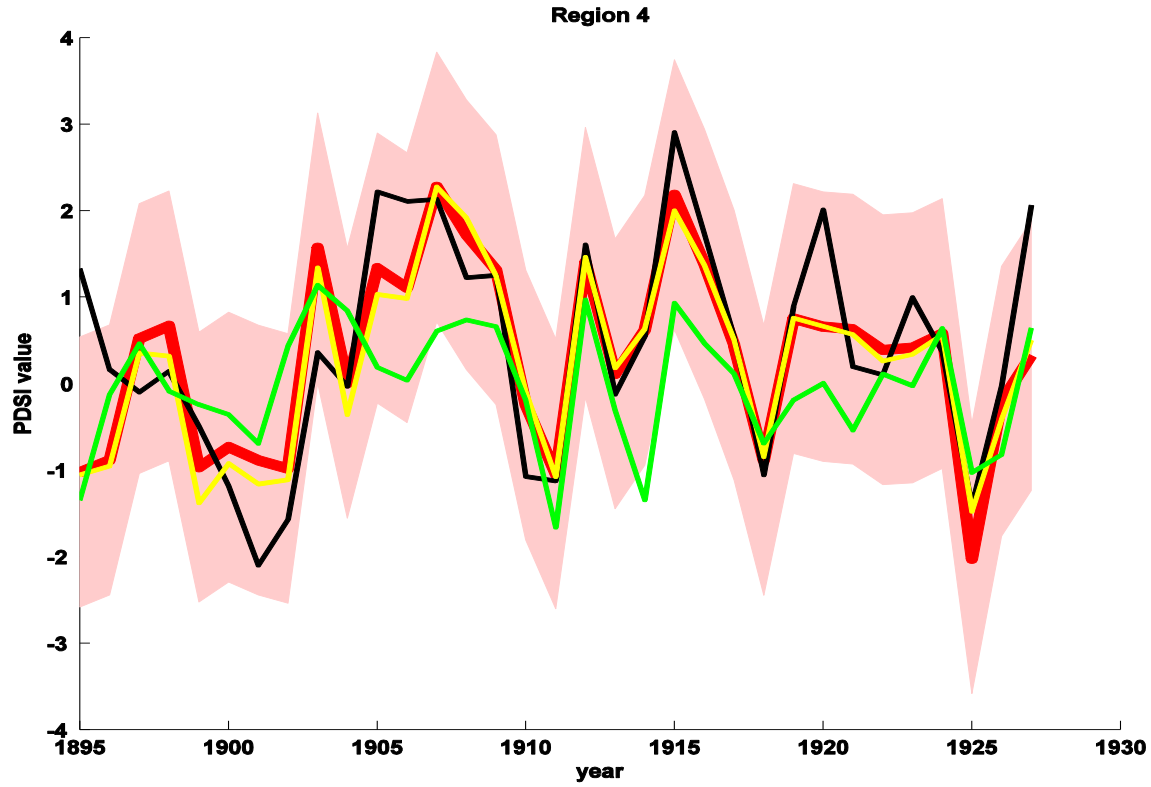
Region 4
PDSI value
year
4
3
2
1
0
-1
-2
-3
-4
1895
1900
1905
1910
1915
1920
1925
1930

(d)

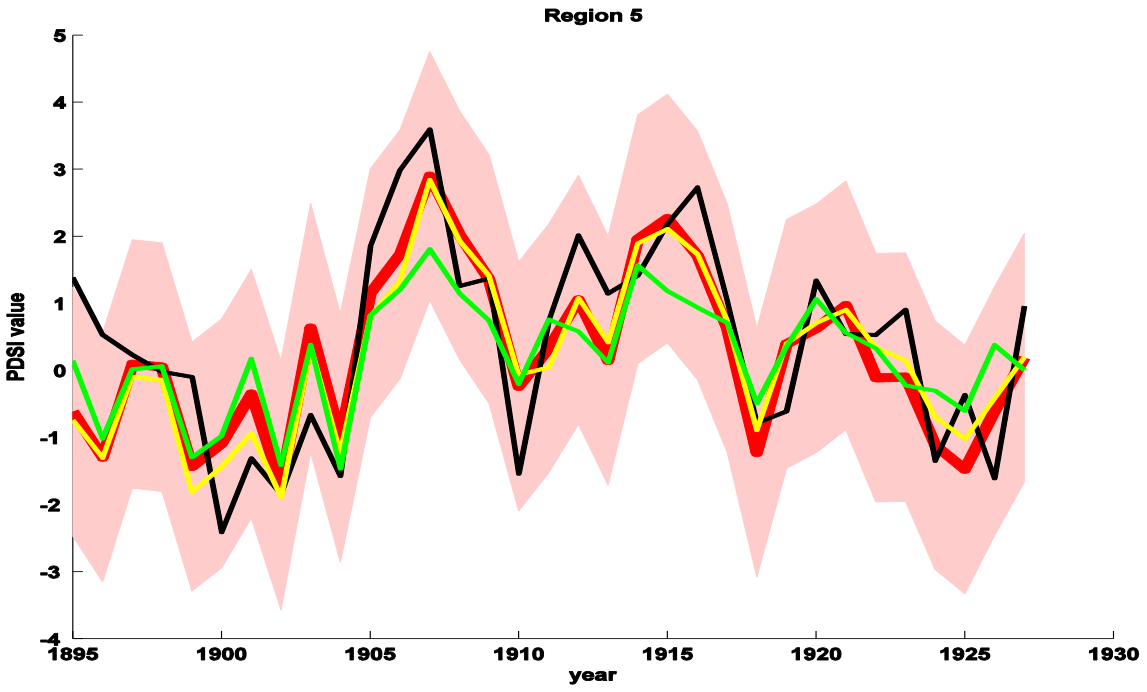
Region 5
PDSI value
year
5
4
3
2
1
0
-1
-2
-3
-4
1895
1900
1905
1910
1915
1920
1925
1930

(e)

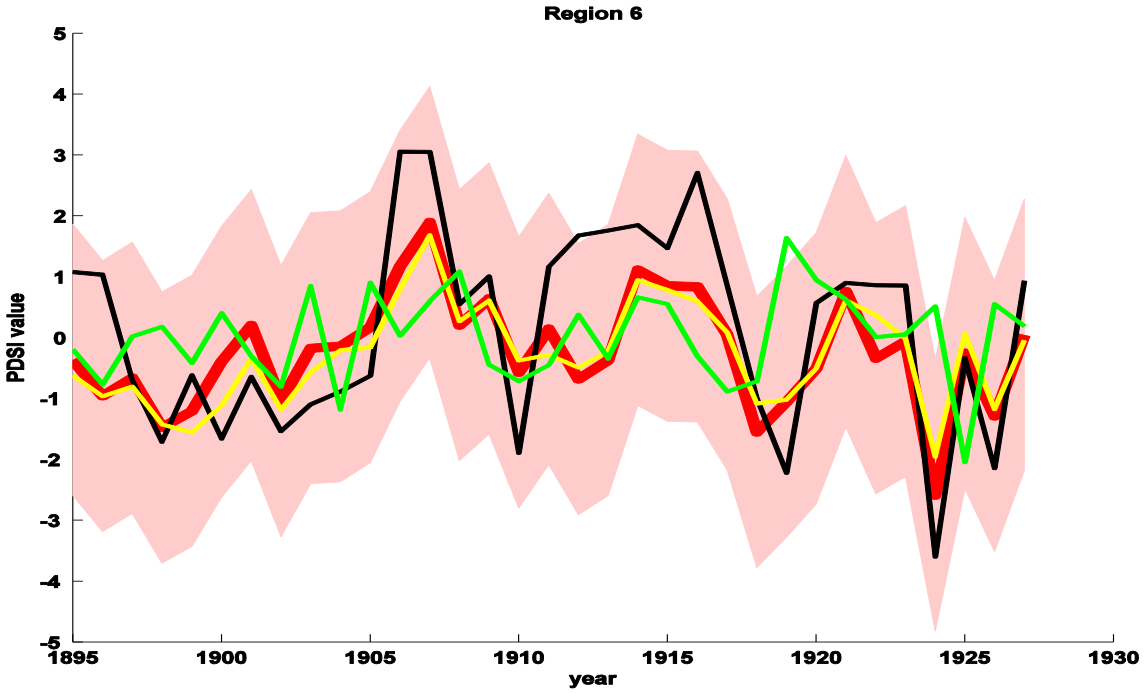
Region 6
PDSI value
year
5
4
3
2
1
0
-1
-2
-3
-4
-5
1895
1900
1905
1910
1915
1920
1925
1930

(f)

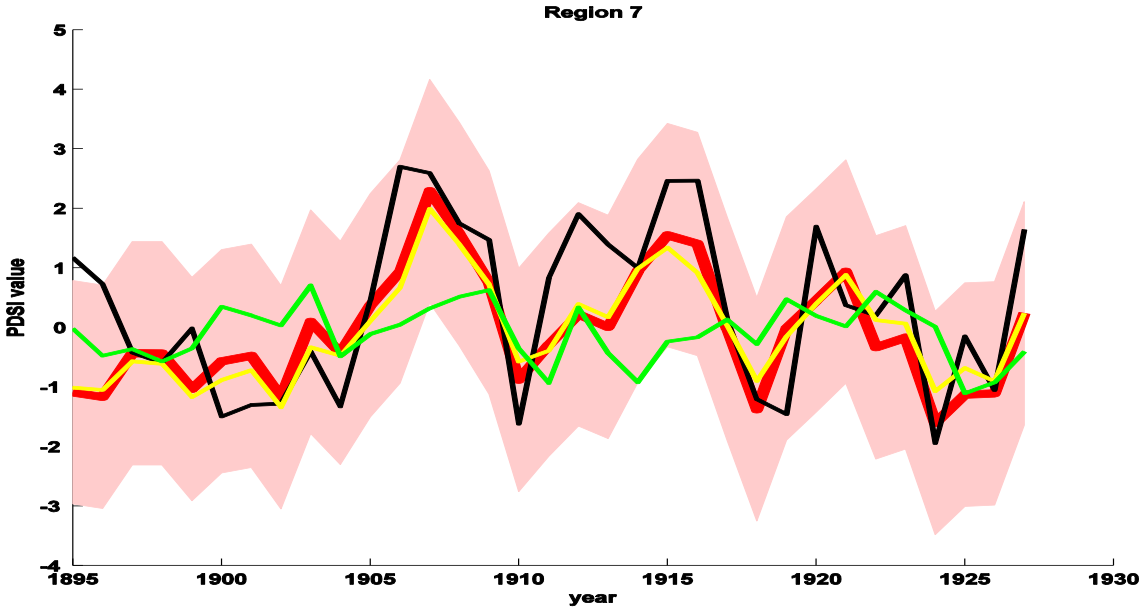

(g)

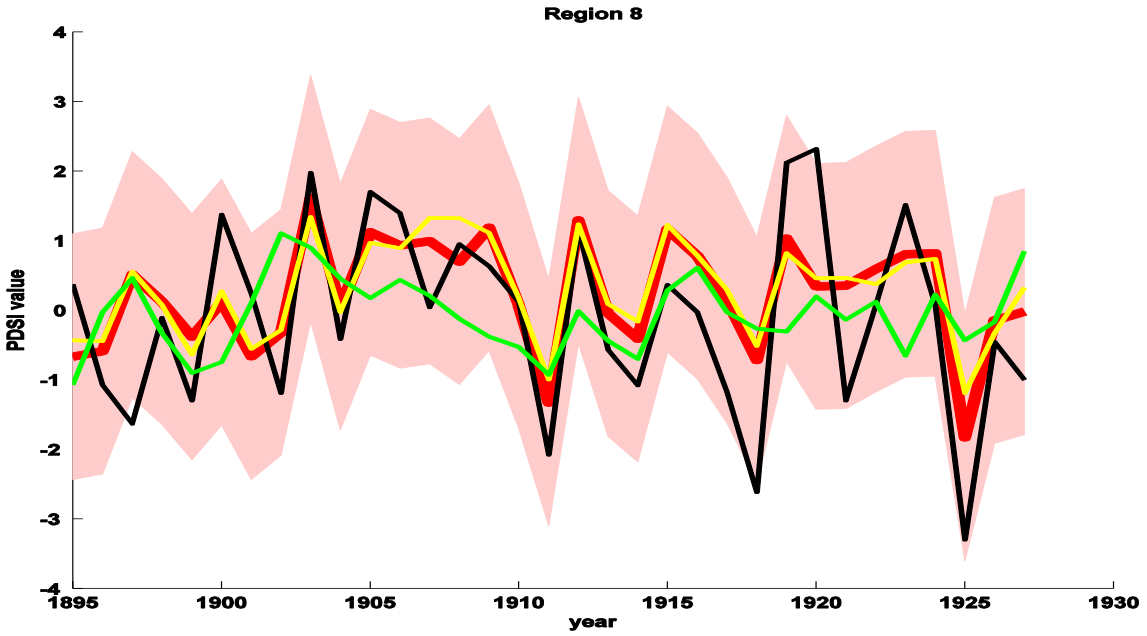

(h)

Figure 4.4 – This series of eight plots ((a) – (h)) shows graphs of the each of the eight regional areal-mean summer PDSI reconstruction series made using the RegEM-ridge method with expanded tree-ring proxy network (Exp. 1) (and their $\pm 2\sigma$ uncertainty bounds), the Zhang et al. (2004) method, and the Cook et al. (1999) method as well as the eight regional areal-mean instrumental series. A legend of graph line colors is given in (a). The full reconstruction period was 1700-1927, but series are shown over the only 1895-1927 validation period.

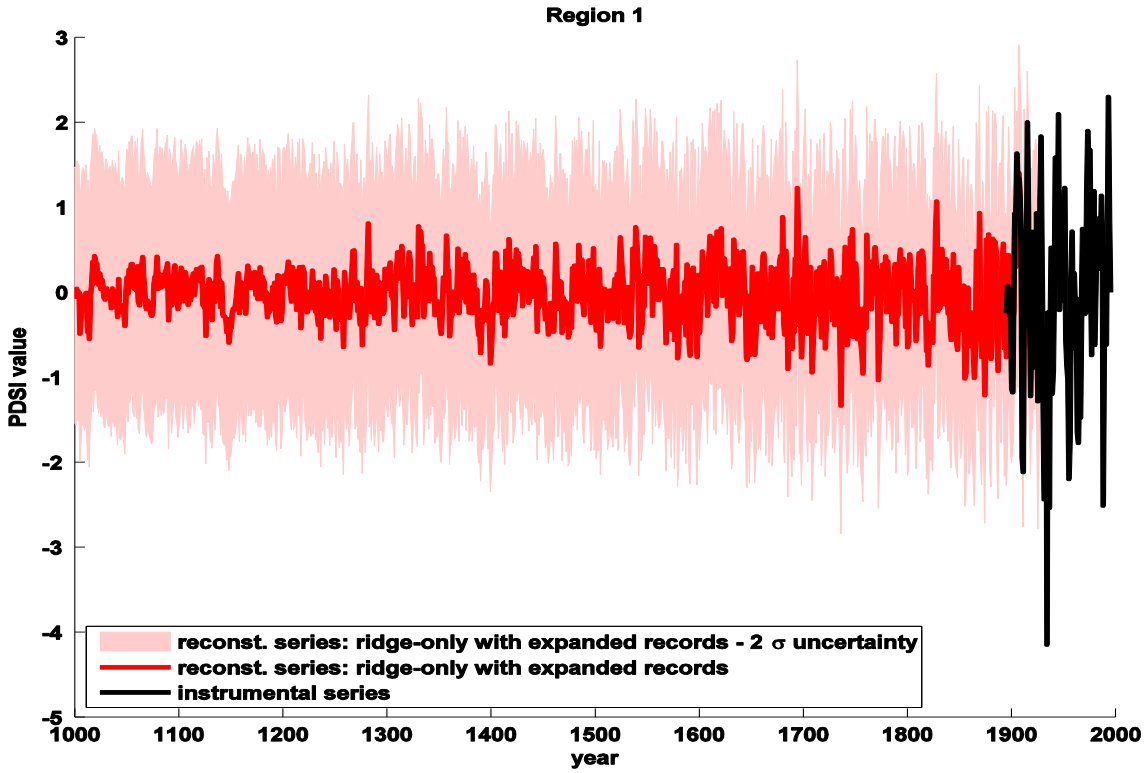

(a) RE = 0.625, CE = 0.617

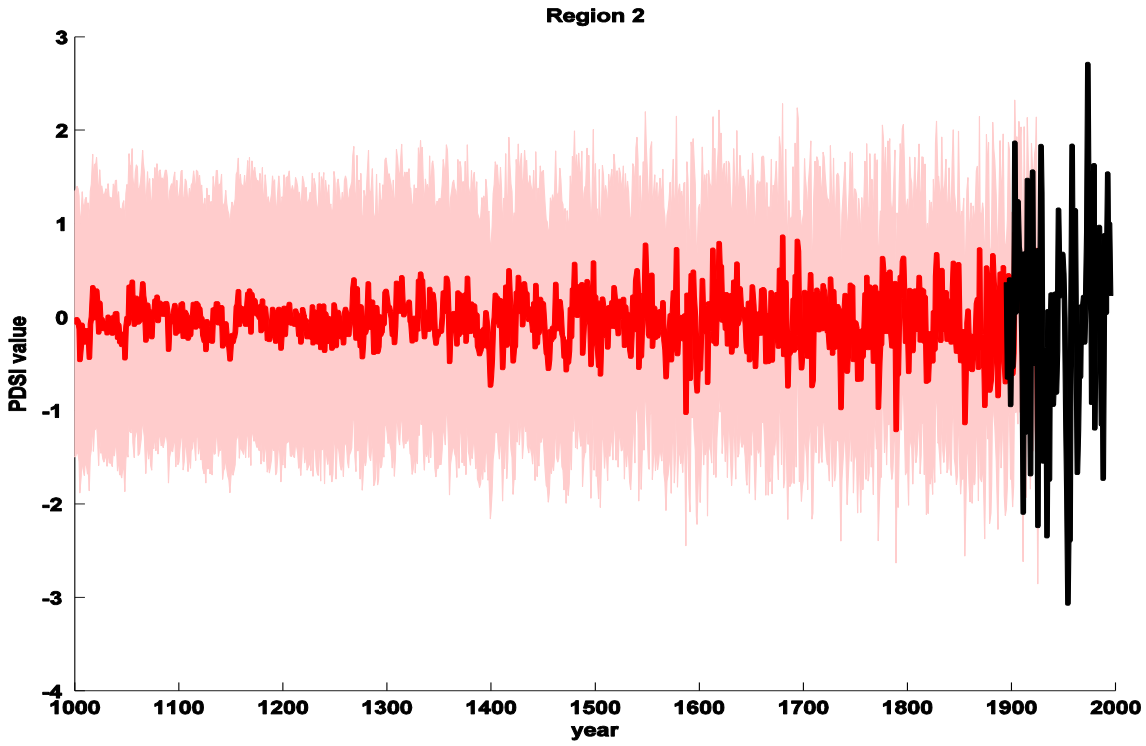

(b) RE = 0.610, CE = 0.603

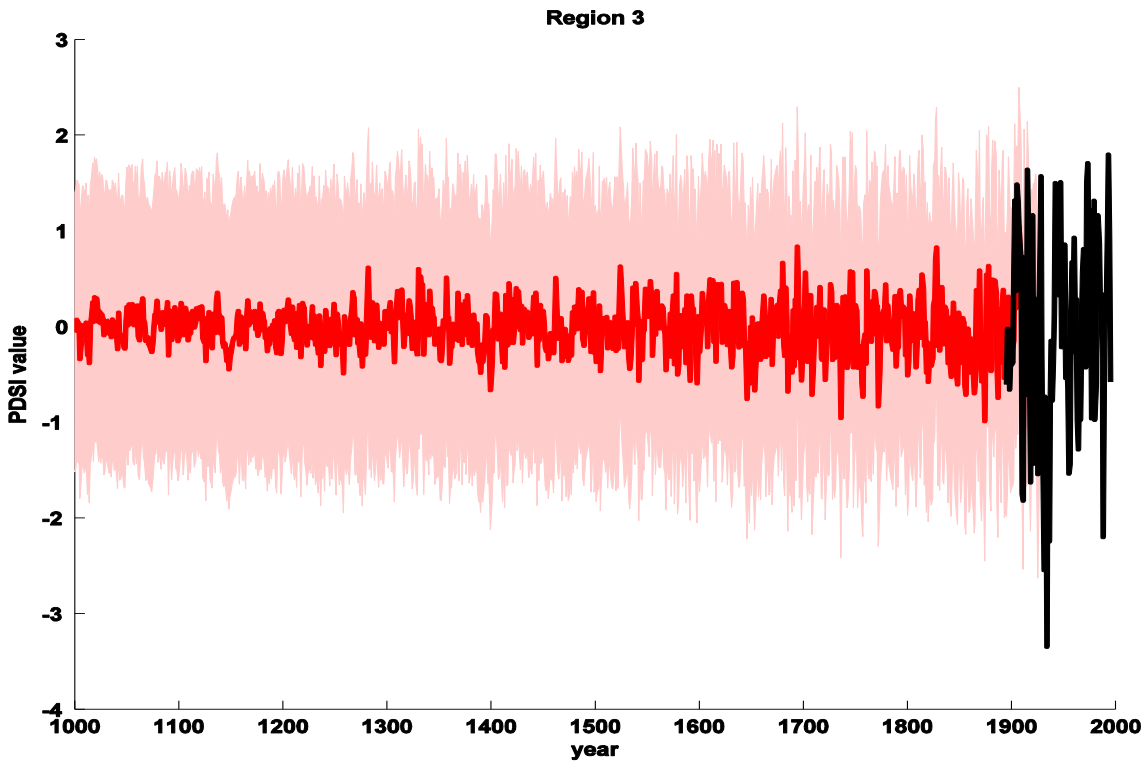

(c) RE = 0.541, CE = 0.538

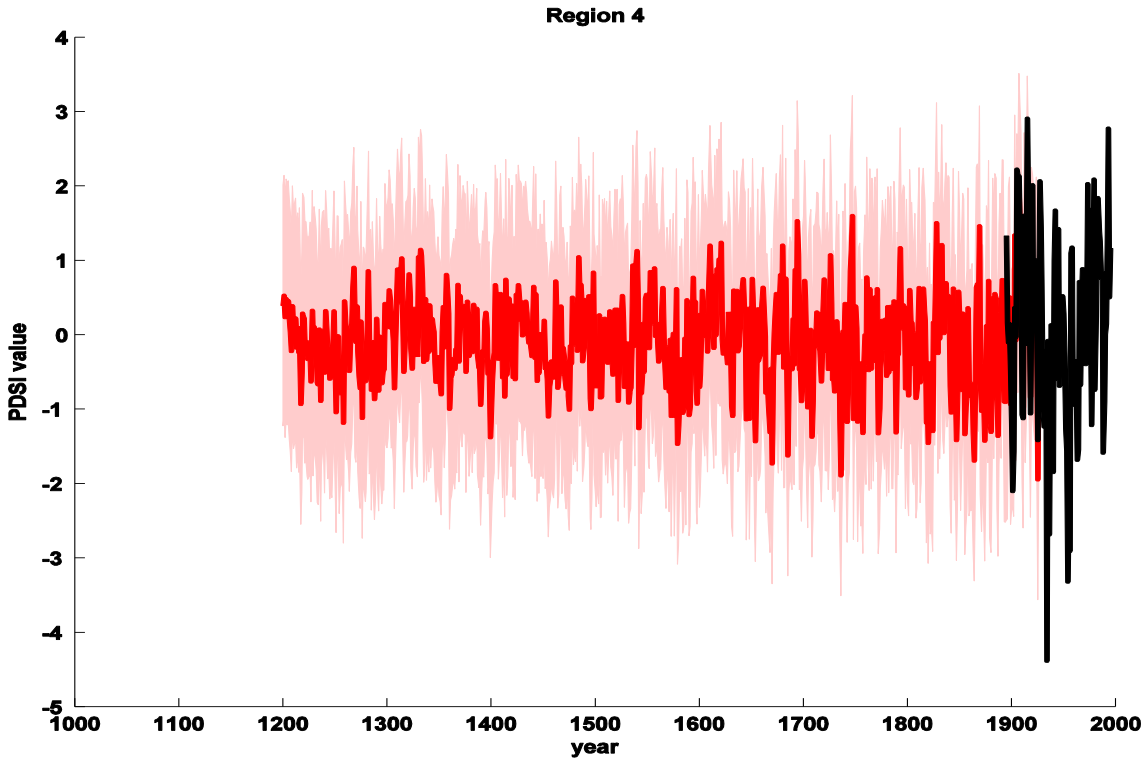

(d) RE = 0.647, CE = 0.572

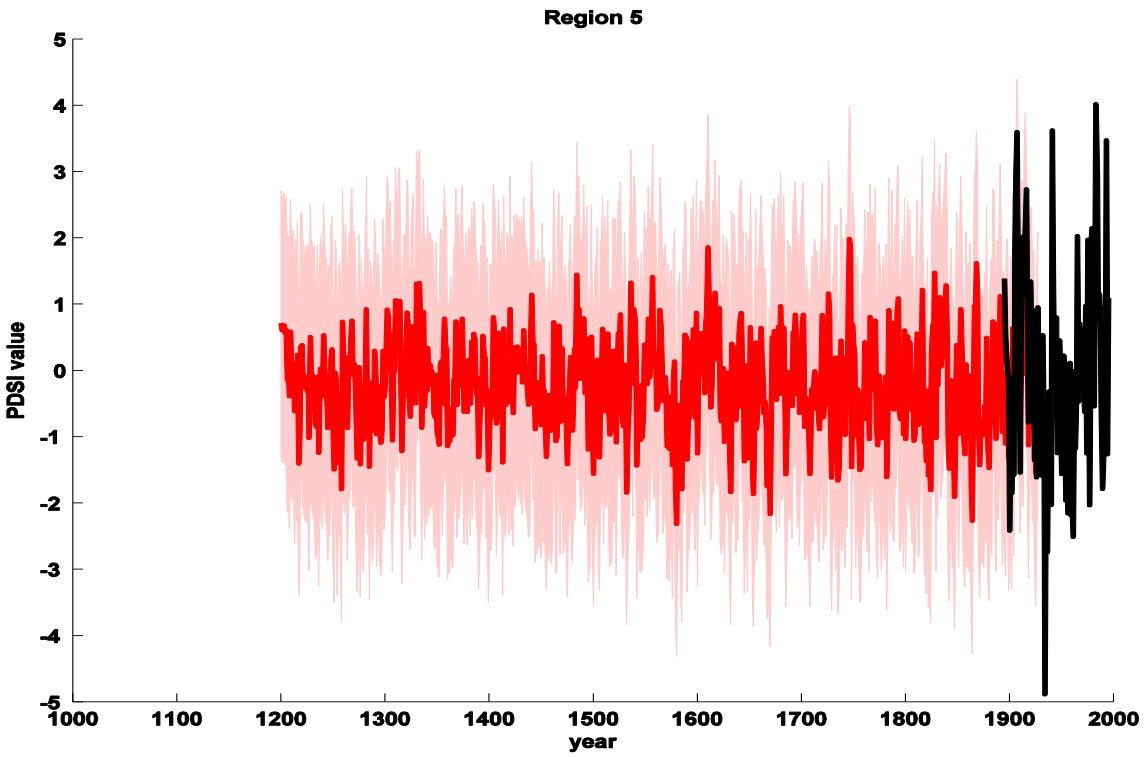

(e) RE = 0.617, CE = 0.539

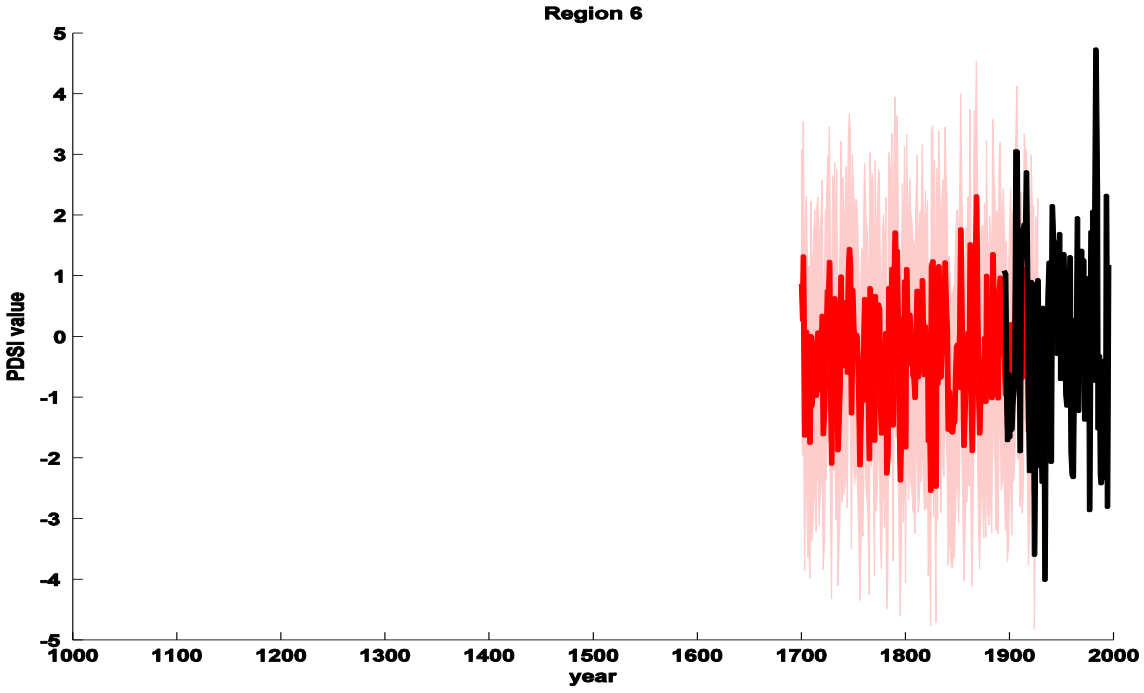

(f) RE = 0.530, CE = 0.509

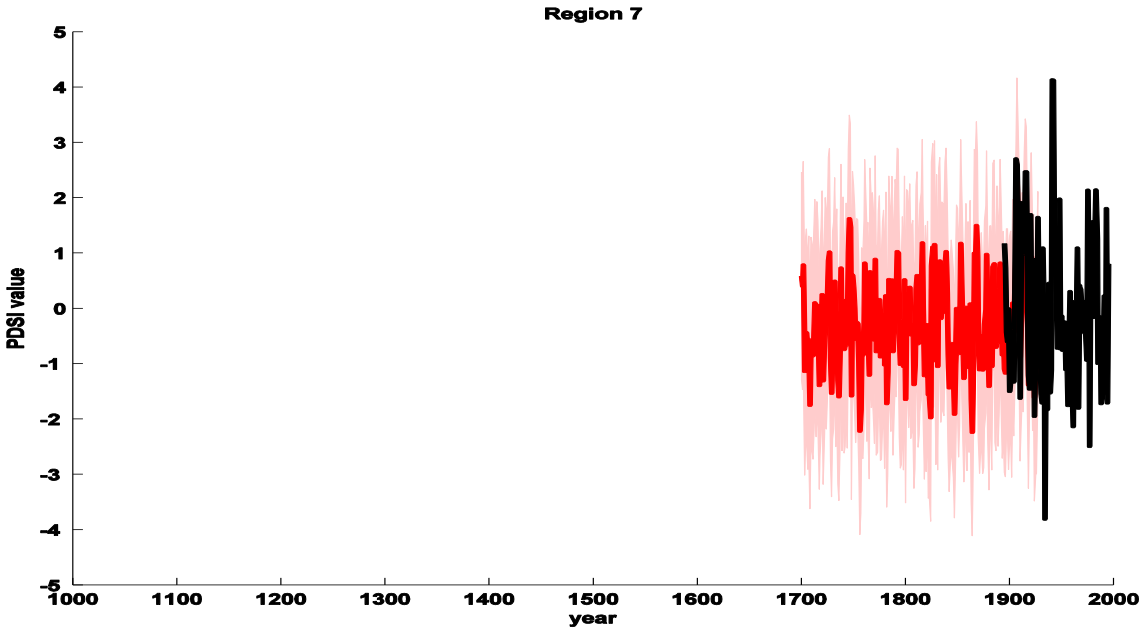

(g) RE = 0.538, CE = 0.469

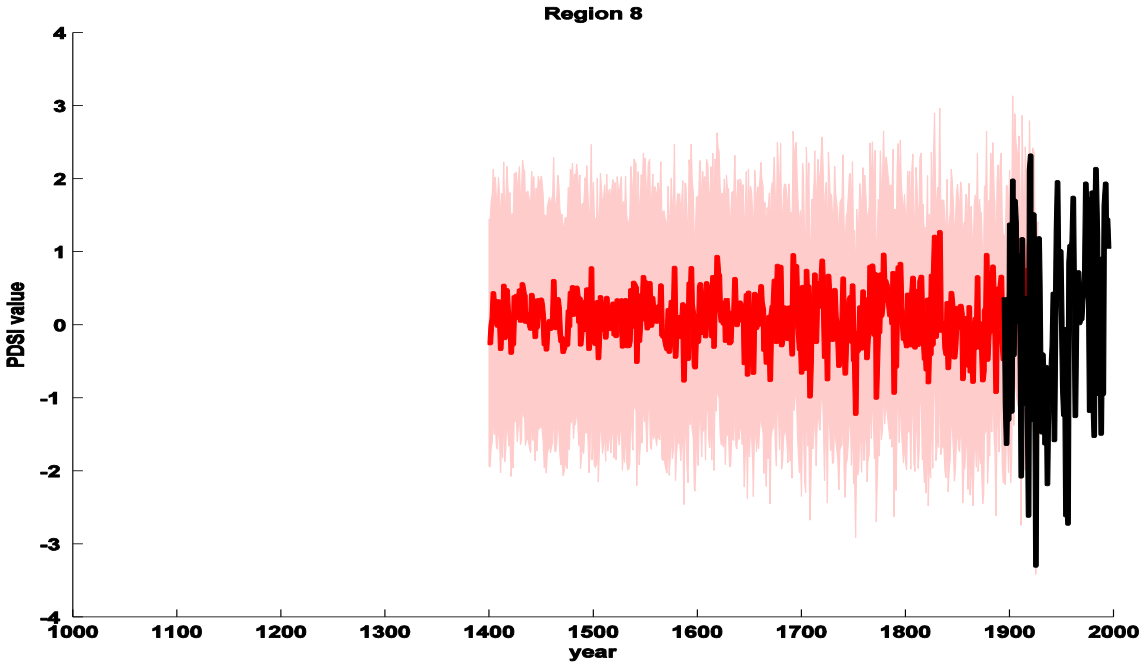

(h) RE = 0.515, CE = 0.509

Figure 4.5 – This series of eight plots ((a) – (h)) shows graphs of the each of the eight regional areal-mean summer PDSI reconstruction series made using the RegEM-ridge method with the expanded tree-ring proxy network (Exp. 1) (and their $\pm 2\sigma$ uncertainty bounds). Noted for each figure are the RE and CE scores for the corresponding reconstruction. All RE and CE P-values are less than 0.05. The reconstructions are shown as far back as a high level of skill remained as explained in more detail in the text. A legend of graph line colors is given in (a).

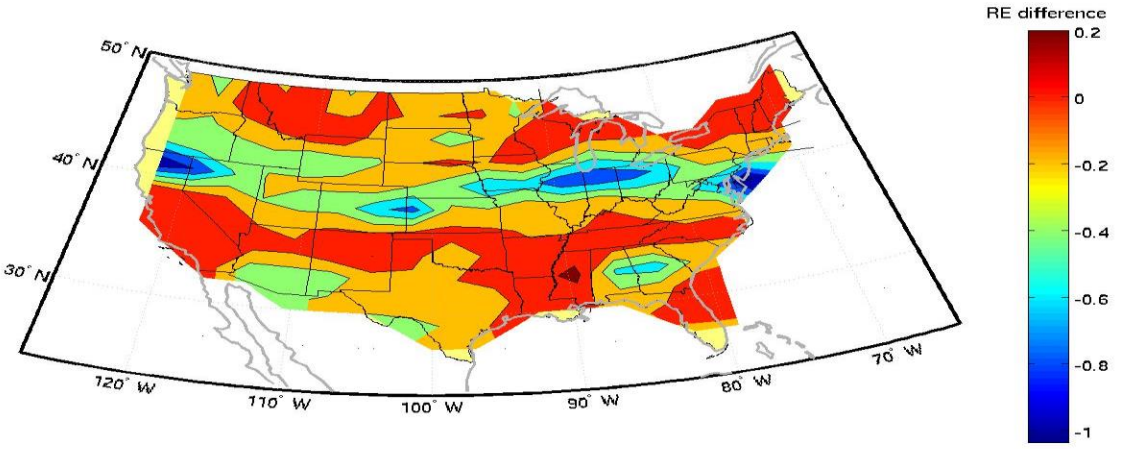

Figure 4.6 – Contour map of the difference in RE scores between those calculated for a 1700-1927 reconstruction of summer PDSI using the hybrid RegEM method with only the tree-ring part of the proxy network (Exp. 2) and those calculated for a reconstruction of the same target using the RegEM-ridge method with expanded tree-ring network (Exp. 2). Scores were calculated for each of 155 grid points and then interpolated. Difference values greater than zero indicate that the hybrid RegEM method had greater reconstructive skill than the RegEM-ridge method – both using the same proxy network.

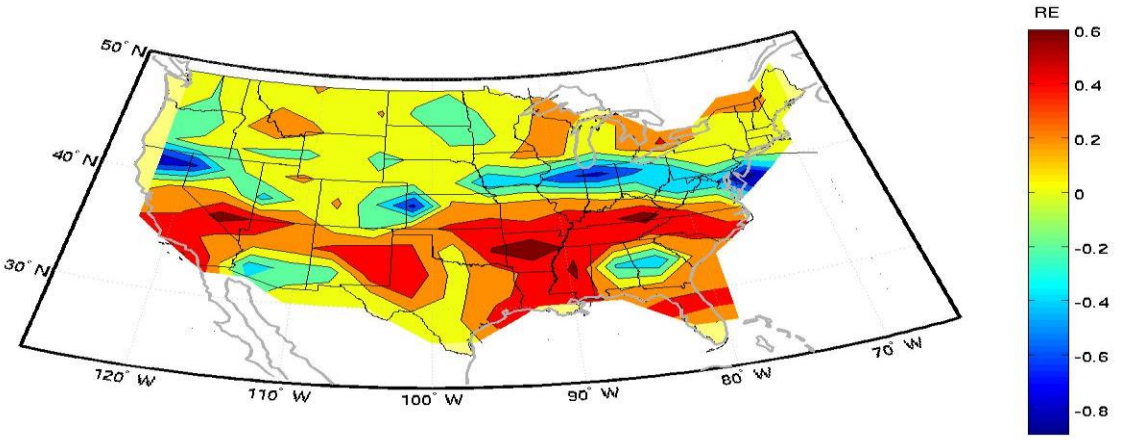

Figure 4.7 – Contour map of RE scores, as calculated for each of 155 grid points and then interpolated, for the 1700-1927 reconstruction of summer PDSI using the hybrid RegEM-ridge method with only the tree-ring part of the proxy network (Exp. 2). Warmer colors indicate greater values of RE score, and cooler colors indicate lesser values. The map of CE scores is qualitatively similar.

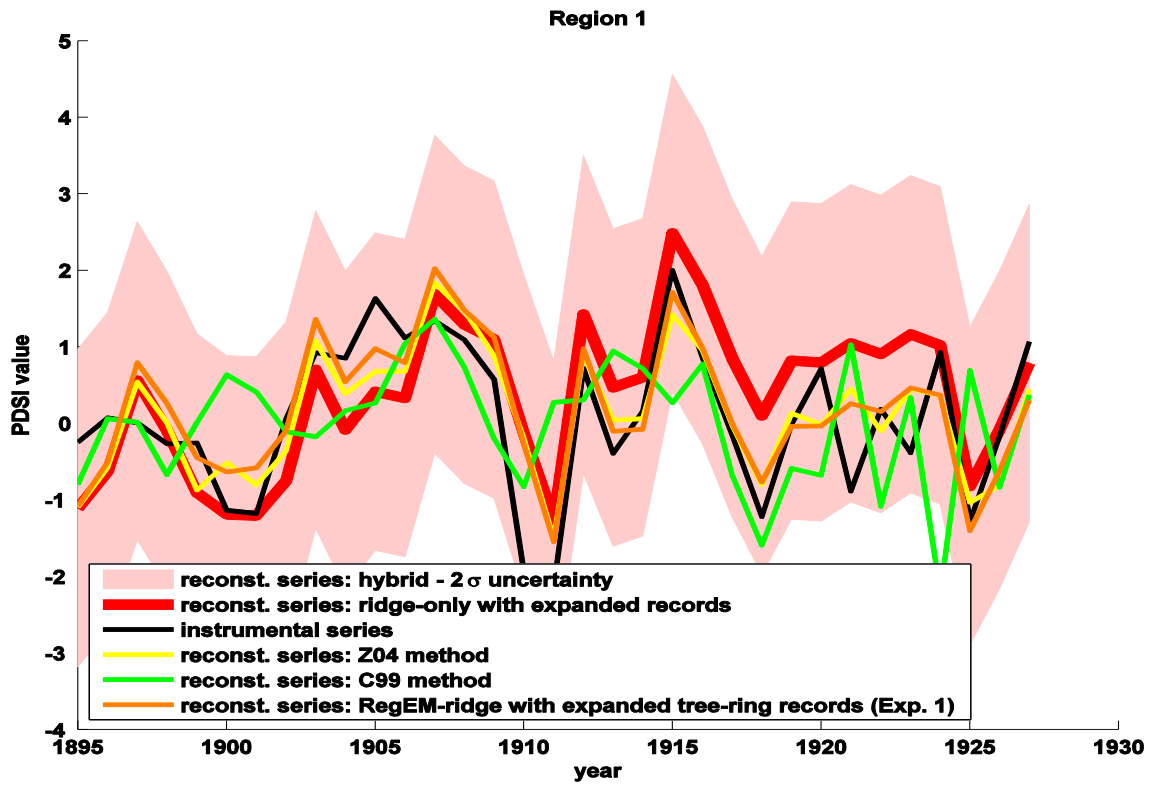
Region 1
PDSI value
year
reconst. series: hybrid - 2 σ uncertainty
reconst. series: ridge-only with expanded records
instrumental series
reconst. series: Z04 method
reconst. series: C99 method
reconst. series: RegEM-ridge with expanded tree-ring records (Exp. 1)

(a)

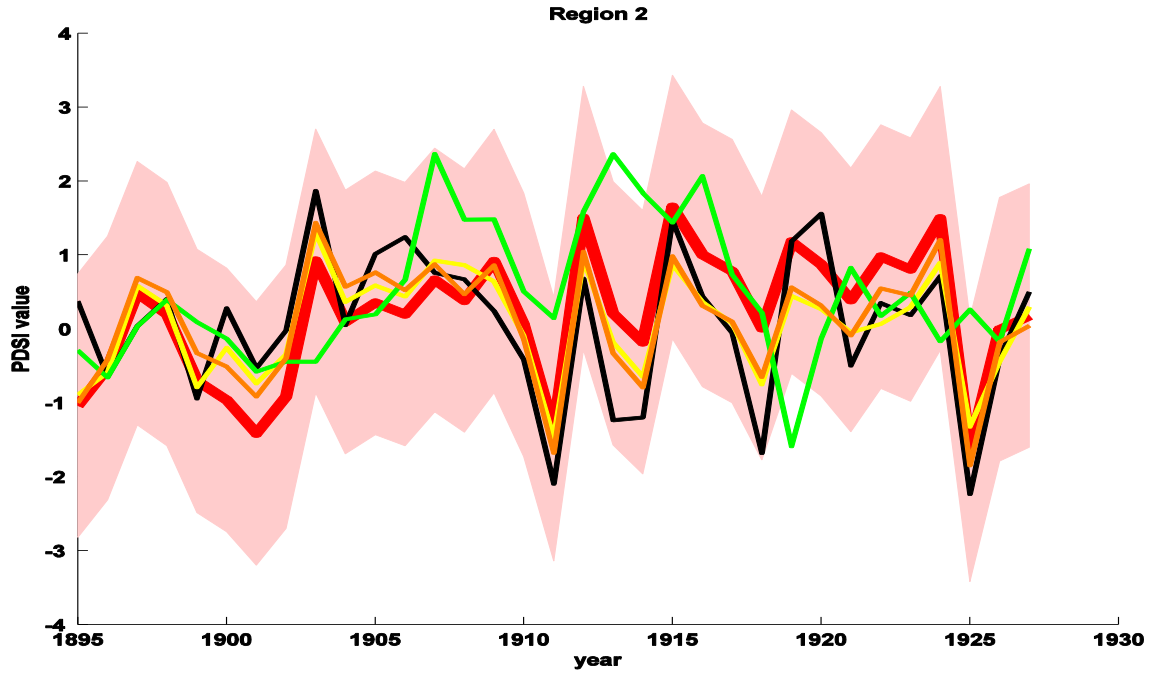
Region 2
PDSI value
year

(b)

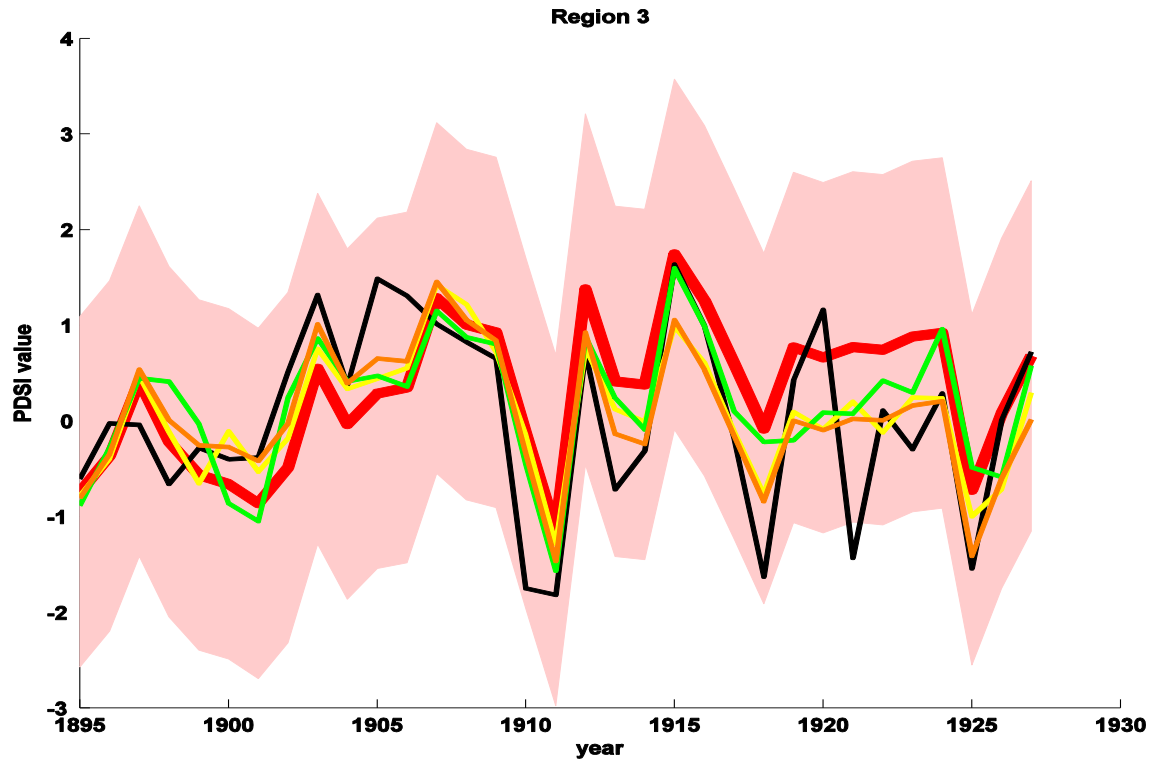
Region 3
PDSI value
year
4
3
2
1
0
-1
-2
-3
1895
1900
1905
1910
1915
1920
1925
1930

(c)

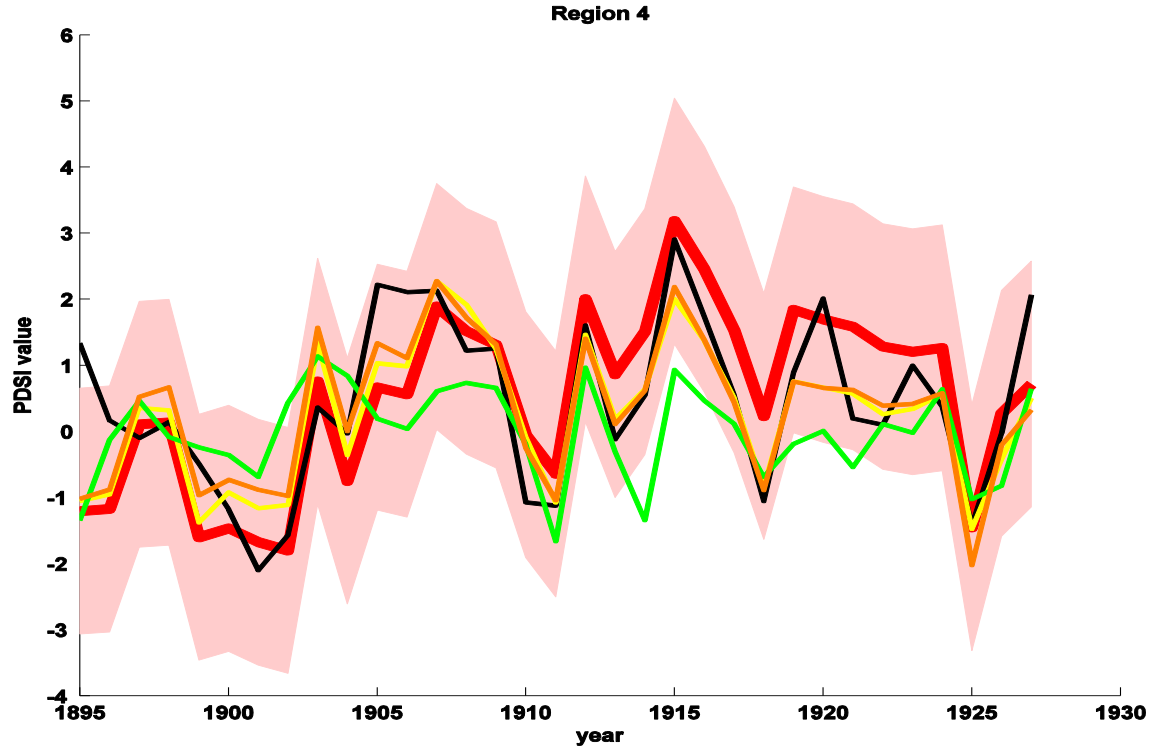
Region 4
PDSI value
year
6
5
4
3
2
1
0
-1
-2
-3
-4
1895
1900
1905
1910
1915
1920
1925
1930

(d)

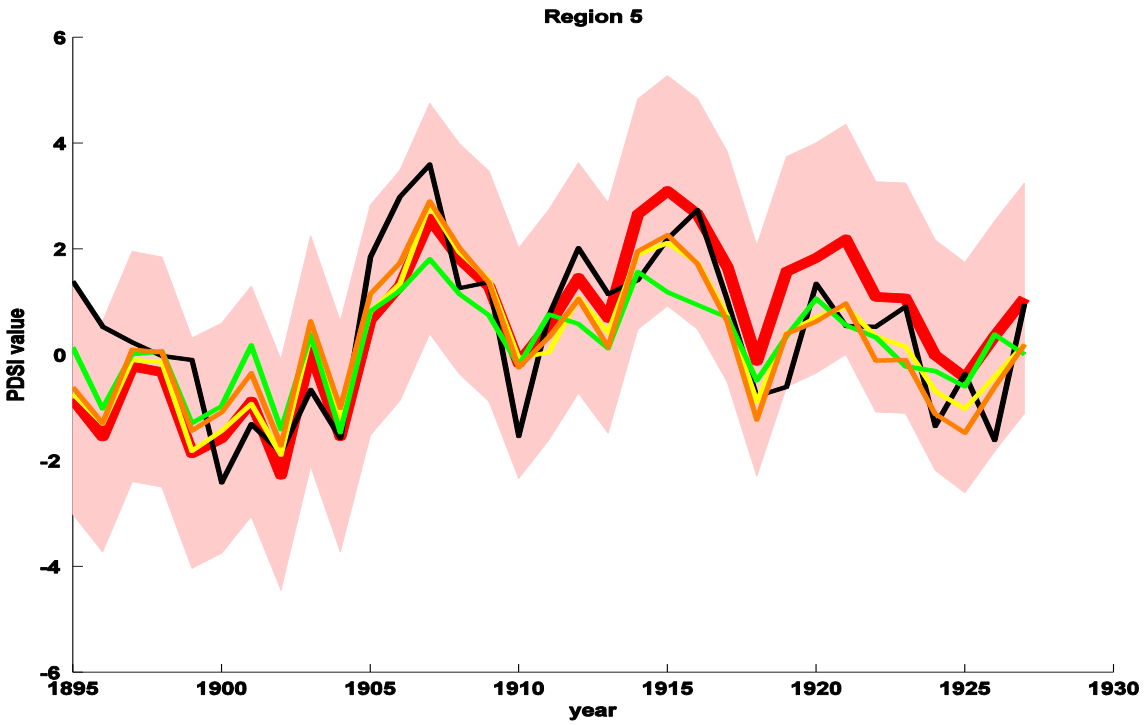
Region 5
PDSI value
year
6
4
2
0
-2
-4
-6
1895
1900
1905
1910
1915
1920
1925
1930

(e)

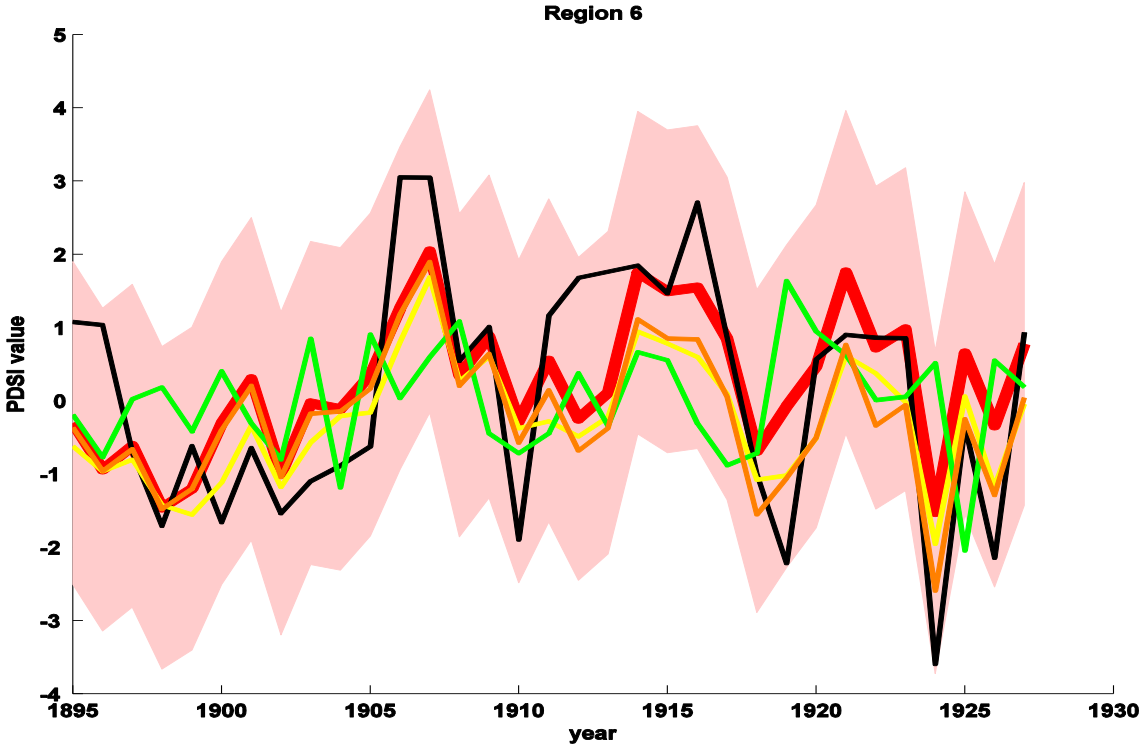
Region 6
PDSI value
year
5
4
3
2
1
0
-1
-2
-3
-4
1895
1900
1905
1910
1915
1920
1925
1930

(f)

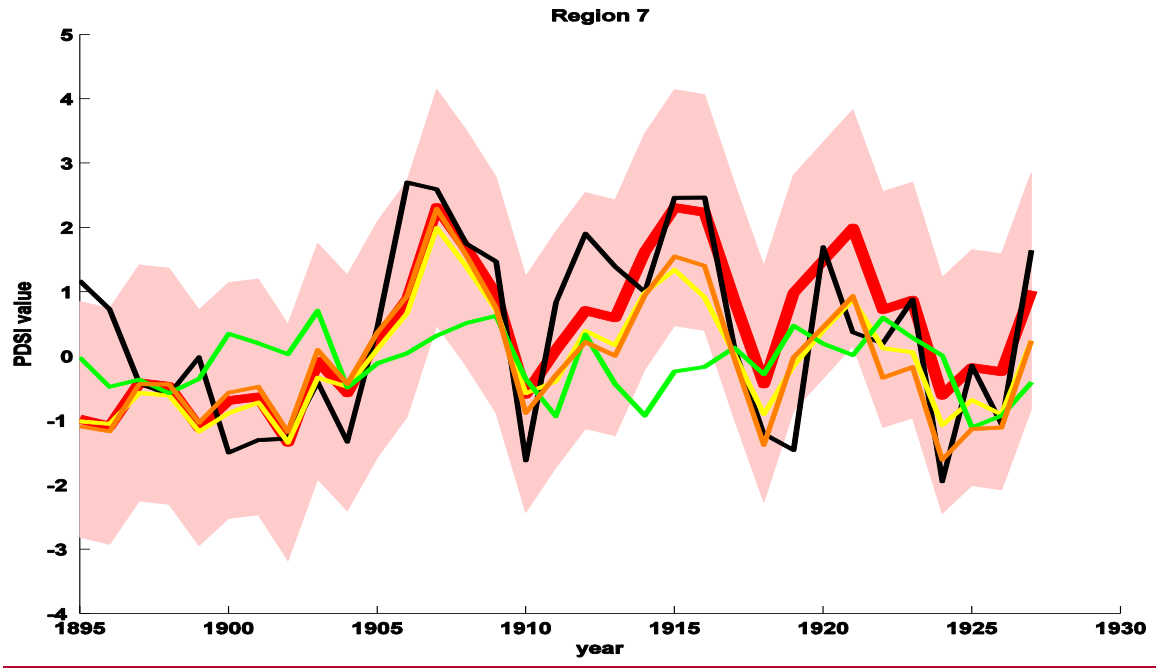

(g)

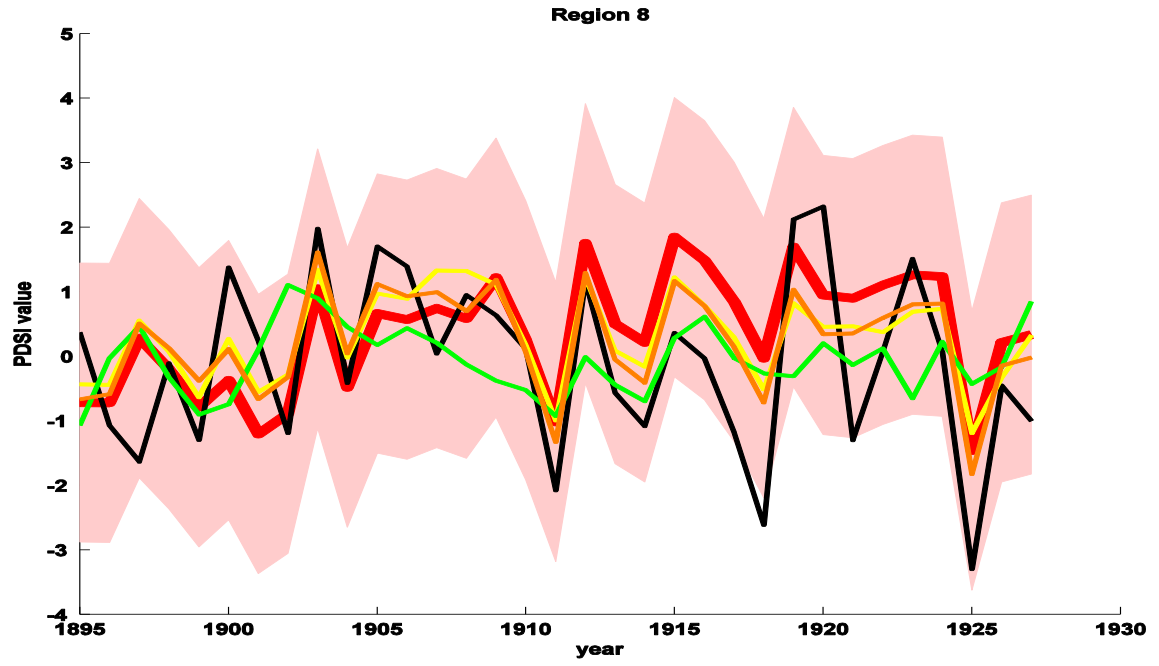

(h)

Figure 4.8 – This series of eight plots ((a) – (h)) shows graphs of the each of the eight regional areal-mean reconstruction series made using the hybrid RegEM method with only the tree-ring part of the proxy network (Exp. 2)(and their $\pm 2\sigma$ uncertainty bounds), the RegEM-ridge method with expanded tree-ring proxy network, the Zhang et al. (2004) method, and the Cook et al. (1999) method as well as the eight regional areal-mean instrumental series. A legend of graph line colors is given in (a). The full reconstruction period was 1700-1927, but series are shown over the only 1895-1927 validation period.

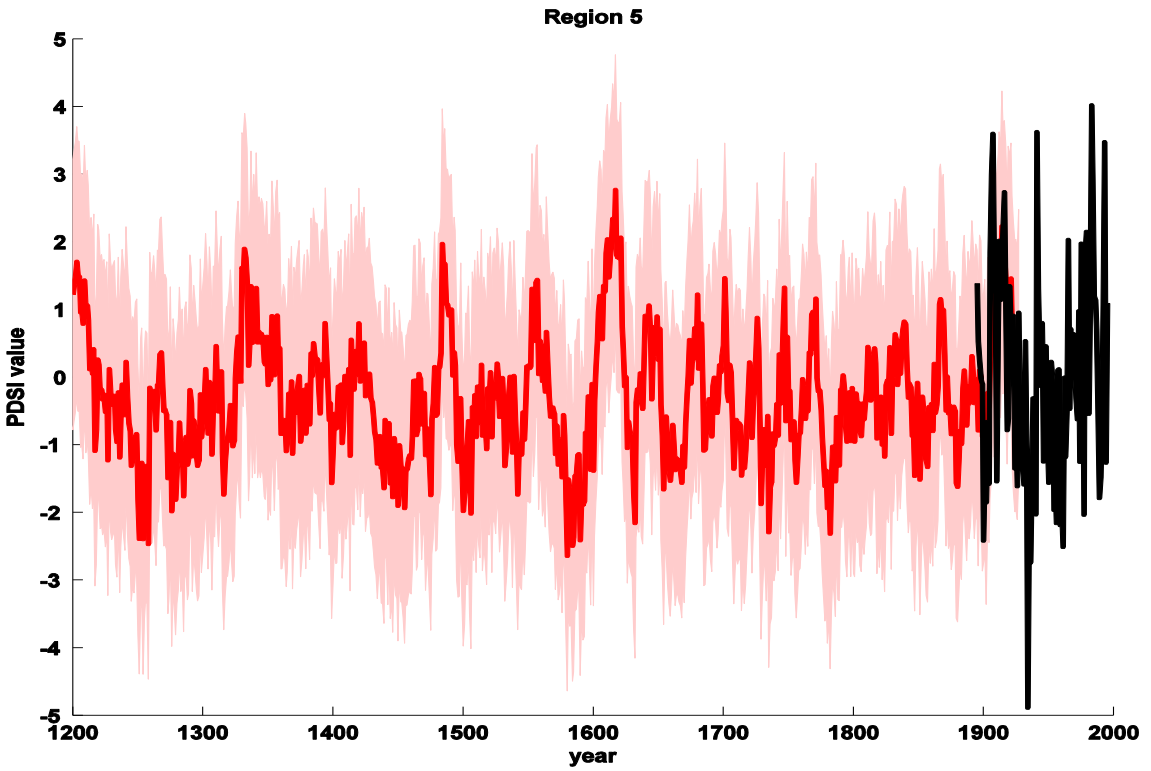

RE = 0.478, CE = 0.371, RE P-value = 0.000, CE P-value = 0.000

Figure 4.9 – This plot shows the graph (in red) of the Region 5 regional areal-mean 1200-1927 summer PDSI reconstruction series (and its $\pm 2\sigma$ uncertainty bounds), made using the hybrid RegEM method with only the tree-ring part of the proxy network (Exp. 2), that exhibited a moderate or high level of skill as explained in more detail in the text. Noted are the RE and CE scores for the reconstruction and their P-values. Also shown is the graph (in black) of the Region 5 1895-1995 instrumental series.

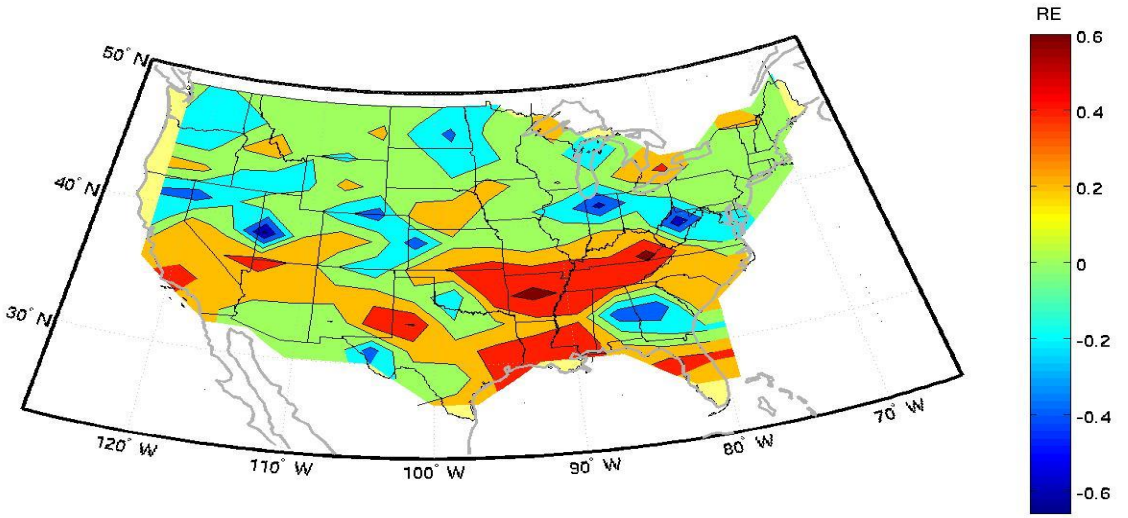

Figure 4.10 – Contour map of RE scores, as calculated for each of 155 grid points and then interpolated, for the 1700-1927 reconstruction of summer PDSI using the hybrid RegEM method with only the tree-ring part of the proxy network used in the ridge sub-reconstruction and the full proxy network used in the TTLS sub-reconstruction (Exp. 3). Warmer colors indicate greater values of RE, and cooler colors indicate lower values of CE. The map of CE scores is qualitatively similar.

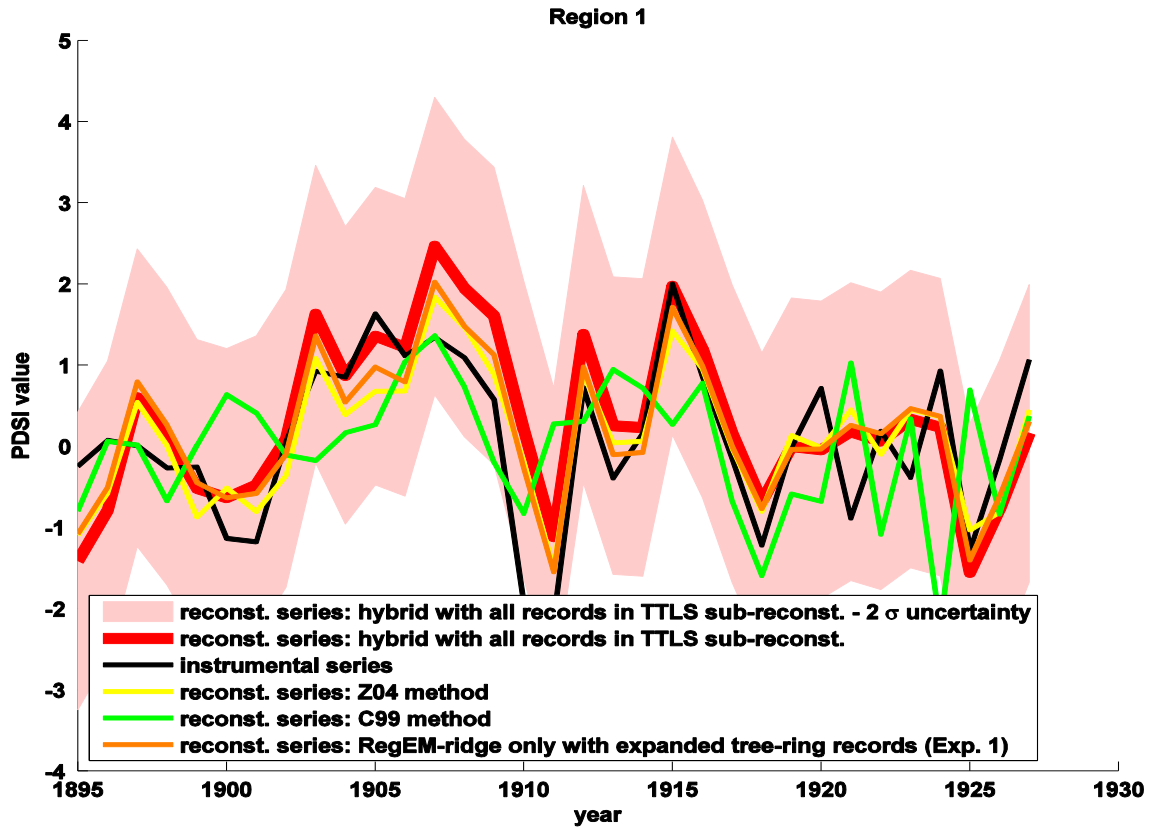
Region 1
PDSI value
year
reconst. series: hybrid with all records in TTLS sub-reconst. - 2 σ uncertainty
reconst. series: hybrid with all records in TTLS sub-reconst.
instrumental series
reconst. series: Z04 method
reconst. series: C99 method
reconst. series: RegEM-ridge only with expanded tree-ring records (Exp. 1)

(a)

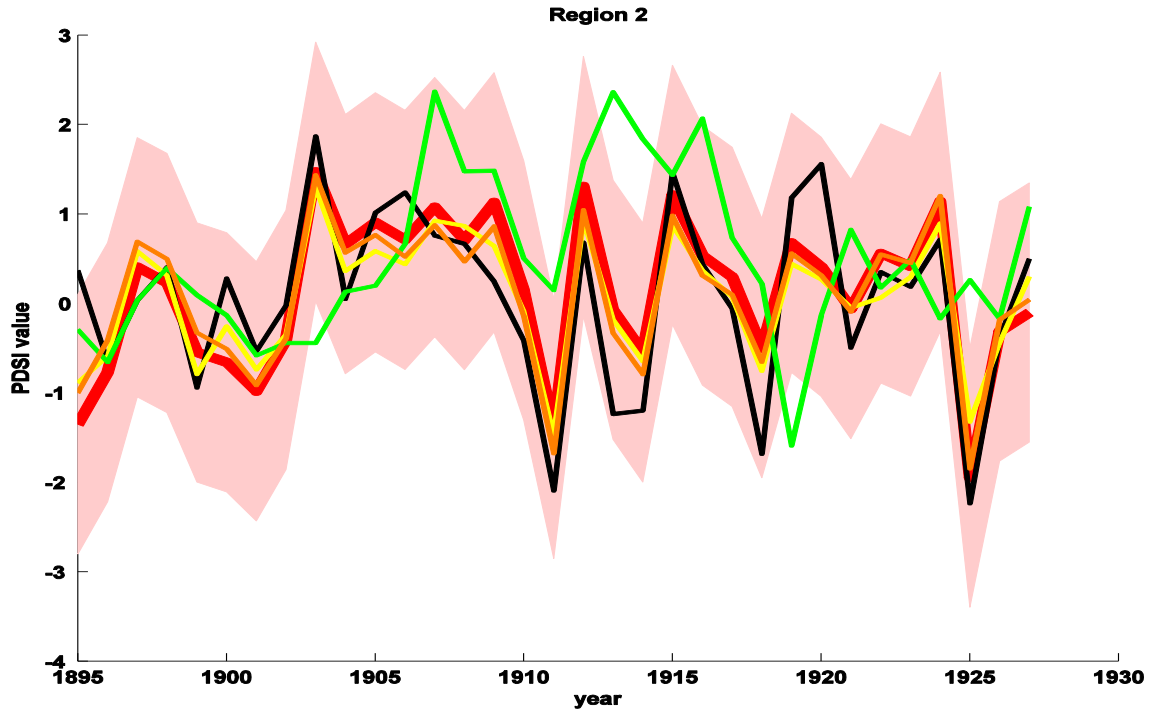
Region 2
PDSI value
year

(b)

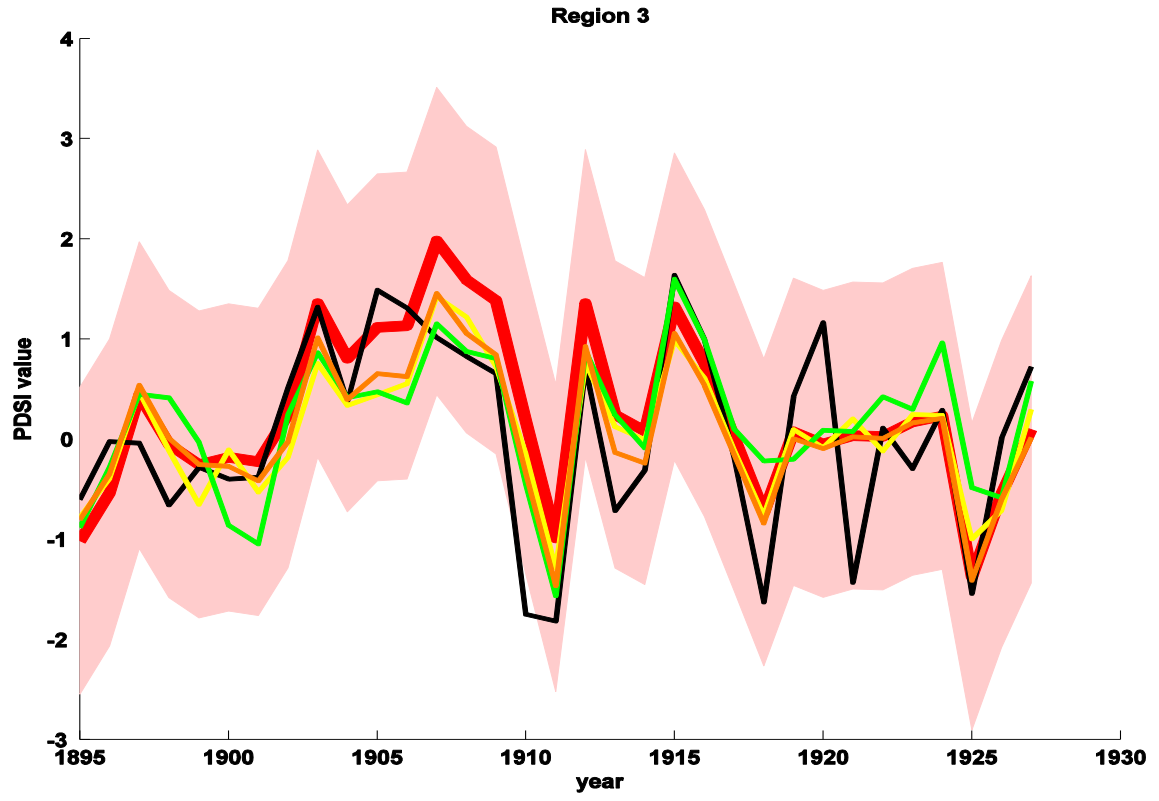
Region 3
PDSI value
year
4
3
2
1
0
-1
-2
-3
1895
1900
1905
1910
1915
1920
1925
1930

(c)

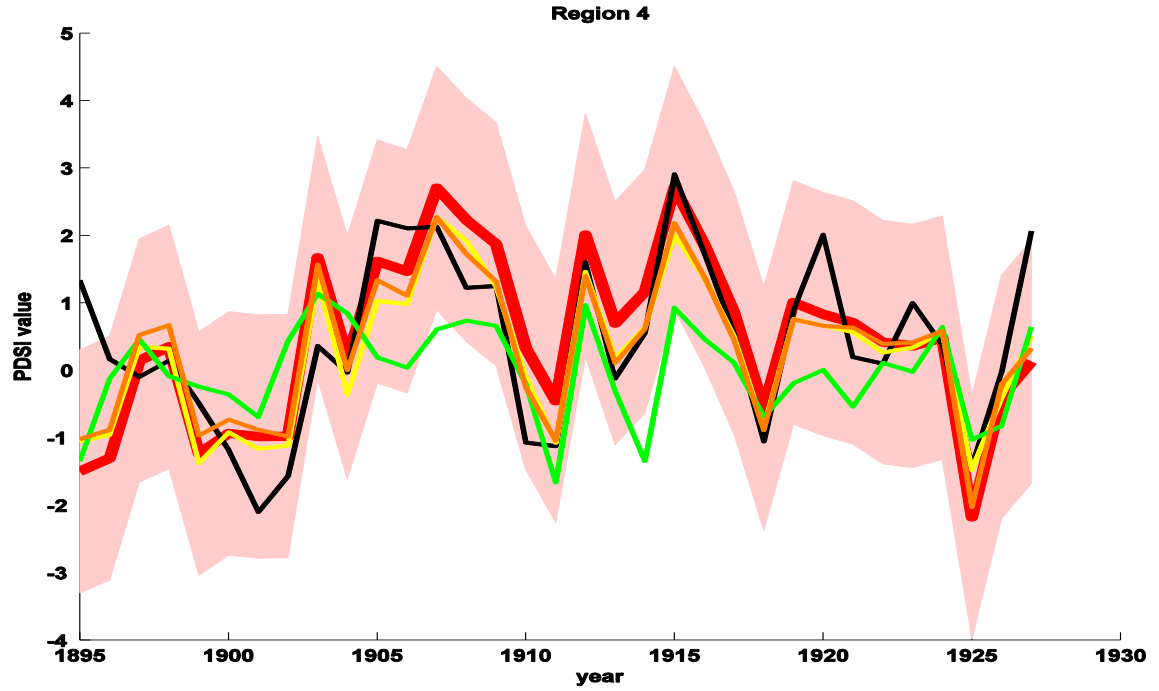
Region 4
PDSI value
year
5
4
3
2
1
0
-1
-2
-3
-4
1895
1900
1905
1910
1915
1920
1925
1930

(d)

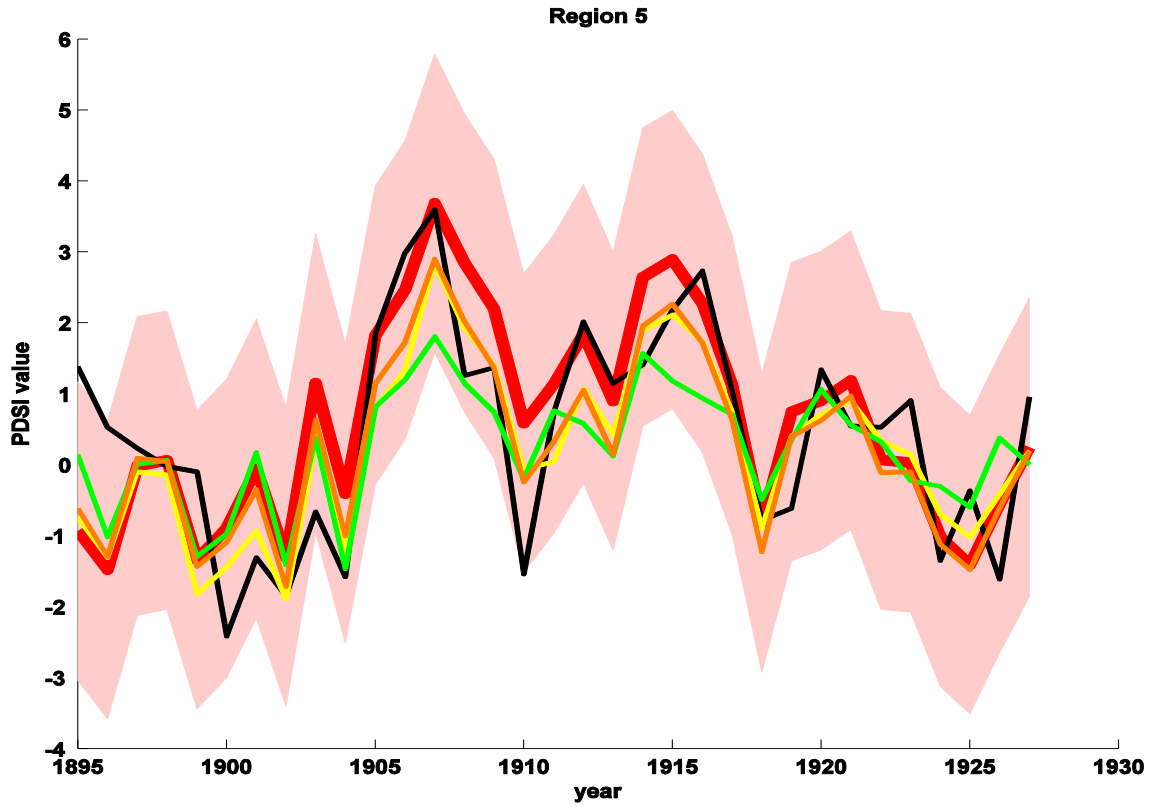
Region 5
PDSI value
year
6
5
4
3
2
1
0
-1
-2
-3
-4
1895
1900
1905
1910
1915
1920
1925
1930

(e)

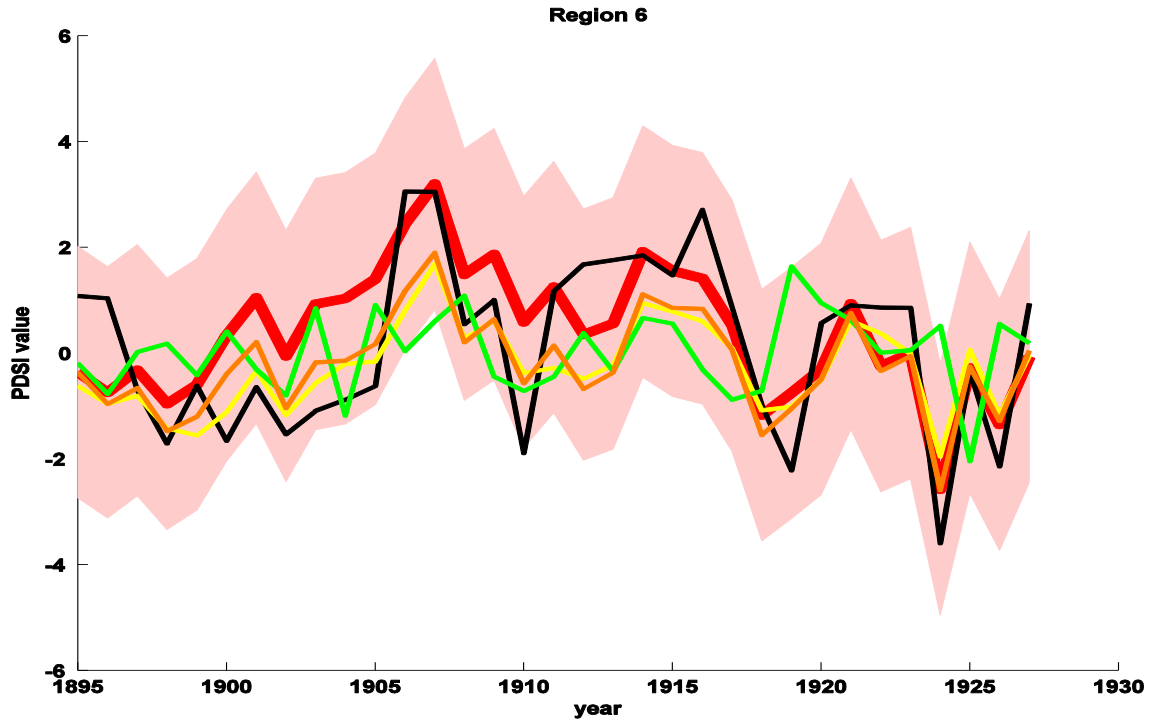
Region 6
PDSI value
year
6
4
2
0
-2
-4
-6
1895
1900
1905
1910
1915
1920
1925
1930

(f)

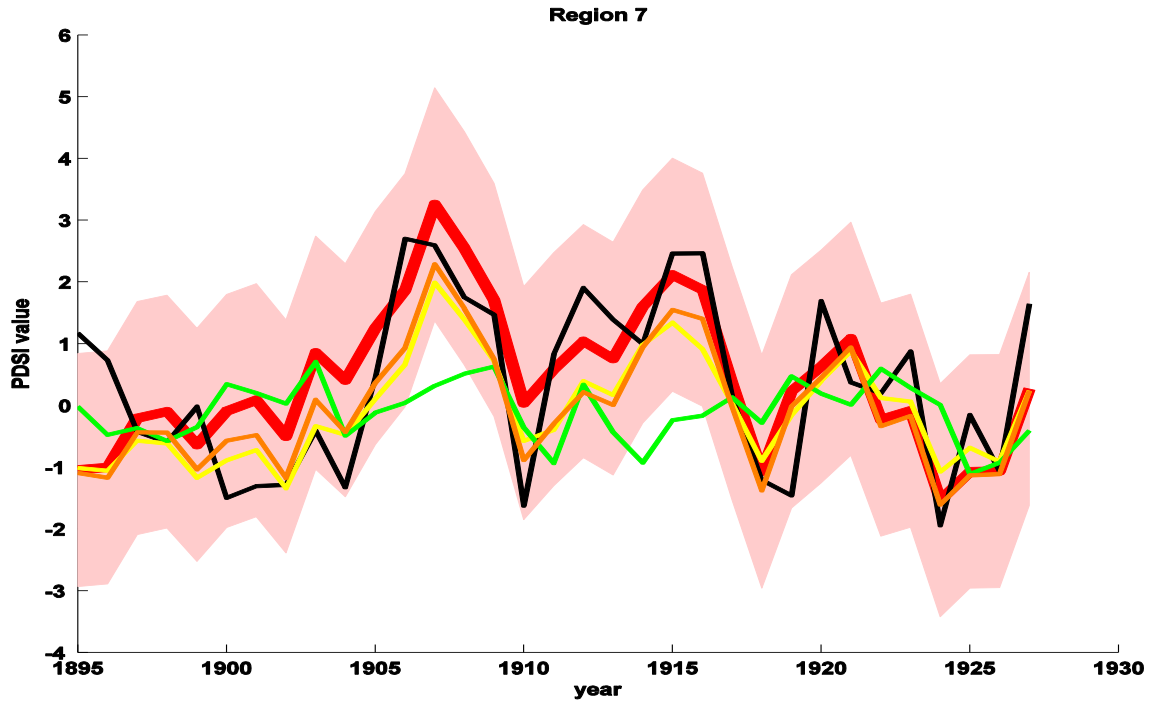

(g)

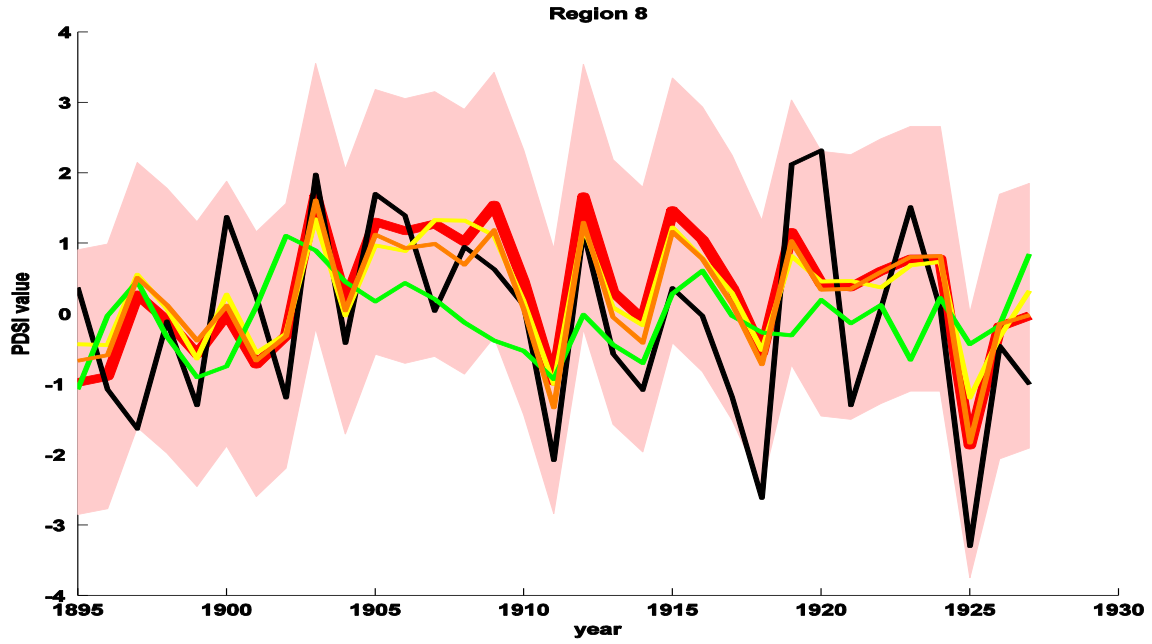

(h)

Figure 4.11 -- This series of eight plots ((a) – (h)) shows graphs of the each of the eight regional areal-mean summer PDSI reconstruction series made using the hybrid RegEM method with only the tree-ring part of the network used in the ridge sub-reconstruction and the full proxy network used in the TTLS sub-reconstruction (Exp. 3) (and their $\pm 2\sigma$ uncertainty bounds), the RegEM-ridge method with expanded tree-ring proxy network (Exp. 1), the Zhang et al. (2004) method, and the Cook et al. (1999) method as well as the eight regional areal-mean instrumental series. A legend of graph line colors is given in (a). The full reconstruction period was 1700-1927, but series are shown over the only 1895-1927 validation period.

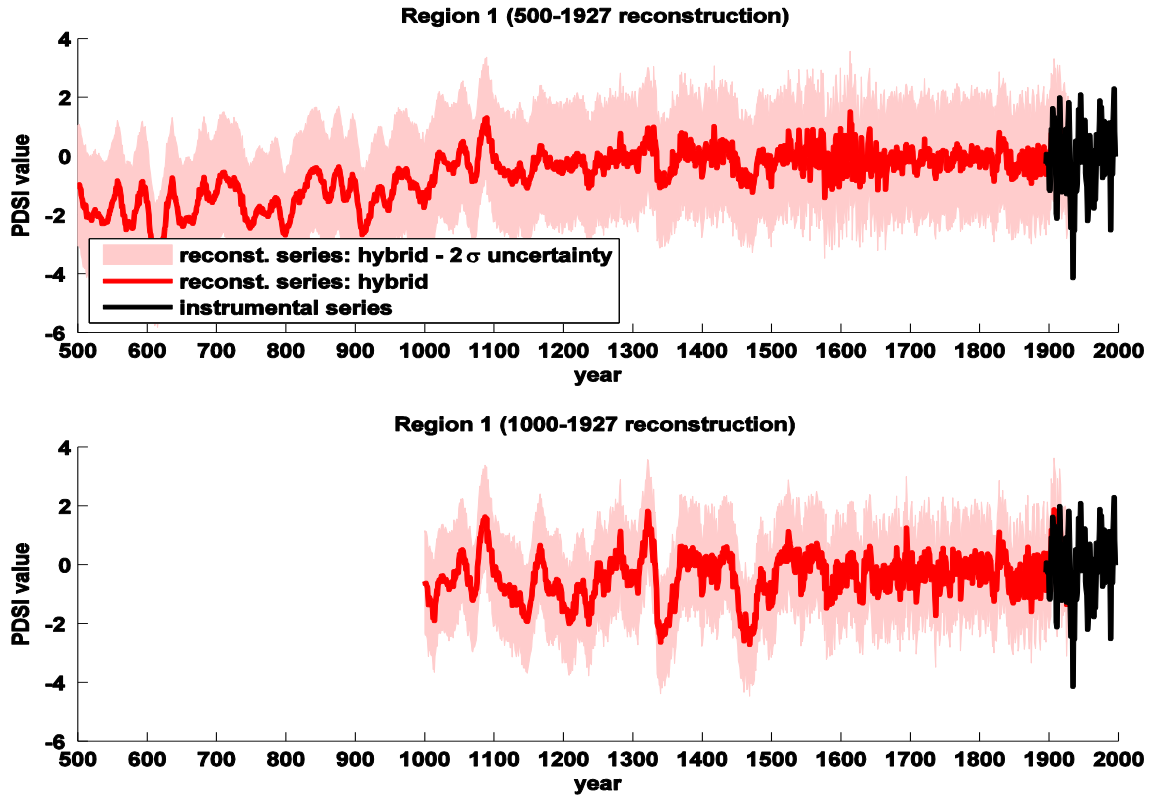

(**a**) 500-1927 reconstruction: RE = 0.307, CE = 0.293 | 1000-1927 reconstruction: RE = 0.497, CE = 0.487

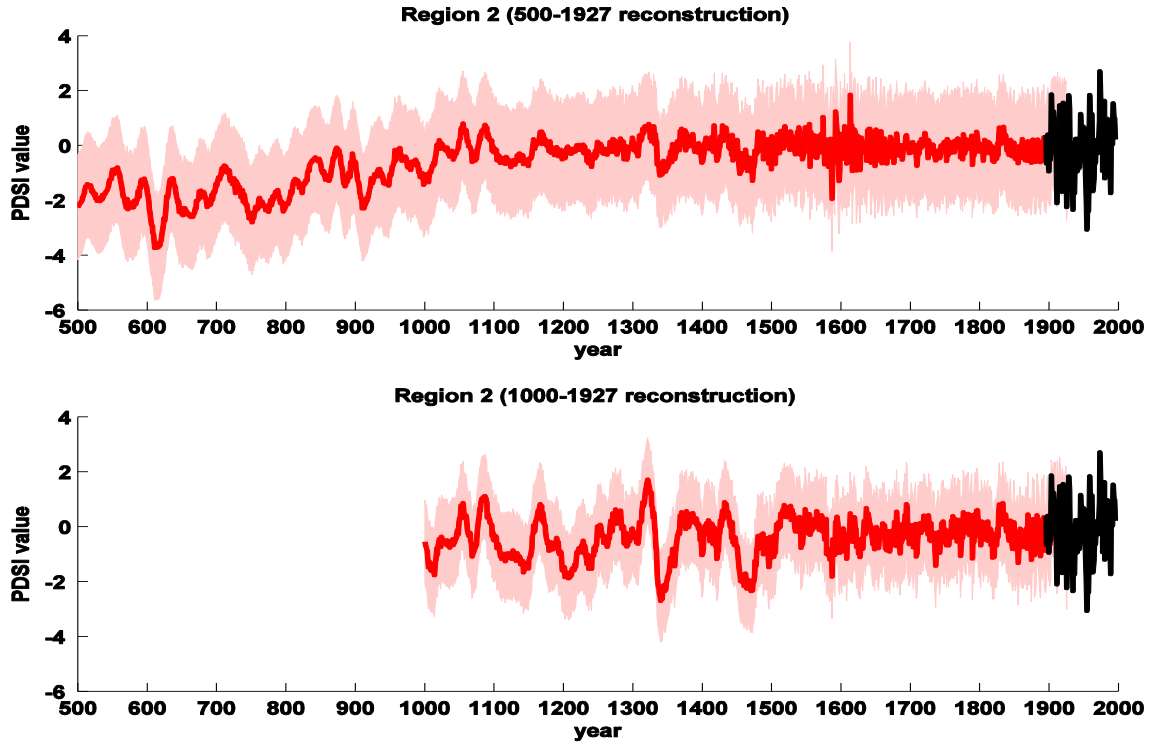

(b) 500-1927 reconstruction: RE = 0.298, CE = 0.286 | 1000-1927 reconstruction: RE = 0.556, CE = 0.549

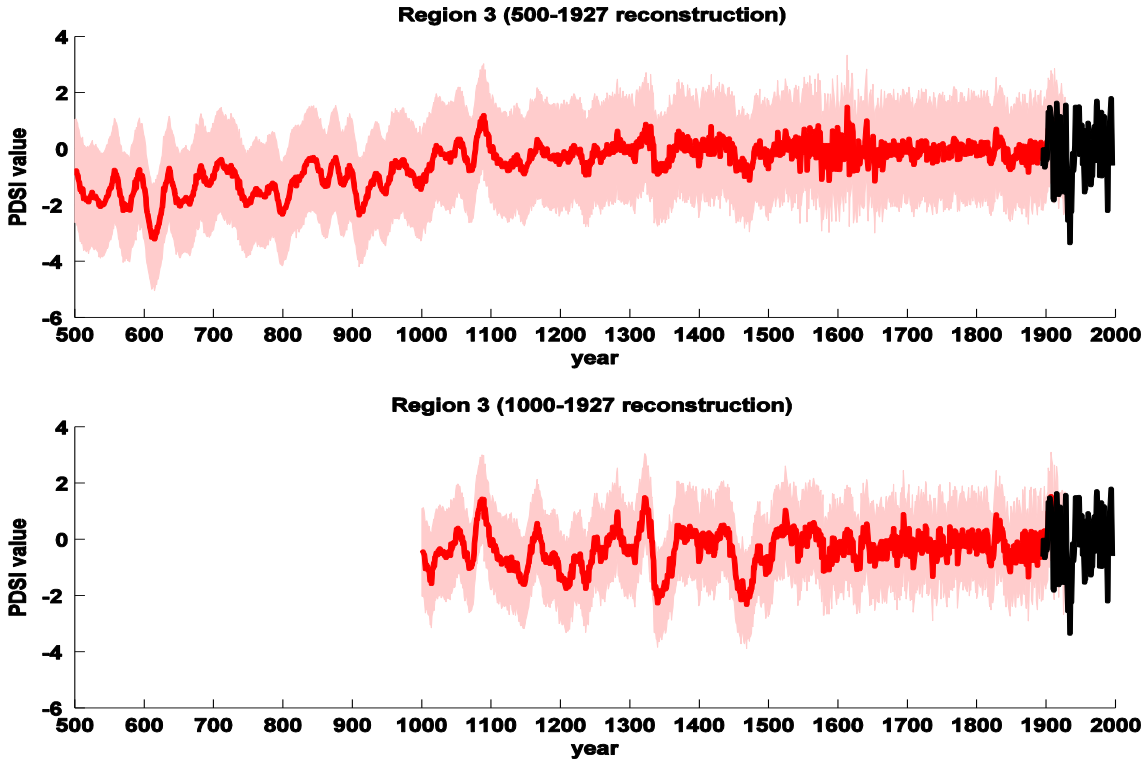

(c) 500-1927 reconstruction: RE = 0.276, CE = 0.271 | 1000-1927 reconstruction: RE = 0.475, CE = 0.471

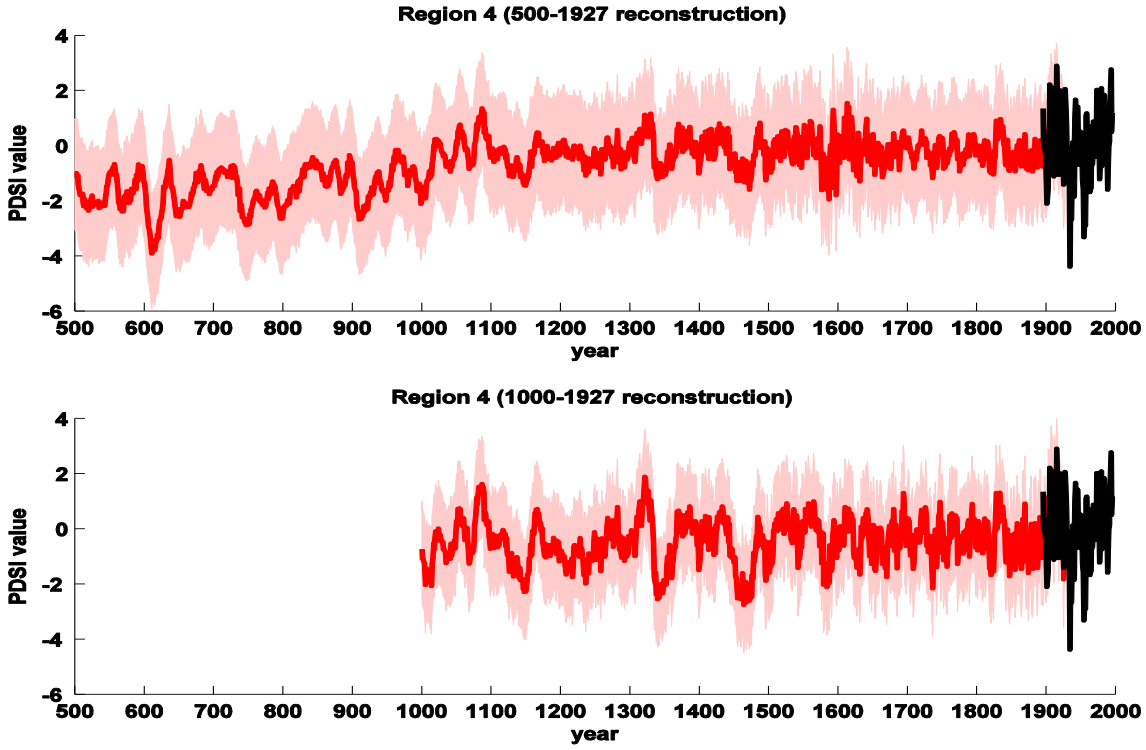

(d) 500-1927 reconstruction: RE = 0.455, CE = 0.338 | 1000-1927 reconstruction: RE = 0.595, CE = 0.508

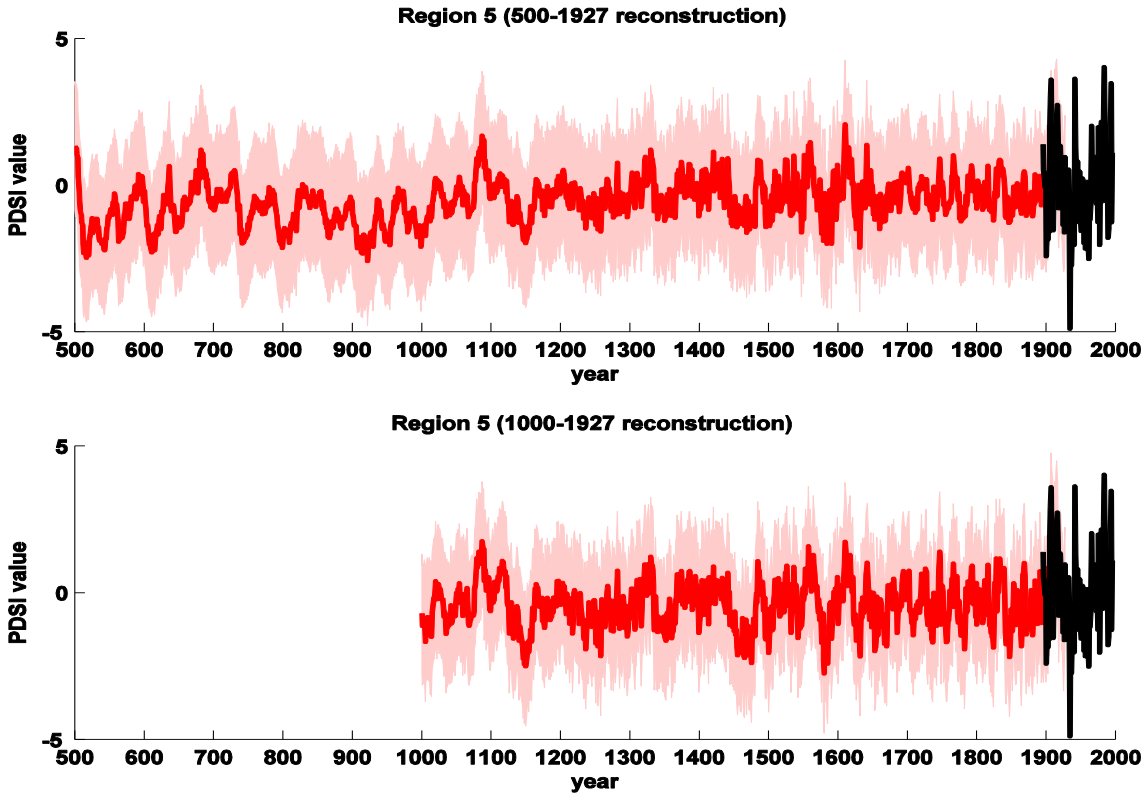

(e) 500-1927 reconstruction: RE = 0.537, CE = 0.443 | 1000-1927 reconstruction: RE = 0.605, CE = 0.524

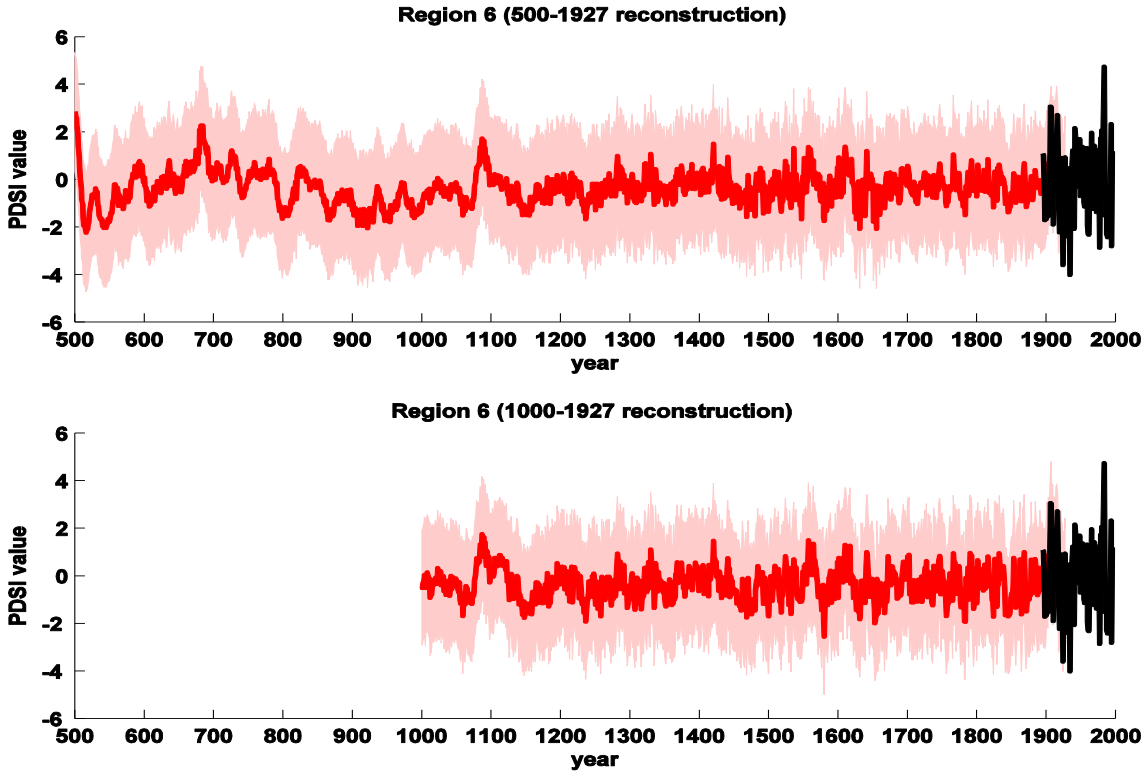

(f) 500-1927 reconstruction: RE = 0.409, CE = 0.379 | 1000-1927 reconstruction: RE = 0.442, CE = 0.415

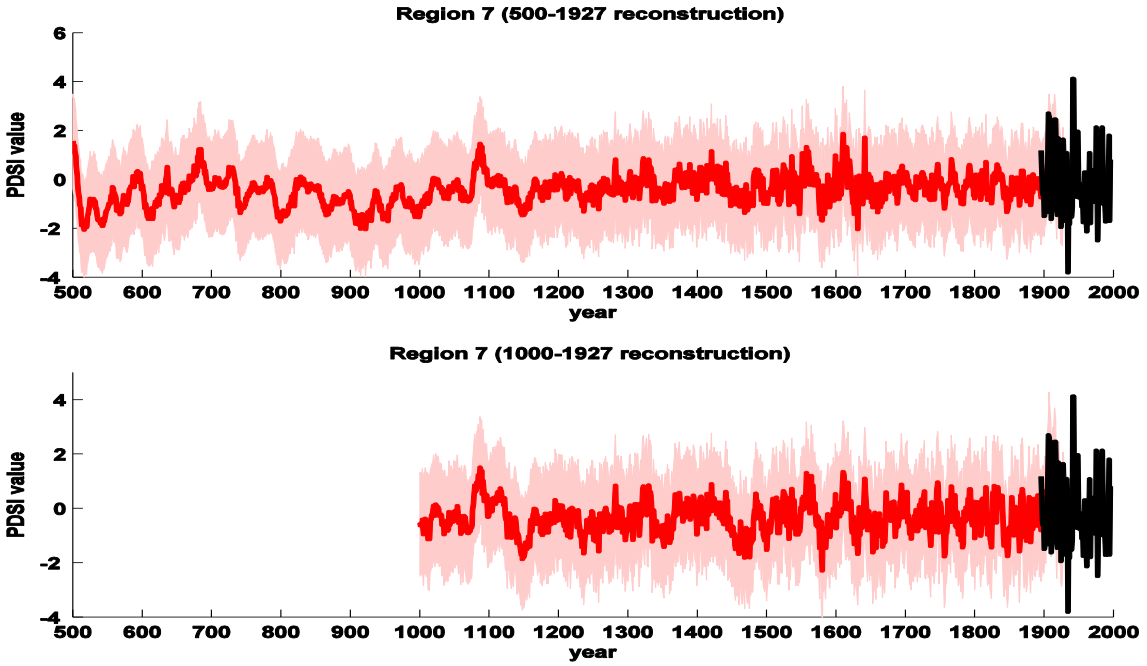

(g) 500-1927 reconstruction: RE = 0.511, CE = 0.438 | 1000-1927 reconstruction: RE = 0.541, CE = 0.472

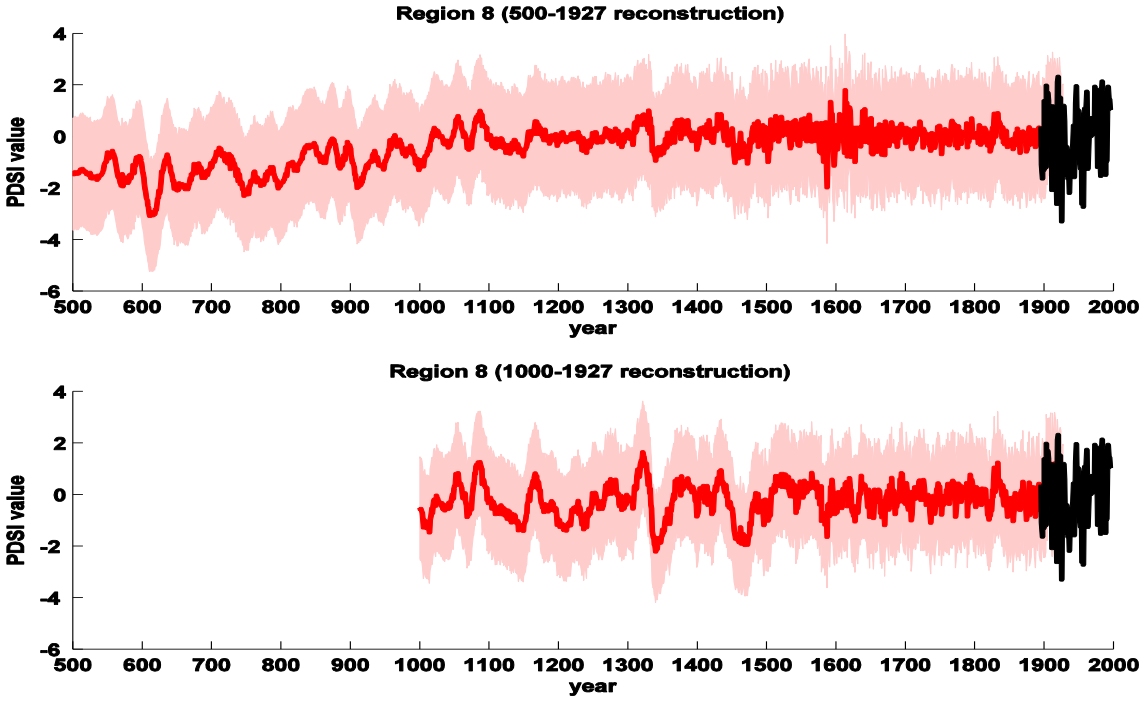

(h) 500-1927 reconstruction: RE = 0.298, CE = 0.286 | 1000-1927 reconstruction: RE = 0.556, CE = 0.549

Figure 4.12 – This series of eight plots ((a) – (h)) shows graphs of the eight regional areal-mean 500-1927 (top panel) and 1000-1927 (bottom panel) summer PDSI reconstruction series (and their $\pm 2\sigma$ uncertainty bounds) made using the hybrid RegEM method with only the tree-ring part of the proxy network in the ridge sub-reconstruction and the full proxy network in the TTLS sub-reconstruction (Exp. 3). In black are the instrumental series from 1895-1995. Noted for each figure are the RE and CE scores for the corresponding reconstruction. The P-values for all RE and CE scores are 0 to three decimal places.

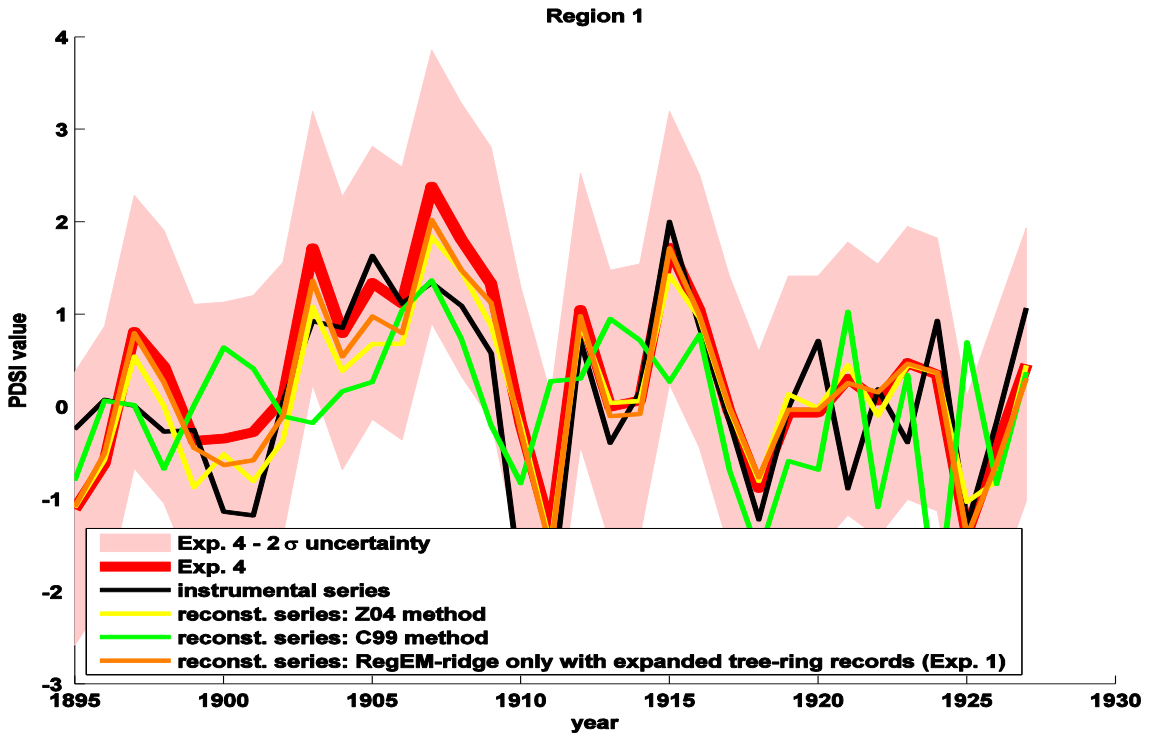
Region 1
PDSI value
year
Exp. 4 - 2 σ uncertainty
Exp. 4
instrumental series
reconst. series: Z04 method
reconst. series: C99 method
reconst. series: RegEM-ridge only with expanded tree-ring records (Exp. 1)

(a)

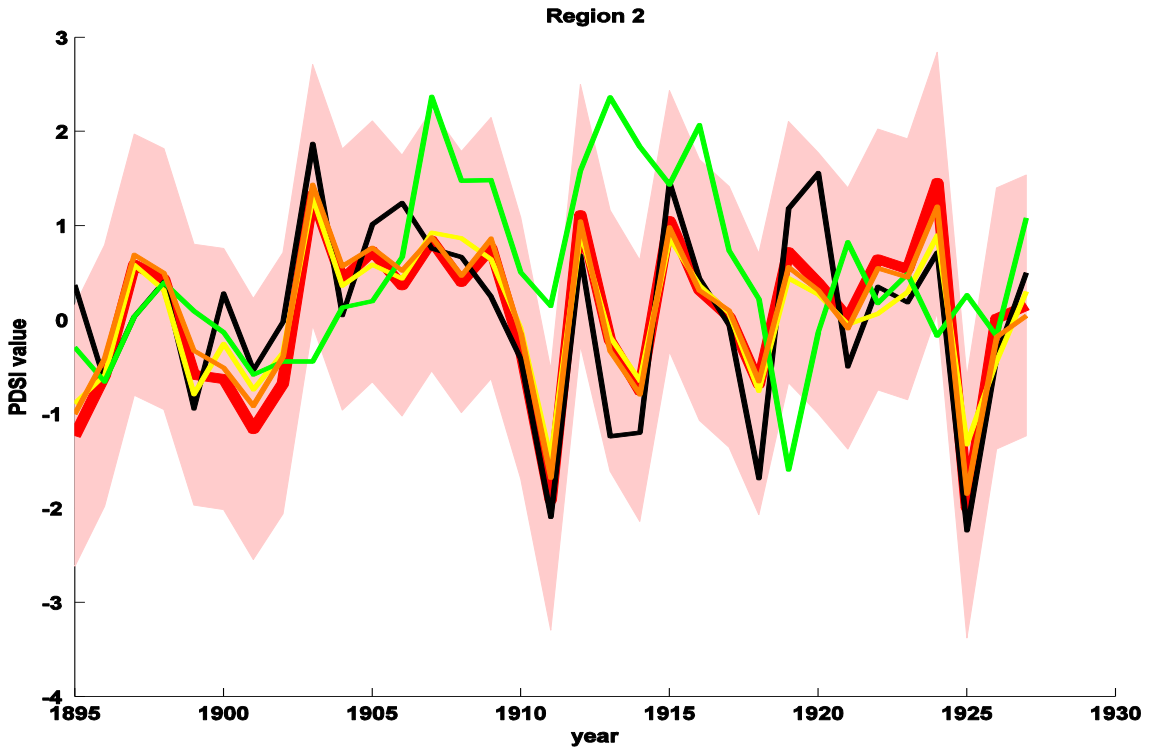
Region 2
PDSI value
year

(b)

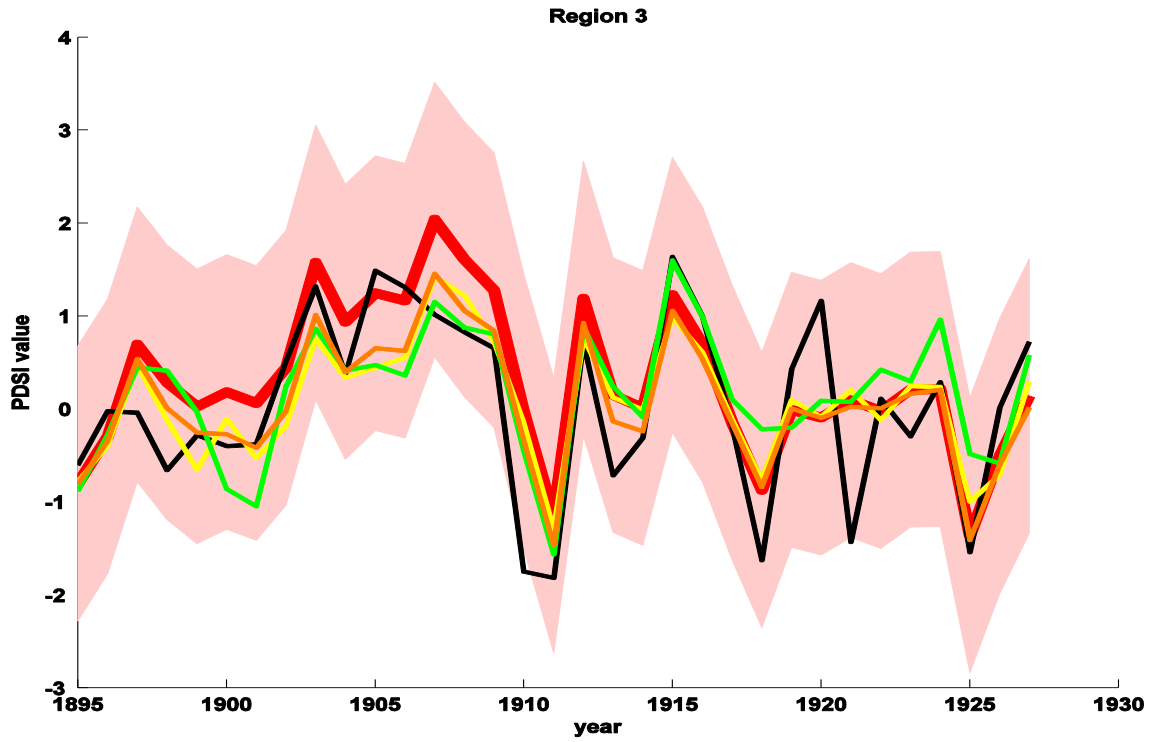
Region 3
PDSI value
year
4
3
2
1
0
-1
-2
-3
1895
1900
1905
1910
1915
1920
1925
1930

(c)

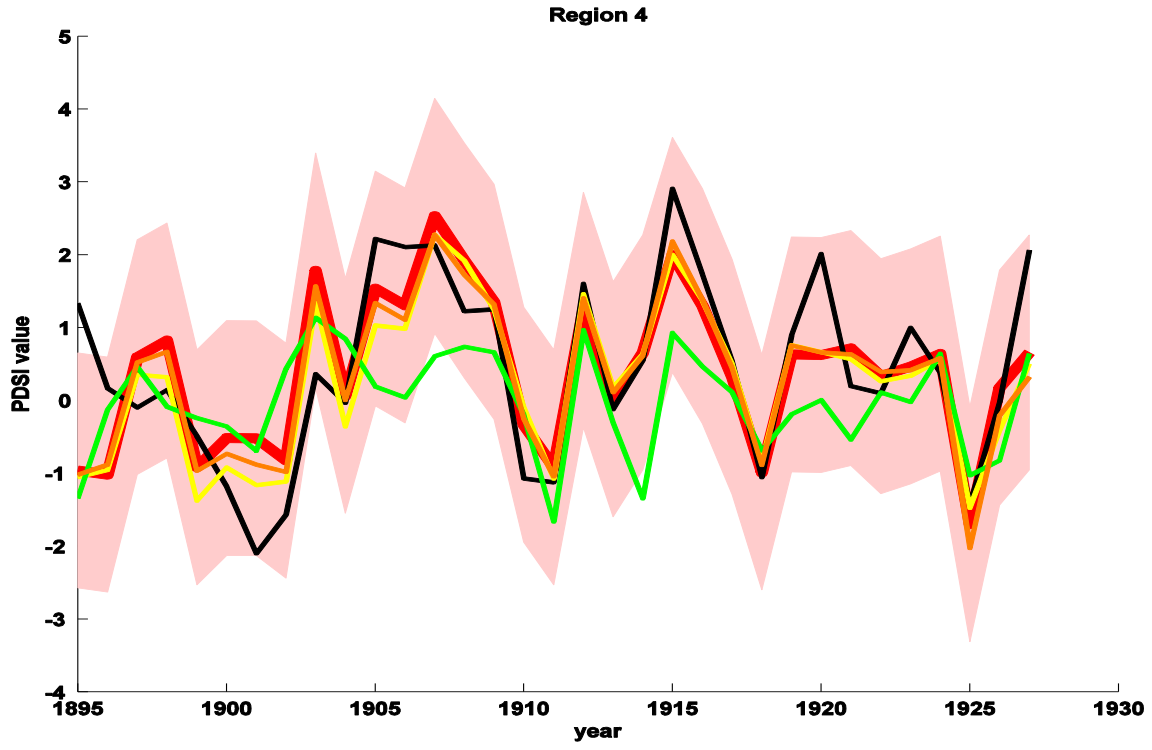
Region 4
PDSI value
year
5
4
3
2
1
0
-1
-2
-3
-4
1895
1900
1905
1910
1915
1920
1925
1930

(d)

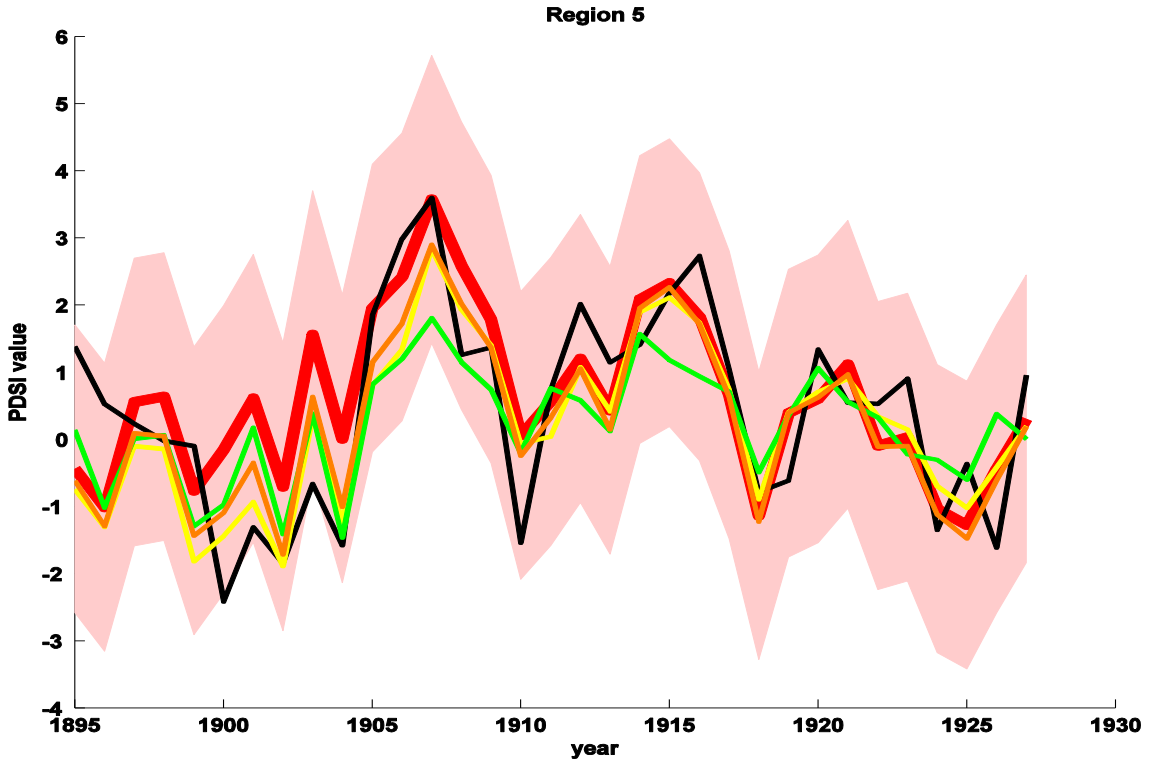
Region 5
PDSI value
year
6
5
4
3
2
1
0
-1
-2
-3
-4
1895
1900
1905
1910
1915
1920
1925
1930

(e)

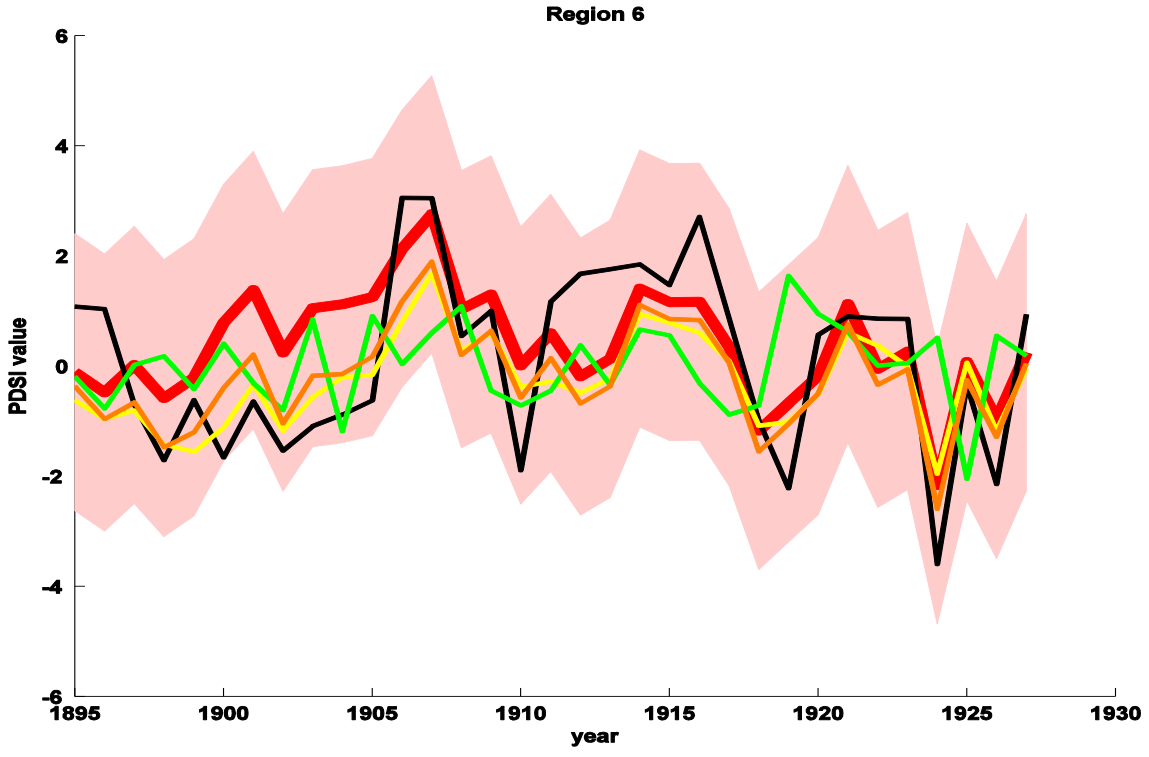
Region 6
PDSI value
year
6
4
2
0
-2
-4
-6
1895
1900
1905
1910
1915
1920
1925
1930

(f)

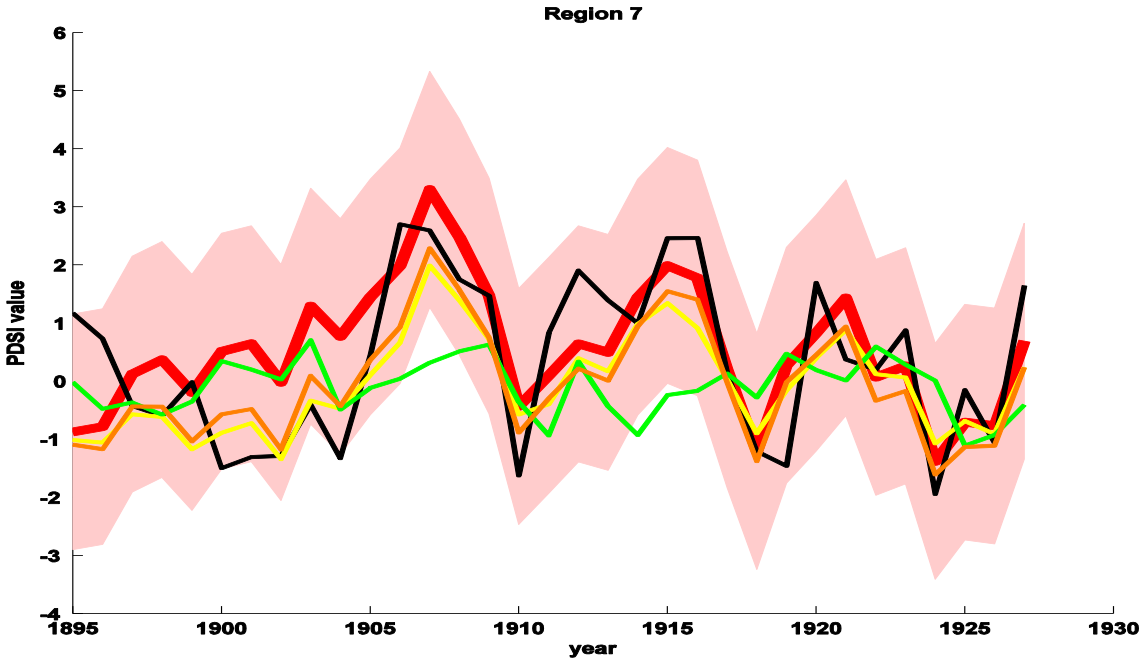

(g)

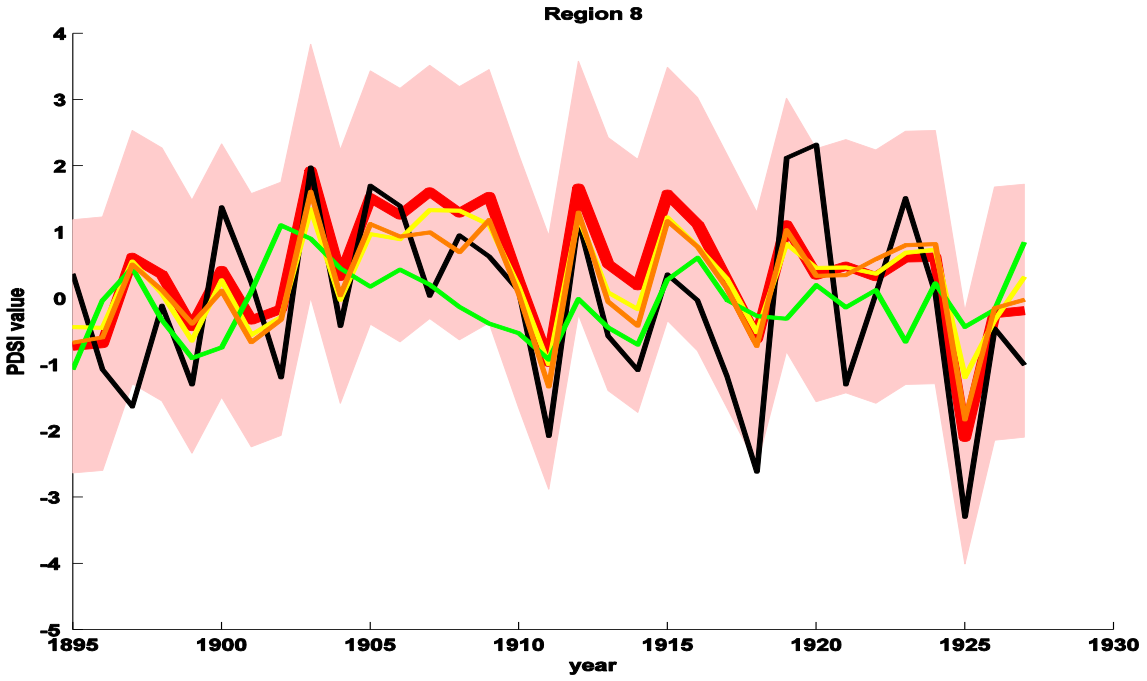

(h)

Figure 4.13 -- This series of eight plots ((a) – (h)) shows graphs of the each of the eight regional areal-mean summer PDSI reconstruction series made using the regionalized hybrid RegEM method (Exp. 4) (and their $\pm 2\sigma$ uncertainty bounds), the RegEM-ridge method with expanded tree-ring proxy network (Exp. 1), the Zhang et al. (2004) method, and the Cook et al. (1999) method as well as the eight regional areal-mean instrumental series. A legend of graph line colors is given in (a). The full reconstruction period was 1700-1927, but series are shown over the only 1895-1927 validation period.

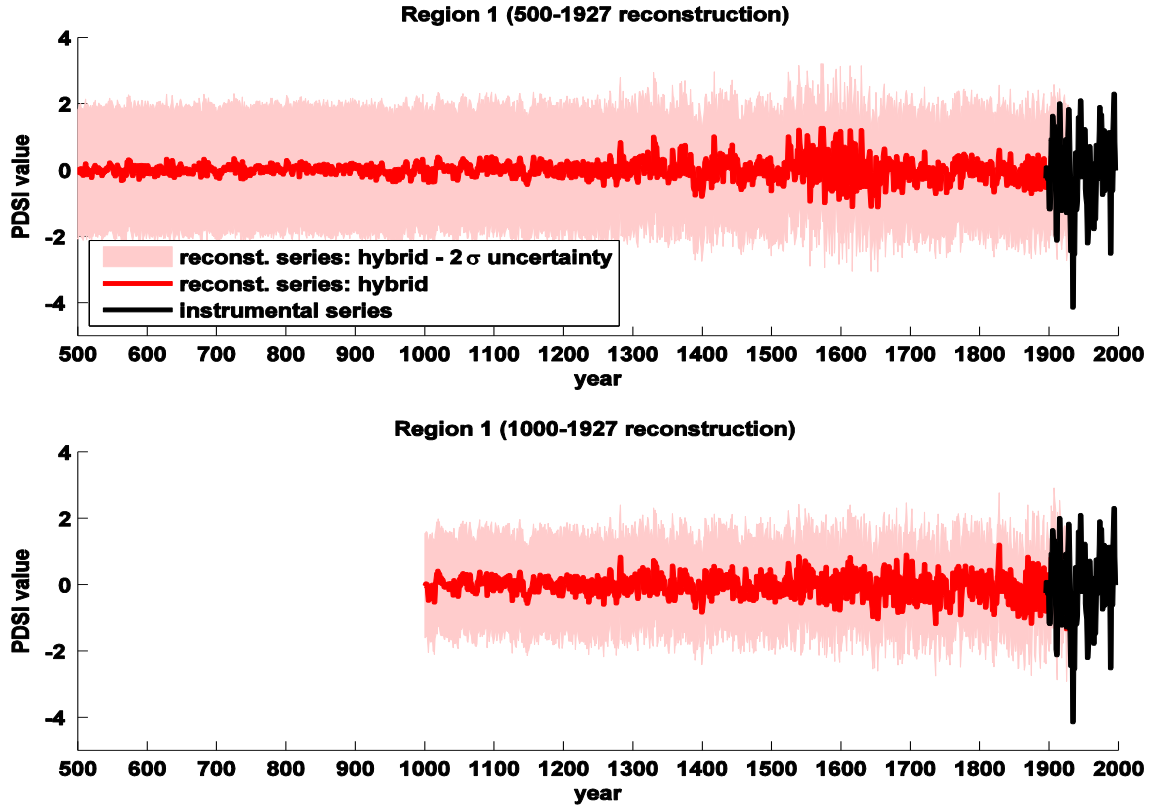

(a) 500-1927 reconstruction: RE = 0.37, CE = 0.34 | 1000-1927 reconstruction: RE = 0.59, CE = 0.58

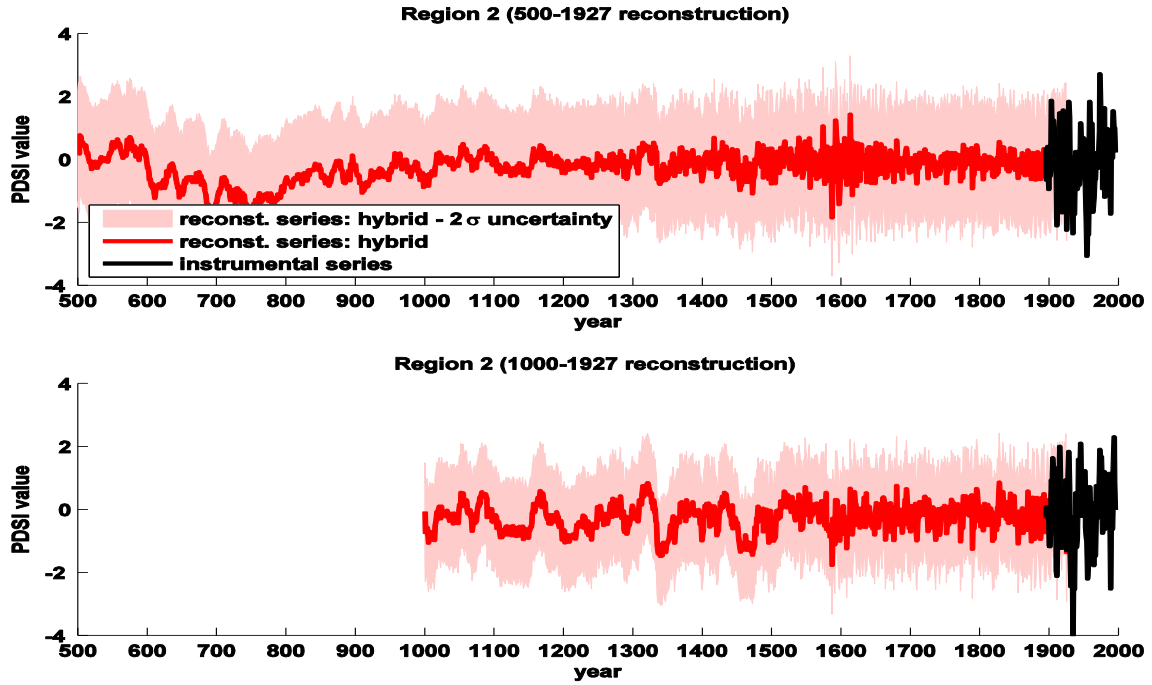

(b) 500-1927 reconstruction: RE = 0.33, CE = 0.32 | 1000-1927 reconstruction: RE = 0.59, CE = 0.58

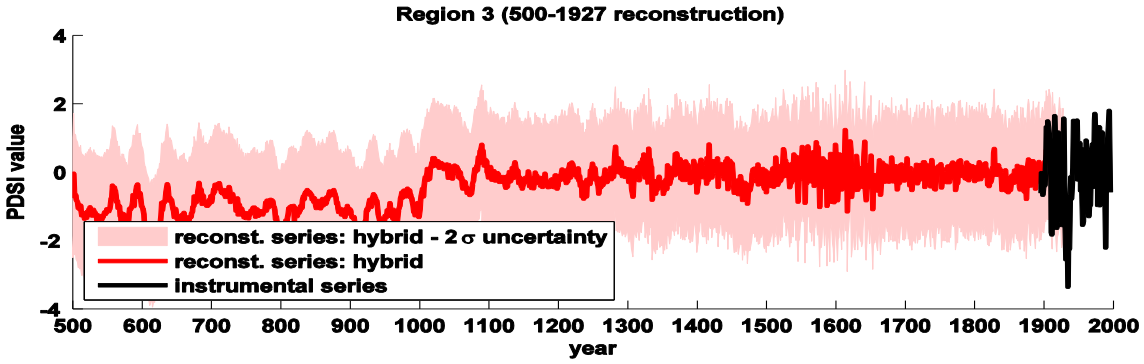

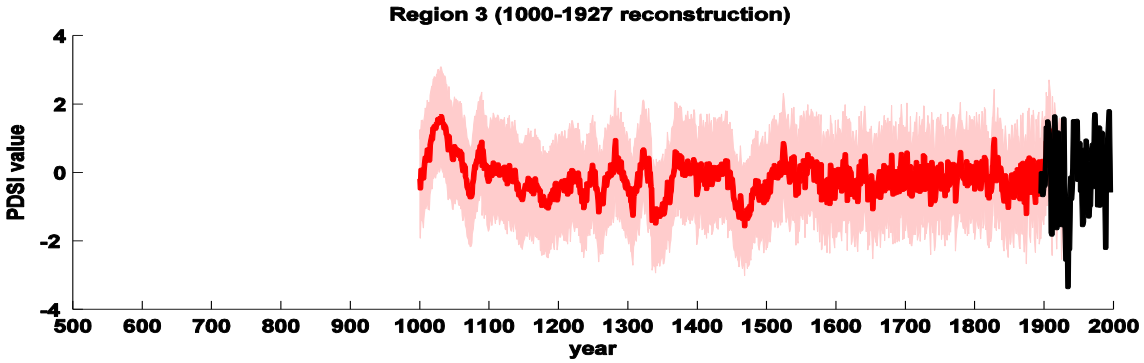

(c) 500-1927 reconstruction: RE = 0.34, CE = 0.33 | 1000-1927 reconstruction: RE = 0.55, CE = 0.54

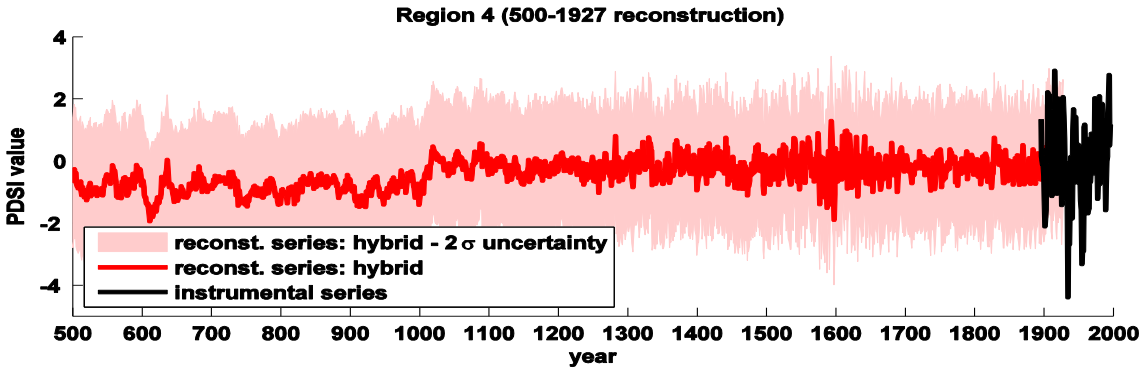

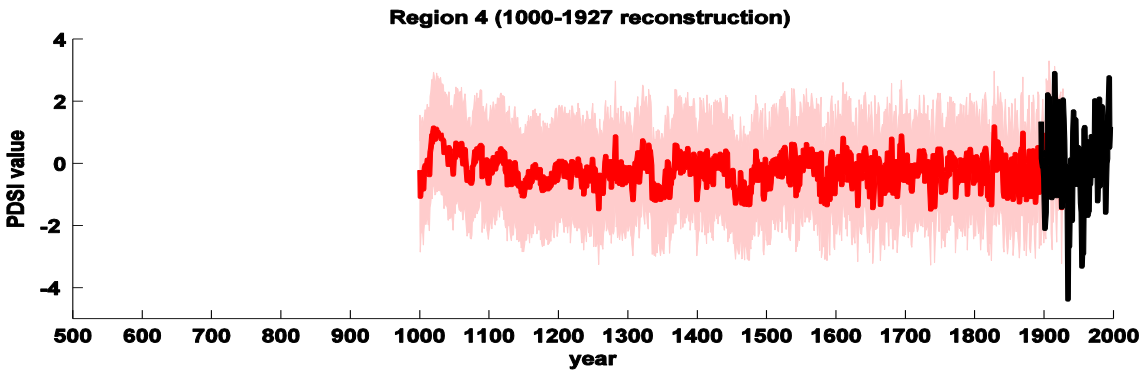

(d) 500-1927 reconstruction: RE = 0.41, CE = 0.27 | 1000-1927 reconstruction: RE = 0.57, CE = 0.47

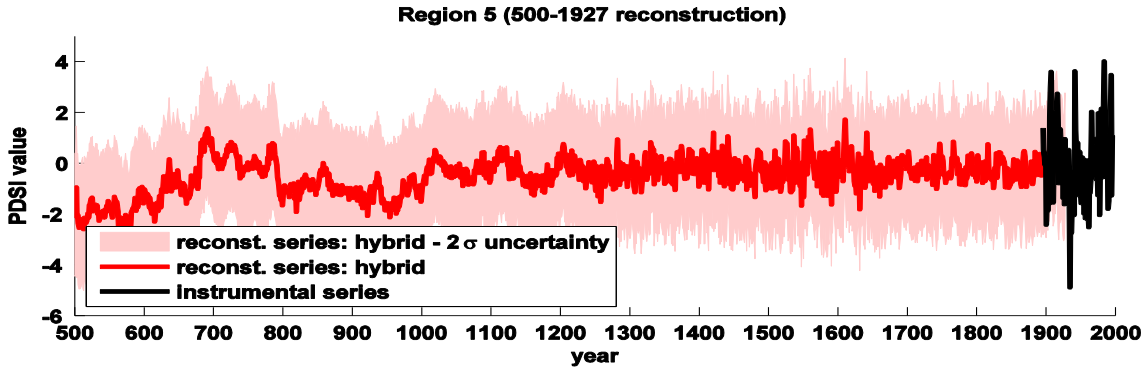

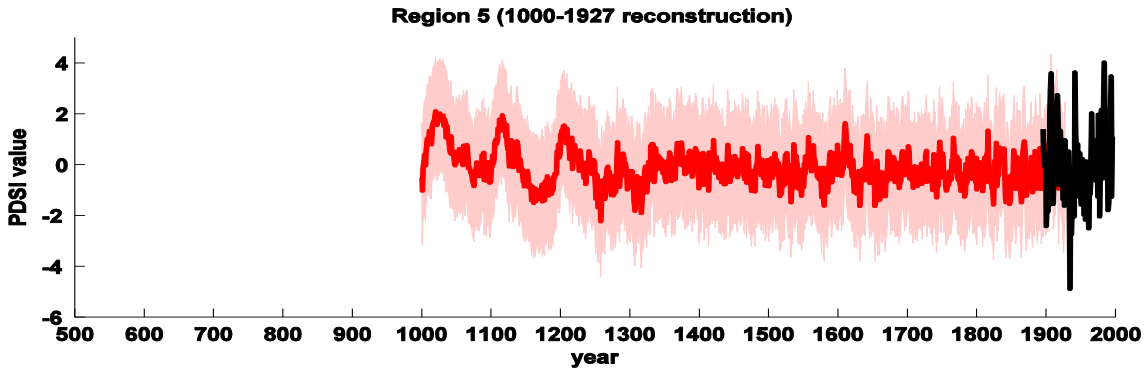

(e) 500-1927 reconstruction: RE = 0.44, CE = 0.32 | 1000-1927 reconstruction: RE = 0.55, CE = 0.45

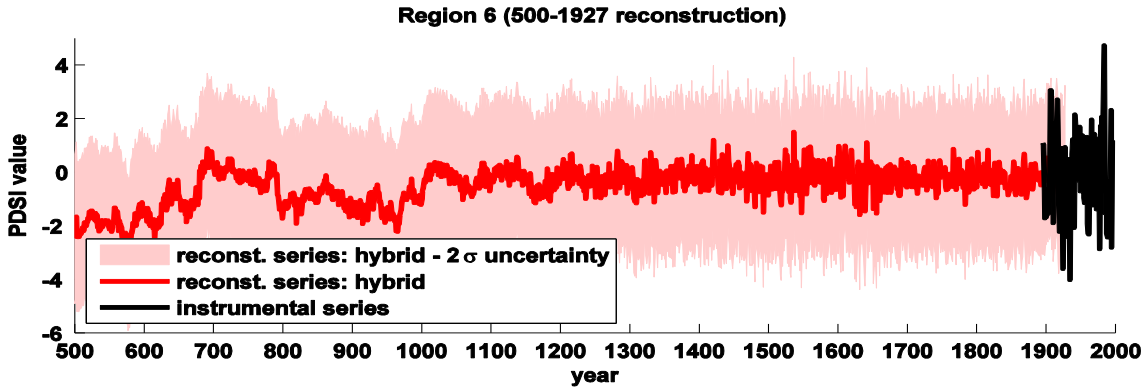

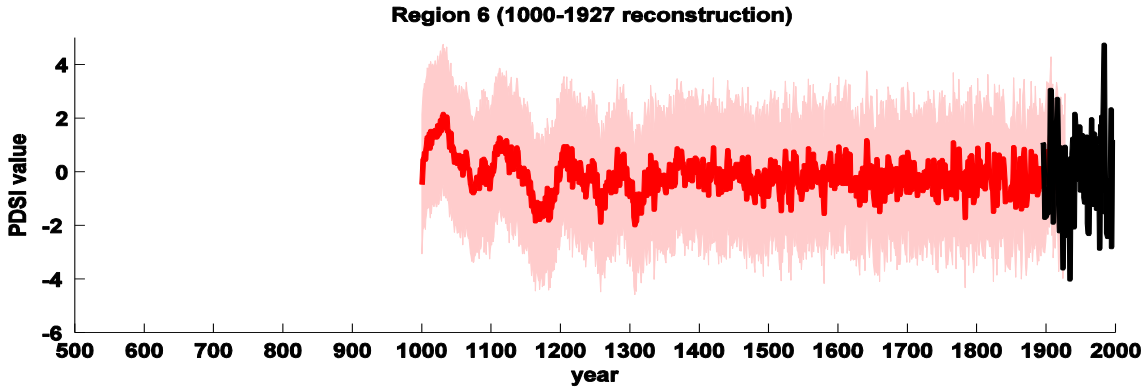

(f) 500-1927 reconstruction: RE = 0.26, CE = 0.22 | 1000-1927 reconstruction: RE = 0.36, CE = 0.33

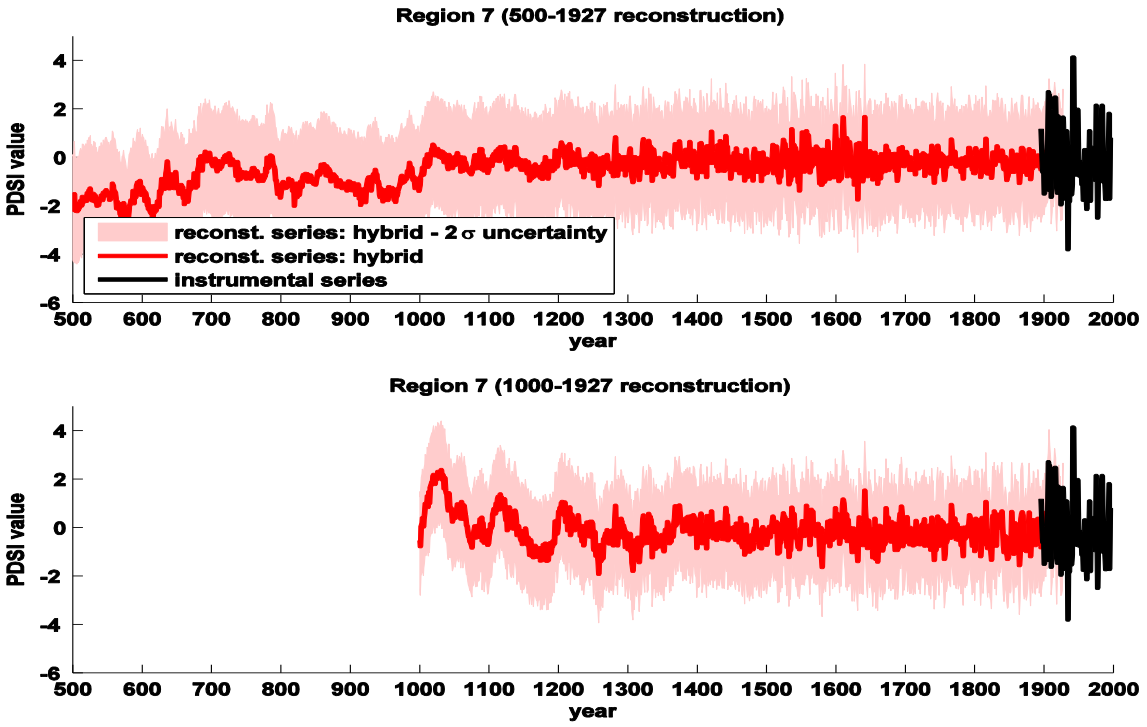

(g) 500-1927 reconstruction: RE = 0.38, CE = 0.28 | 1000-1927 reconstruction: RE = 0.46, CE = 0.37

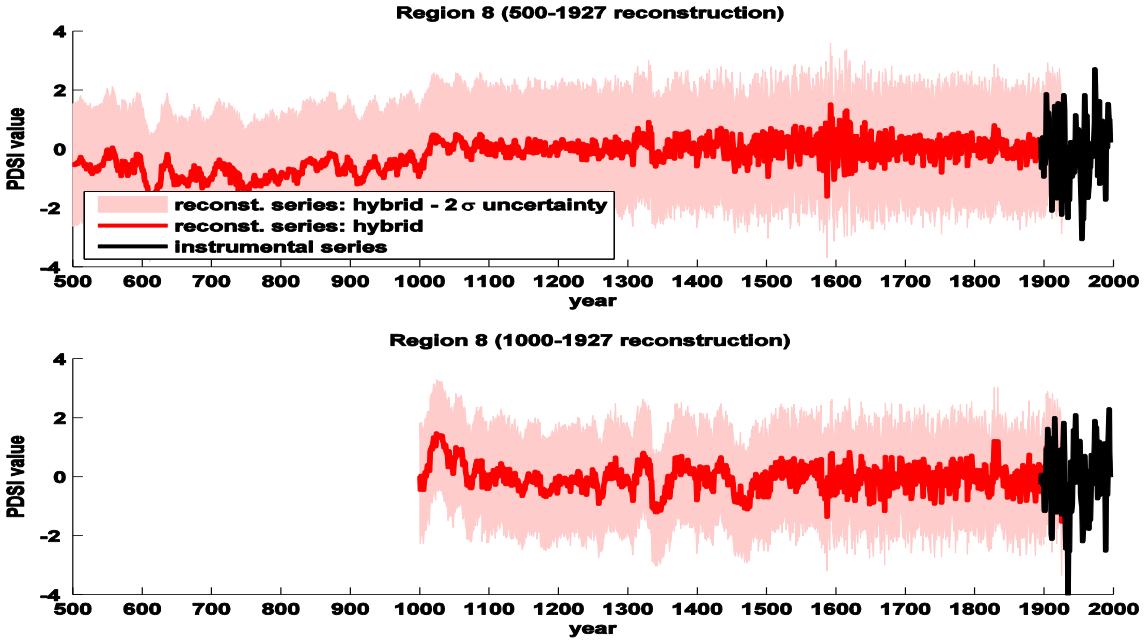

(h) 500-1927 reconstruction: RE = 0.27, CE = 0.26 | 1000-1927 reconstruction: RE = 0.44, CE = 0.43

Figure 4.14 – This series of eight plots ((a) – (h)) shows graphs of the eight regional areal-mean 500-1927 (top panel) and 1000-1927 (bottom panel) summer PDSI reconstruction series (and their $\pm 2\sigma$ uncertainty bounds) made using the regionalized hybrid RegEM method (Exp. 4). In black are the instrumental series from 1895-1995. Noted for each figure are the RE and CE scores for the corresponding reconstruction. The P-values for all RE and CE scores are 0 to three decimal places.

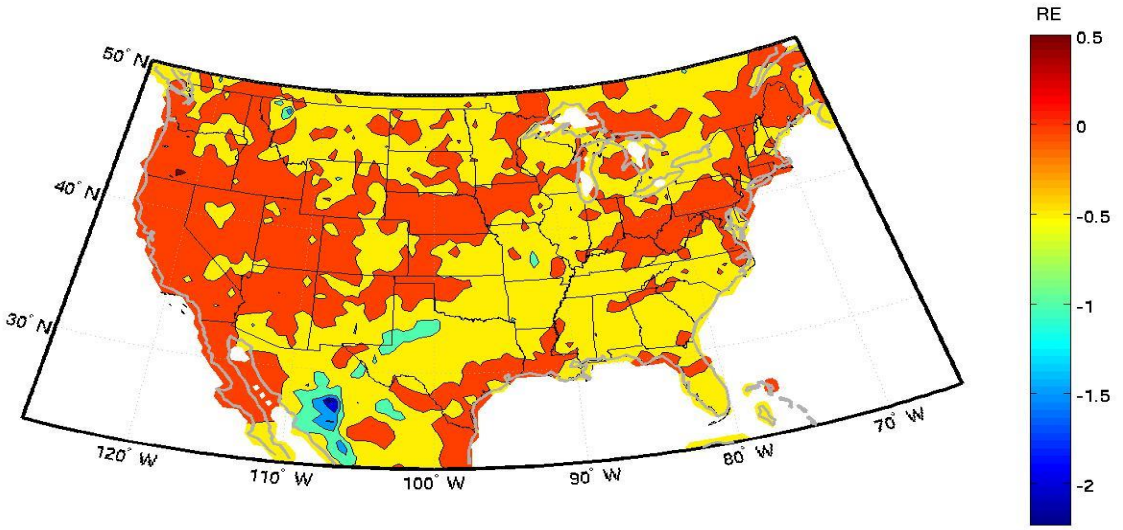

Figure 4.15 – Contour map of RE scores, as calculated for each of 6373 grid points and then interpolated, for the 1700-1930 reconstruction of winter precipitation using the hybrid method in which only the tree-ring part of the proxy network was used in the ridge sub-reconstruction and the entire proxy network was used in the TTLS sub-reconstruction (Exp. 3). Warmer colors indicate greater values of RE, and cooler colors indicate lesser values of RE. Only the areas shaded in red or dark red exhibit skill (RE $\geq$ 0). The map of CE scores is qualitatively similar.

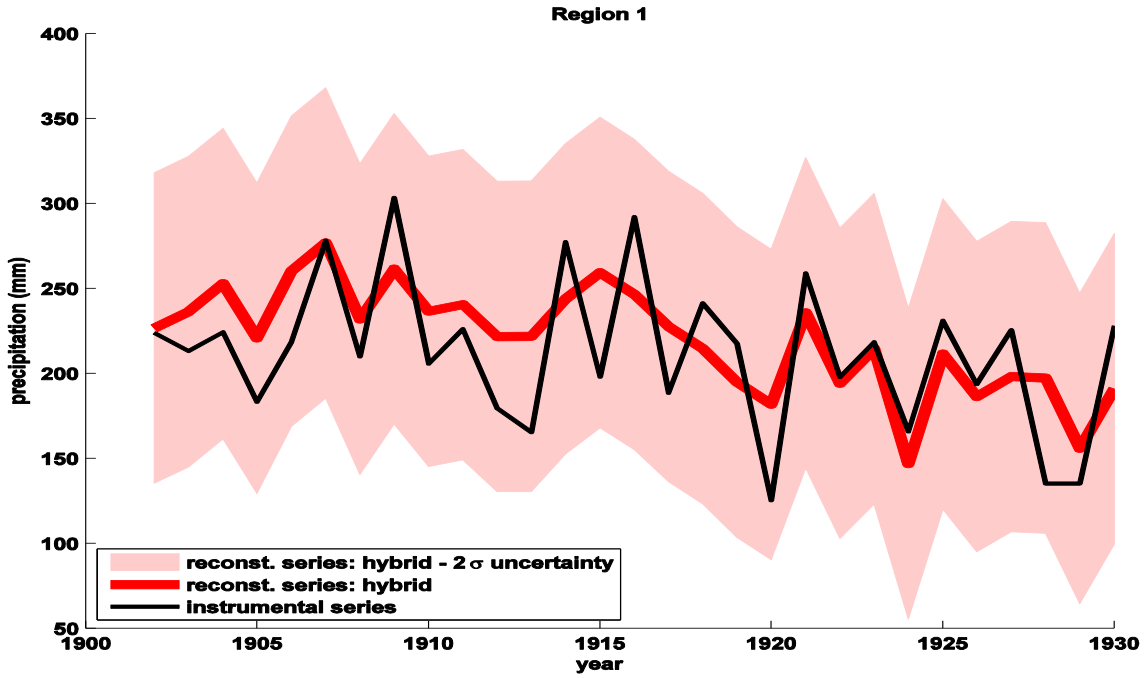

(a)

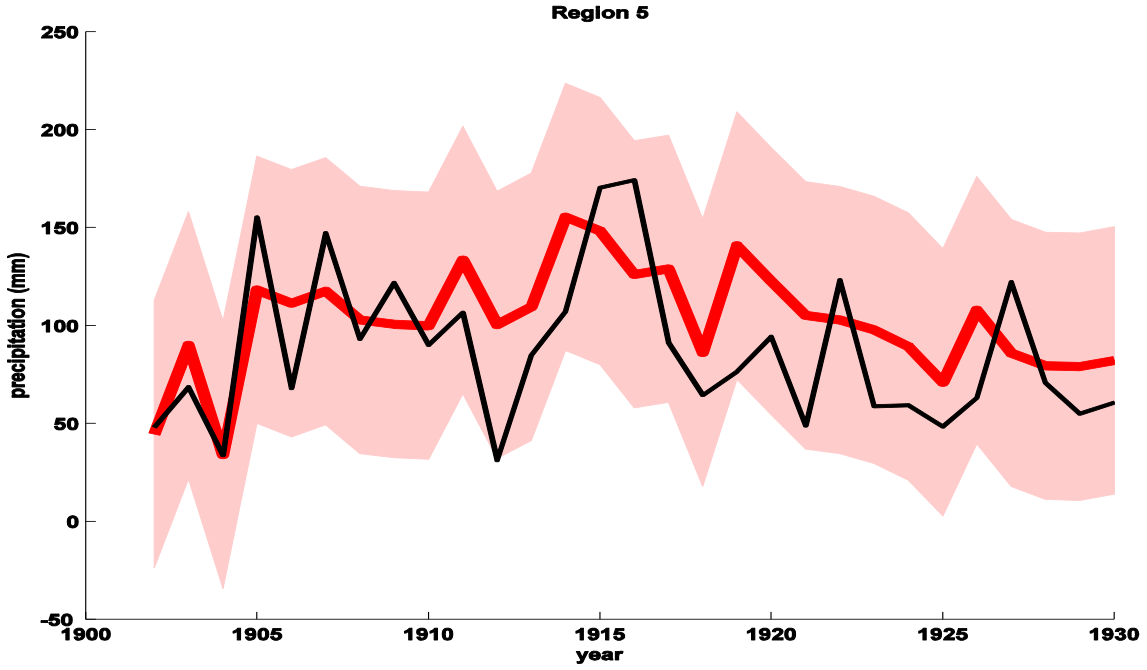

(b)

Figure 4.16 – This series of two plots ((a) – (b)) shows graphs of the validation-period portion (1902-1930) of two regional areal-mean 1700-1930 winter precipitation reconstruction series (and their $\pm 2\sigma$ uncertainty bounds) made using the hybrid RegEM method with only the tree-ring part of the proxy network in the ridge sub-reconstruction and the full proxy network in the TTLS sub-reconstruction (Exp. 3). In black are the instrumental series from 1895-1995. Noted for each figure are the RE and CE scores for the corresponding reconstruction. These two regions were chosen for reasons described in the text.

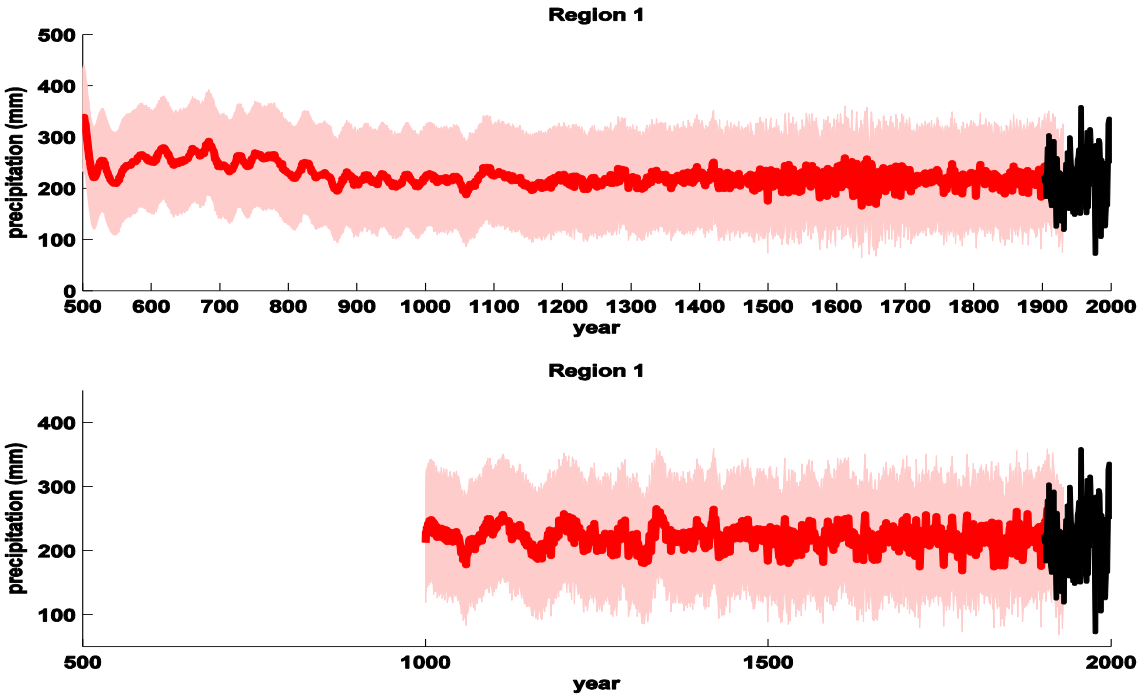

(a) 500-1930 Reconstruction: RE = 0.286, CE = 0.265
1000-1930 Reconstruction: RE = 0.372, CE = 0.354

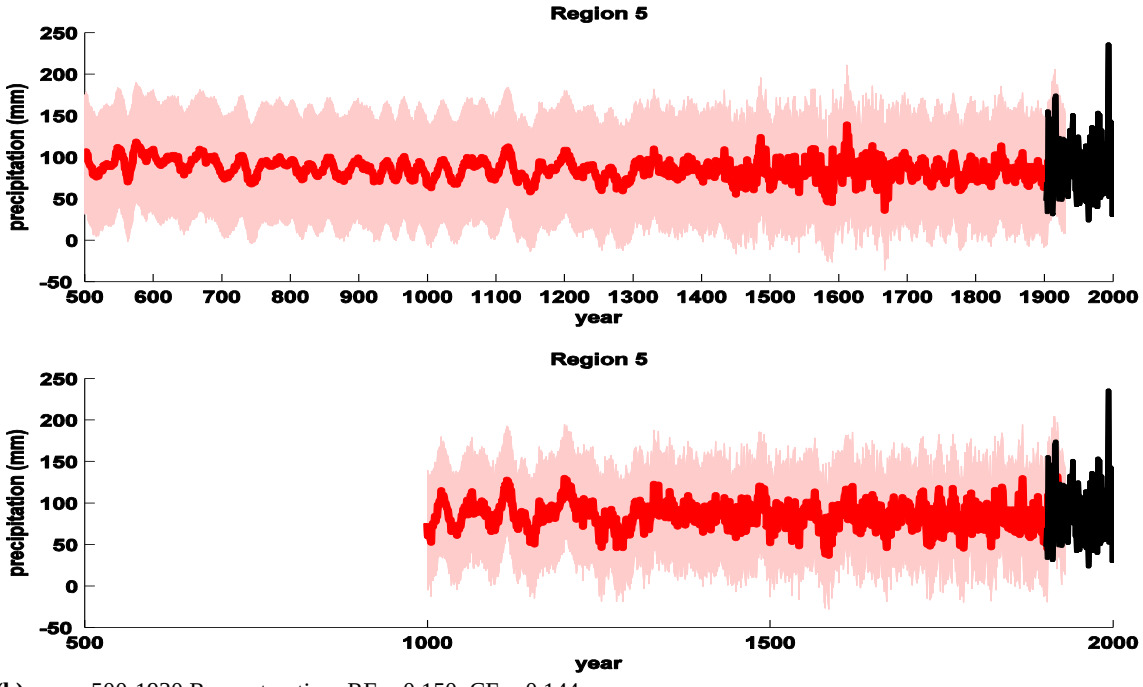

(b) 500-1930 Reconstruction: RE = 0.150, CE = 0.144
1000-1930 Reconstruction: RE = 0.304, CE = 0.299

Figure 4.17 – This series of two plots ((a) – (b)) shows graphs of the 500-1930 (top panel) and 1000-1930 (bottom panel) areal-mean winter precipitation reconstructions (in red; lighter red are their $\pm 2\sigma$ uncertainties) for Regions 1 and 5 that were made using the hybrid RegEM method in which only the tree-ring part of the proxy network was used in the ridge sub-reconstruction and the entire proxy network was used in the TTLS sub-reconstruction (Exp. 3). In black are the areal-mean 1902-2000 instrumental series. RE and CE scores for each reconstruction are also given.

Table 4.1 – This display compares RE scores for areal-mean summer PDSI reconstruction series made using various reconstruction methods described in the text.

METHOD	Rgn. 1	2	3	4	5	6	7	8
Ridge-only with expanded tree-ring proxies (Exp. 1)	0.600	0.657	0.566	0.680	0.679	0.544	0.555	0.462
Hybrid with expanded tree-ring proxies (Exp. 2)	0.289	0.388	0.278	0.534	0.547	0.539	0.559	0.206
Hybrid with tree-ring records only in ridge sub-reconst. and low-frequency records only in TTLS sub-reconst.	0.030	-0.019	-0.153	0.486	0.639	-0.75	0.169	0.057
Hybrid with tree-ring records only in ridge sub-reconst. and full network in TTLS sub-reconst. (Exp. 3)	0.445	0.596	0.494	0.561	0.576	0.465	0.533	0.401
Exp. 3 Hybrid method with regionalization (Exp. 4)	0.640	0.630	0.530	0.650	0.560	0.400	0.460	0.380
Zhang et al. (2004) 'global-global'	0.602	0.682	0.520	0.671	0.670	0.502	0.532	0.371
Cook et al. (1999)	0.550	0.748	0.593	0.510	0.639	0.678	0.605	0.616

Table 4.2 -- As in Table 4.1 but CE scores.

METHOD	Rgn. 1	2	3	4	5	6	7	8
Ridge-only with expanded tree-ring proxies (Exp. 1)	0.592	0.652	0.563	0.612	0.614	0.522	0.489	0.456
Hybrid with expanded tree-ring proxies (Exp. 2)	0.274	0.377	0.273	0.435	0.454	0.516	0.494	0.197
Hybrid with tree-ring records only in ridge sub-reconst. and low-frequency records only in TTLS sub-reconst.	0.010	-0.037	-0.161	0.376	0.565	-0.84	0.045	0.046
Hybrid with tree-ring records only in ridge sub-reconst. and full network in TTLS sub-reconst. (Exp. 3)	0.433	0.589	0.491	0.467	0.490	0.438	0.463	0.394
Exp. 3 Hybrid method with regionalization (Exp. 4)	0.625	0.626	0.528	0.571	0.474	0.371	0.375	0.378
Zhang et al. (2004) 'global-global'	0.594	0.677	0.516	0.601	0.603	0.477	0.463	0.364
Cook et al. (1999)	0.549	0.542	0.503	0.485	0.601	0.674	0.575	0.565

Table 4.3 – This displays shows the RE and CE scores for the eight regional areal-mean 1700-1930 winter precipitation reconstruction series made using the hybrid RegEM method in which only the tree-ring part of the proxy network was used in the ridge sub-reconstruction and the entire proxy network was used in the TTLS sub-reconstruction (Exp. 3).

	1	**2**	**3**	**4**	**5**	**6**	**7**	**8**
RE score	0.405	0.121	0.199	-0.061	0.219	-0.110	-0.168	0.064
CE score	0.387	0.006	0.189	-0.089	0.213	-0.294	-0.171	-0.08

Table 4.4 – This displays shows the P-values, calculated from 1000 realizations of a Monte Carlo simulation (as described in the text), for the RE and CE scores for the eight regional areal-mean 1700-1930 winter precipitation reconstruction series made using the hybrid RegEM method in which only the tree-ring part of the proxy network was used in the ridge sub-reconstruction and the entire proxy network was used in the TTLS sub-reconstruction (Exp. 3).

	1	**2**	**3**	**4**	**5**	**6**	**7**	**8**
RE P-value	0.000	0.000	0.001	0.064	0.000	0.019	0.031	0.010
CE P-value	0.000	0.016	0.000	0.084	0.000	0.113	0.036	0.050

Chapter 5
Conclusions and Future Work

A series of experiments was undertaken to develop a method based on the RegEM algorithm to make skillful proxy-based reconstructions of summer drought and winter precipitation for the contiguous United States going back to AD 500.

It was found that, back to 1700, reconstructions arising from the RegEM-ridge (Exp. 1) method exhibited the greatest and most widespread skill for summer PDSI while also minimizing variance loss and was, thus, preferred. However, for reconstructions of that same target that extended farther back in time, the regionalized hybrid RegEM method in which low-frequency records are used in the calibration (Exp. 4) was preferred because it produced reconstructions that depicted low-frequency variability going back in time with moderate to high cross-validation skill though not quite as high as realized in some previous work. For winter precipitation, reconstructive skill was much more limited, restricted to the western part of the reconstruction domain. In that part of the domain, a hybrid method was preferred for similar reasons as it was for the longer reconstructions of summer PDSI.

In assessing the skill of the reconstructions, comparison was made to the skill of 1700-present reconstructions published by C99. In the present study, the highest skill was seen in reconstructions of summer PDSI back to 1700 using the Exp. 1 method (RegEM-ridge, tree-ring records only), but even that skill was still lower than that of the C99 reconstruction. On the other hand, the skill was generally higher than that realized from reconstructions made using the method and proxy network of Z04. The Z04 method was the same, but their proxy network consisted of fewer records. Thus, it appeared that the

addition of proxy records improved reconstructive skill. Beneficial future work might examine the sensitivity of the reconstructions, particularly by region, to the addition of these data.

Additionally, the Exp. 1 method yields areal-mean reconstruction series that suffer from variance loss and consequent unsatisfactory depiction of low-frequency variability going back in time. Applying the hybrid RegEM method with low-frequency records included in the proxy network (Exp. 3) resolves the variance-loss weakness of the Exp. 1 method, but a cost of that improvement is a decrease in skill. The skill is still moderate to high, but it is generally lower than that of the reconstruction made using the Exp. 1 method and the C99 reconstruction, which only extend back to 1700. Follow-up work might use the C99 method, which is point-by-point regression of the PDSI gridpoints on proximal tree-ring proxy records, in conjunction with the multi-proxy network of the current study. Doing so may demonstrate the limitations of their methodology, which relies on tree-ring records, with respect to depicting low-frequency variability over long time-scales.

Some concern exists about possible enhanced low-frequency variability in the early parts of the longer reconstructions. It seems likely that such enhancement, if it exists at all, is linked to the choice of low-frequency records in the proxy network. A possible way to probe at this enhancement would be a simple data-denial sensitivity analysis in which the impact of removing each low-frequency record from the network, one at a time, on how low-frequency variability is depicted. Furthermore, additional, high-quality low-frequency records could be identified for inclusion in the network.

The skill of the winter precipitation reconstruction was disappointingly low, regardless of method used. Intuition suggests that precipitation, an intensely spatially

variable quantity, would be more difficult to reconstruct on a large spatial scale. It also suggests that it would be more difficult to reconstruct it at high resolution as was attempted in this study. The limited results reported in this study, as well as a mounting body of peer-reviewed literature, suggest that it is critical that winter precipitation be reconstructed. Future efforts might be aimed at re-attempting the reconstruction using a coarser target grid compared to the 0.5^{o} resolution grid used in the current study. Such a future effort is motivated by the idea that the spatial density of records in the proxy network is insufficient to resolve the fine grid used in this study.

Past work (e.g., Steinman et al. 2014) has hinted at the idea of a dipole pattern in hydroclimate in western North America and how the focus for this dipole shifts geographically on centennial time-scales. It has been remarked that the polar jet stream in the Pacific Northwest can shift into southern Canada at these time-scales, resulting in drier conditions across the United States part of this region. An extension of the reconstructions into southern Canada would be a fruitful future effort so that this entire area of interest could be examined.

Appendix
Metadata

Table A.1 – This table displays various metadata for the 787 tree-ring records included in the full proxy network for the reconstructions. These metadata include ITRDB record identification number, latitude and longitude coordinates for record location, and start and end years for the record's chronology series. In the record identification number, the first two letters refer to the state abbreviations employed by the United States Postal Service; for example, 'pa' refers to Pennsylvania.

ITRDB Record ID Number	Latitude (ºN)	Longitude (ºW)	Start Year	End Year
al001	33.817	85.7	1679	1985
ar009	35.65	93.07	1713	1972
ar018	34.72	94.05	1650	1980
ar021	34.08	91.07	1764	1980
ar024	36.08	94.4	1725	1982
ar027	34.8	92.93	1667	1980
ar033	34.37	93.97	1708	1982
ar036	38.17	91.82	1779	1980
ar039	33.68	93.87	1766	1980
ar042	34.63	91.75	1522	1980
ar048	35.85	90.95	1417	1980
ar049	34.95	91.22	1133	1985
ar050	35.15	91.3	1019	1980
ar052	35.55	91.25	998	1990
ar053	33.77	92.33	1262	1985
ar054	35.63	90.45	1321	1990
ar055	36.08	93.3	1359	1992
ar056	36.07	93.32	1670	1992
ar057	36.07	93.18	1620	1993
ar060	36.3	92.2	1637	1993
ar061	35.93	92.87	1692	1993
ar064	34.25	94.17	1658	1991
ar065	34.63	93.63	1762	1991

ar067	36.2	92.37	1764	1976
ar070	32.55	93.28	1480	1991
ar072	35.83	94	1625	1991
ar073	34.62	93.72	1729	1991
az077	34.07	110.62	1642	1971
az078	34.05	110.67	1695	1971
az079	34.05	110.65	1677	1971
az080	36.1	109.35	1598	1971
az081	36.08	109.37	1601	1971
az083	36.22	109.35	1500	1971
az084	36.17	110.5	1470	1971
az086	36.83	110.73	1365	1971
az088	35.4	111.57	1679	1972
az089	34.25	109.82	1596	1972
az090	35.67	109.33	1611	1972
az091	35.57	111.65	1689	1972
az099	34.5	109.95	1687	1973
az101	34.75	111.1	1534	1972
az104	36.75	113.73	1594	1971
az106	35.82	112.07	1448	1975
az109	35	113	1598	1971
az127	36.73	112.23	1581	1976
az129	36.63	112.1	1482	1976
az135	35.08	113.9	1569	1971
az139	35.7	109.37	1620	1972
az143	35.95	113.08	1643	1972
az144	36.83	112.05	1481	1975
az505	36.42	112	1693	1975
az506	32.35	110.72	1766	1987

az509	34.88	111.57	1728	1985
az510	35.5	111.67	548	1983
az511	32.7	109.87	1696	1990
az512	32.7	109.88	1752	1989
az513	33.7	109.23	1570	1986
az514	33.8	109.32	1580	1987
az515	32.42	110.73	1610	1987
az516	32.2	110.55	1720	1987
az517	34.88	111.82	1630	1986
az518	33.47	109.48	1640	1987
az519	32.38	110.68	1550	1986
az520	32.38	110.68	1460	1986
az521	35.27	111.75	1550	1987
az522	34.38	110.42	1660	1986
az523	34.07	110.62	1700	1985
az524	32.22	110.55	1690	1987
az525	32.22	110.55	1720	1987
az526	31.7	110.87	1720	1987
az527	34.32	110.77	1630	1986
az528	32.65	109.82	1770	1987
az529	32.22	110.55	1780	1987
az530	32.22	110.55	1720	1987
az531	32.22	110.55	1640	1987
az532	32.22	110.55	1700	1987
az533	33.9	111.4	1570	1987
az534	31.93	109.27	1650	1986
az535	35.32	111.72	1770	1987
az536	32.68	109.88	1610	1986
az538	34.72	111.5	1670	1986

az539	35.38	111.53	1630	1986
az541	33.42	109.37	1660	1987
az542	34.25	109.93	1630	1986
az543	35.5	111.83	1600	1986
az544	31.72	110.83	1600	1986
az545	32.2	110.55	1660	1987
az546	32.2	110.55	1670	1987
az547	35.17	111.52	1420	1987
az548	35.17	111.52	1680	1986
az549	32.7	109.93	1557	1991
az553	35.43	110.2	1453	1983
az556	31.45	110.35	1630	1995
az557	32.45	110.78	1321	1998
az560	36.13	111.88	1800	1995
ca051	34.12	116.82	-42	1970
ca064	39.57	120.25	1415	1980
ca065	41.62	120.7	1357	1980
ca066	40.15	120.6	1471	1980
ca067	40.15	120.6	1484	1980
ca073	41.77	120.75	1310	1980
ca074	39.32	120.35	1510	1980
ca076	37.75	119.75	1441	1980
ca079	38.13	120.05	1557	1980
ca082	39.43	122.68	1500	1980
ca084	39.67	122.97	1318	1980
ca085	39.6	122.95	1497	1980
ca087	37.28	119.08	1140	1981
ca089	35.43	118.28	1505	1981
ca091	38.75	119.67	1556	1983

ca092	36.72	118.88	1434	1981
ca094	35.53	118.43	1528	1981
ca095	41.72	121.8	1548	1982
ca512	33.73	117.55	1610	1972
ca514	36.03	118.18	1607	1981
ca517	41.72	120.75	1654	1980
ca520	41.15	120.57	1653	1980
ca523	41.33	122.52	1388	1981
ca525	41.5	121.17	1627	1979
ca526	41.18	120.12	1526	1979
ca527	40.22	120.92	1623	1979
ca528	36.77	118.37	898	1987
ca529	36.45	118.6	699	1987
ca530	36.45	118.22	917	1987
ca531	36.77	118.35	1027	1987
ca532	36.45	118.62	1050	1987
ca533	37.5	118.22	626	1983
ca536	34.27	117.28	1654	1988
ca537	34.27	117.33	1725	1988
ca538	34.22	117.3	1784	1988
ca539	33.98	116.75	1560	1988
ca540	34.02	116.9	1757	1988
ca541	34.05	116.97	1787	1988
ca543	34.12	116.98	1793	1988
ca544	34.17	117.12	1707	1988
ca545	34.17	117.1	1772	1988
ca546	34.17	117.07	1741	1988
ca547	34.17	117.05	1684	1988
ca548	34.15	117.02	1800	1988

ca550	34.22	117.22	1621	1988
ca551	34.22	117.27	1781	1988
ca552	34.1	116.97	1628	1988
ca553	34.17	116.73	1540	1988
ca554	33.97	116.75	1701	1988
ca555	40.03	122.87	1177	1988
ca602	37.83	119.42	1532	1991
ca603	37.92	119.23	1430	1996
ca604	37.92	119.28	1520	1996
ca605	37.87	119.28	885	1996
ca606	37.83	119.22	800	1996
ca607	37.72	119.67	1681	1991
ca608	38.02	122.8	1760	1997
ca609	34.12	116.8	1560	1995
ca610	32.87	116.42	1660	1995
ca611	33.35	116.85	1640	1992
ca612	34.65	119.37	1470	1993
ca613	33.73	117.55	1660	1995
ca614	35.3	120.27	1455	2004
ca615	39.02	122.82	1620	2004
ca616	37.72	120.42	1531	2005
ca617	39.82	123.07	1535	1996
ca618	39.52	121.43	1572	2004
ca619	40.27	121.85	1363	2004
ca621	35.52	118.67	1585	2003
ca623	37.87	121.95	1582	2004
ca624	37.87	121.95	1621	1996
ca625	37.05	121	1510	2003
ca626	36.47	121.18	1577	2003

ca627	37.03	119.67	1710	1996
ca628	40.15	120.6	1450	1998
ca629	41.45	120.9	1152	1998
ca633	37.75	118.68	680	2000
ca641	37.87	119.37	1700	2005
ca642	37.88	119.37	1700	2005
ca643	37.87	119.37	1700	2005
ca645	37.67	121.78	1697	2003
ca646	36.82	120.88	1379	2003
ca647	36.57	120.87	1409	2003
ca648	40.88	120.03	1582	2004
ca649	39.35	122.73	1546	2004
ca650	40.47	122.75	1649	2004
ca651	36.48	118.78	1596	2003
ca652	40.42	122.63	1519	2004
ca653	35.92	118.67	1448	2003
ca654	40.15	122.05	1601	2005
ca655	38	120.62	1695	2004
ca656	34.73	120	1293	2003
ca657	36.65	121.92	1460	2004
ca658	36.2	121.77	1494	2003
ca659	36.92	118.9	1494	2004
ca660	34.92	119.4	1333	2004
ca661	39.82	122.62	1532	2004
ca662	35.7	120.43	1538	2004
ca663	38.67	122.45	1534	2004
ca664	37.15	119.75	1557	2004
ca665	37.87	119.98	1408	2005
ca671	37.617	119.02	1610	2009

cana032	44.82	64	1572	1982
cana033	45.8	78.2	1550	1982
cana034	45.17	78.75	1641	1982
cana035	46.63	71.88	1524	1982
cana036	48.58	65.92	1404	1982
cana037	47	79.92	1644	1983
cana106	48.47	79.28	1186	1987
cana107	49.52	123.07	1687	1992
cana109	49.53	123.03	1539	1992
cana110	49.53	123.03	1344	1993
cana127	45.42	78.6	1662	1994
cana135	51.17	114.67	1315	1992
cana136	49.58	114.22	1466	1992
cana137	49.58	114.2	1467	1992
cana147	50.82	119.9	1665	1994
cana161	51.03	119.05	1710	1996
cana162	51.03	119.05	1773	1996
cana269	46.83	71.17	1540	2005
cana327	52.19	116.44	1576	2007
cana328	52.048	116.4	1018	2008
cana329	51.97	116.72	1617	2007
cana330	52	116.45	1062	2007
cana331	52.072	116.39	1555	2008
cana332	49.9	114.2	1482	2004
cana333	49.7	114	1380	2004
cana334	50	114.2	1572	2004
cana335	49.6	114.6	1450	2004
cana338	51.3	114.7	1341	2004
cana339	49.9	114.1	1525	2004

cana343	49.9	114.4	1618	2004
cana347	49.9	114.2	1509	2004
co066	37.58	108.55	1457	1978
co067	37.58	108.55	1270	1978
co076	37.17	108.52	1390	1971
co083	40.07	105.58	1539	1979
co509	37.18	108.48	1373	1978
co511	40.03	105.58	1169	1989
co517	40.05	105.58	1610	1982
co522	39.63	105.58	525	1983
co523	39.32	106.08	1050	1985
co524	38.77	104.98	560	1983
co525	38.1	105.63	1048	1983
co526	40.42	105.47	1650	1980
co527	40.22	105.42	1800	1983
co529	38.07	105.13	1726	1984
co532	40.37	105.58	1640	1987
co535	38.77	104.97	1320	1987
co537	40.53	105.2	1800	1987
co538	40.53	105.13	1670	1987
co539	39.68	105.2	1550	1987
co541	39.45	105.13	1710	1987
co542	40.17	105.28	1690	1987
co544	40.1	105.73	1430	1987
co545	40.05	105.55	1330	1987
co546	40.33	105.83	1770	1987
co547	40.4	105.67	1070	1987
co549	40.37	105.67	1510	1987
co550	40.37	105.25	1690	1987

co551	40.05	105.43	1750	1987
co555	37.78	105.5	1260	1995
co556	37.72	105.47	1035	1995
co557	37.78	106.82	1654	1997
co559	37.38	106.28	1600	1997
co560	37.63	106.68	1675	1997
co561	37.38	108.12	1484	1994
co562	37.55	105.42	1180	1994
co563	40.42	105.57	1698	2001
co564	39.5	104.22	1709	1997
co565	39.38	104.2	1779	1998
co566	39.07	104.43	1534	1998
co567	37.5	103.53	1743	1997
co568	37.23	103.25	1628	1998
co572	40.32	105.55	894	1998
co579	39.95	106.52	1320	2002
co580	39	108.15	1135	2002
co581	40.75	106.85	1539	2000
co582	38.67	108.35	1569	1999
co583	39.72	106.98	1402	2002
co584	39.7	106.73	1336	1999
co586	39.87	105.87	1224	1992
co588	37.47	106.3	1632	2004
co589	38.73	106.8	1319	1999
co590	40.67	105.52	1392	2002
co591	40.98	105.67	1423	2001
co592	40.42	105.28	1550	2000
co593	38.08	107	1366	2002
co594	38.25	106.67	1437	2002

co595	39.83	108.2	1168	2001
co596	39.93	105.3	1545	2003
co597	39.6	105.9	1372	2002
co598	40.37	105.58	1547	2000
co599	39.6	108.8	1382	2000
co600	38.25	108.33	1536	2000
co601	39.38	105.17	1401	1998
co602	38.87	105.43	1507	1997
co603	39.93	105.27	1541	2003
co604	39.85	106.23	1378	2000
co605	38.6	107.58	1383	2002
co606	40.07	106.13	1571	1999
co607	40.13	105.42	1354	2000
co608	39.68	105.2	1487	2003
co609	38.85	106.02	1541	1997
co610	37.58	108.58	1270	2002
co611	39.55	105.27	1553	2002
co612	38.38	108.02	1440	2002
co613	40.92	106.33	1486	2001
co614	40.8	105.18	1508	2002
co615	40.05	108.3	1126	2001
co616	40.78	108.97	1270	2000
co617	38.8	106.23	1169	2002
co618	38.8	106.23	1462	1999
co620	38.53	107.22	1524	2000
co621	39.67	107.88	1352	2000
co622	40.72	105.58	1436	2002
co623	38.32	107.2	1511	2000
co624	38.4	106.43	1275	2002

co625	37.67	106.65	1566	2002
co626	38.02	108.92	1490	2002
co627	38.53	107.32	1541	1999
co628	38.33	105.27	1480	1997
co629	38.83	108.57	1296	2002
co630	40.03	106.07	1454	1999
co631	39.02	108.23	1146	2002
co632	37.9	105.15	1336	1997
co637	37.55	105.57	1450	2003
co638	37.217	107.85	1566	2002
co639	39.017	105.37	1620	2003
co640	38.4	105.3	1577	2003
co641	39.8	105.25	1566	2003
ct001	41.95	73.22	1659	1985
ct002	41.97	73.22	1650	1985
fl001	30.45	85.92	899	1992
fl005	29.73	82.95	1725	1993
fl006	29.73	82.93	1798	1992
fl007	29.02	82.72	1618	2005
fl008	28.92	82.27	1516	2003
fl009	28.3	82.08	1622	2005
ga003	32.35	81.22	990	1985
ga004	32.05	83.3	1202	1984
ia002	40.62	93.75	1672	1982
ia003	40.72	91.97	1715	1981
ia004	40.83	91.37	1724	1984
ia005	41.9	91.5	1770	1983
ia015	42.62	91.57	1735	1977
ia016	41.88	95.92	1714	1977

ia020	41.68	93.68	1654	1980
ia021	41.72	93.7	1654	1981
ia023	42	93.88	1663	1981
ia024	41.28	94.07	1635	1981
ia025	41.28	93.58	1574	1980
ia026	42.42	94.1	1698	1979
ia027	42.38	94.08	1685	1981
ia029	43.18	91.25	1651	1980
ia030	42.63	91.13	1631	1980
ia032	42.7	91.13	1711	1980
ia033	42.55	96.47	1796	1991
id001	47.63	116.47	1712	1976
id002	47.53	115.9	1672	1976
id006	42.52	116.8	1492	1984
id010	43.97	114.97	955	1991
id011	43.97	114.97	1210	1992
id013	44.62	114.5	1305	1997
id015	43.75	116.1	1488	2011
il002	41.65	88.58	1752	1980
il008	41.3	89	1633	1980
il009	41.22	88	1686	1980
il010	39.97	89.85	1671	1980
il011	39.42	88.17	1674	1980
il012	40.13	87.75	1670	1980
il013	37.53	88.98	1655	1981
il014	37.6	89.2	1652	1981
il016	37.27	89.05	1468	1985
in001	41.05	86.7	1692	1985
ks001	38.4	94.77	1714	1982

ks004	37.78	95.95	1728	1982
ks007	37.58	95.95	1738	1982
ks010	37.27	95.77	1724	1982
ky003	37.08	83	1660	1982
ky004	37.18	86.1	1649	1985
la001	32.25	92.97	997	1988
ma001	42.63	72.98	1697	1971
ma002	42.62	72.97	1697	1980
me005	45.03	70.32	1776	1976
me010	44.77	70.77	1667	1976
me015	46.07	68.85	1728	1976
me016	45.92	68.9	1610	1981
me017	44.42	68.15	1665	1982
me018	44.42	68.15	1665	1982
me019	45.5	68.28	1697	1981
me020	45.32	68.25	1686	1981
me021	46.23	69	1639	1986
me022	46.77	69.17	1674	1986
me023	46	69.33	1692	1982
me024	44.58	68.17	1692	1982
mexi001	31.17	115.5	1449	1971
mexi004	29.52	106.82	1569	1971
mexi014	28.93	102.62	1675	1971
mexi019	31.9	115.93	1786	1995
mexi020	30.97	115.5	1560	1995
mexi022	26.4	106.68	1376	1993
mexi023	26.4	106.68	1376	1993
mexi025	27.7	107.62	1644	1993
mexi027	23.75	105.75	1481	1993

mexi028	28.33	108	1583	1993
mexi031	30.4	108.4	1621	1993
mexi034	23.1	99.23	1772	1995
mexi035	23.15	99.15	1474	1995
mexi036	21.68	99.78	1574	1996
mi001	44.67	84.75	1770	1987
mi004	46.32	86.62	1652	1983
mi005	42.67	83.42	1581	1983
mi006	46.2	89.3	1570	1983
mi009	46.47	84.87	1510	1983
mi010	46.7	88.75	1635	1983
mn002	48.22	90.9	1671	1971
mn008	47.18	95.23	1727	1971
mn009	47.2	95.25	1672	1971
mn010	47.2	95.25	1731	1971
mn013	47.35	94.52	1700	1982
mn015	48.08	91.97	1700	1982
mn016	48.32	95.7	1715	1983
mn017	47.22	95.22	1666	1982
mn019	47.18	95.23	1672	1971
mn022	47.27	94.38	1785	1988
mn026	48.23	90.9	1719	1988
mo001	37.27	91.27	1636	1981
mo002	37.12	91.5	1776	1981
mo003	37.12	91.5	1693	1981
mo007	37.72	90.2	1777	1982
mo008	37.72	90.2	1669	1982
mo014	38.6	90.72	1641	1980
mo015	38.65	91.5	1662	1982

mo018	36.6	93.82	1724	1982
mo021	38.5	92.12	1688	1982
mo024	37.67	92	1620	1992
mo027	37.97	92.75	1660	1982
mo030	38.03	93.33	1732	1982
mo033	36.68	92.82	1696	1992
mo036	36.6	93.82	1689	1982
mo037	36.57	90.48	1185	1992
mo038	37.17	92.5	1553	1992
mo041	37.43	91.65	1410	1991
mo042	37.1	91.05	1391	1991
mo043	37.1	91.53	1138	1990
mo044	37.25	91.27	1588	1992
ms001	32.87	89.13	1546	1983
ms002	30.58	88.02	1466	1992
mt006	45	110.72	1185	1971
mt007	45	110.72	1410	1971
mt104	45.42	111.27	1623	1971
mt109	45.17	109.52	1660	1999
mt110	45.3	111.33	819	2000
mt111	45.3	111.33	500	2000
mt116	46.28	113.15	999	1998
mt117	48.72	113.65	1766	2006
nc001	35.73	82.33	1609	1983
nc002	35.6	83.43	1558	1983
nc003	36.07	81.82	1560	1983
nc004	35.22	83.97	1641	1983
nc007	35.88	81.93	1617	1977
nc009	36.45	76.62	1524	1984

nc014	35.6	83.42	1771	1997
nc022	35.5	82.625	1716	1996
nd001	46.6	103.47	1592	1990
nd002	47.15	101.02	1788	1990
nd004	47.42	102.92	1777	1990
nd005	48.98	100.35	1676	1990
ne005	42.7	100.87	1728	1998
ne006	42.67	99.72	1732	1997
ne008	42.63	103.25	1567	1997
nh002	44.22	71.4	1509	1981
nh003	44.1	71.38	1610	1979
nh004	44.28	71.27	1678	1976
nh005	43.8	71.83	1690	2008
nj001	40.5	74.57	1620	1982
nj002	40.5	74.57	1674	1982
nm020	32.35	106.55	1597	1970
nm021	37	107.82	1555	1971
nm022	37	107.82	1660	1971
nm023	37	107.82	1575	1971
nm024	36.68	107.32	1643	1971
nm025	35.6	108.13	1381	1972
nm026	36.35	106.52	1362	1972
nm027	35.23	107.68	1691	1972
nm028	35.23	107.68	1611	1972
nm029	35.4	108.52	1595	1972
nm030	35.4	108.52	1411	1972
nm031	35.43	108.53	1478	1972
nm032	35.03	108.35	1638	1972
nm033	35.03	108.35	1536	1972

nm034	34.92	107.83	1662	1972
nm035	34.22	108.63	1490	1972
nm036	34.77	106.32	1691	1972
nm037	34.77	106.32	1656	1972
nm038	35.45	105.73	1556	1972
nm039	35.53	105.57	1690	1972
nm040	35.53	105.57	1579	1972
nm043	35.7	106.63	1658	1972
nm047	36.82	103.02	1640	1974
nm048	33.78	107.62	1666	1974
nm050	35.08	106.38	1641	1976
nm051	35.58	107.25	1687	1976
nm052	35.58	107.25	1638	1976
nm053	35.9	107.63	1629	1976
nm055	36.68	107.32	1594	1971
nm061	33.25	108.5	1690	1979
nm063	33.25	108.5	1636	1980
nm111	34.23	105.78	1660	1981
nm118	35.08	105.65	1564	1982
nm119	32.93	108.02	1655	1982
nm500	36.12	105.73	1708	1972
nm501	35.78	106.28	1727	1972
nm520	35.97	108.8	1540	1977
nm529	35.97	108.8	1652	1977
nm537	36.68	107.32	1570	1978
nm546	33.55	106.67	1644	1981
nm547	33.25	106.75	1687	1990
nm548	36.73	105.47	1592	1981
nm549	36.73	105.47	1639	1987

nm550	35.88	106.67	1532	1986
nm551	36.33	105.37	1700	1981
nm552	36.3	105.42	1581	1981
nm553	32.72	106.37	1751	1990
nm554	36.12	105.52	1690	1986
nm555	35.8	106.62	1604	1986
nm556	35.78	106.62	1572	1986
nm557	36.15	105.6	1555	1986
nm558	35.82	106.57	1653	1987
nm560	36.73	105.47	837	1989
nm561	33.05	106.53	1799	1990
nm562	32.7	106.35	1659	1990
nm563	36.67	106.2	1786	1983
nm564	34.22	108.62	1410	1987
nm565	33.38	108.23	1470	1986
nm567	33.22	108.27	1530	1987
nm568	32.95	108.02	1670	1986
nm572	34.97	108.1	-136	1992
nm573	32.8	105.9	1610	1994
nm574	36.8	103.98	1613	1998
nm576	36.77	103.95	1626	1998
nm577	36.07	104.35	1595	1998
nm578	36.78	103.93	1635	1992
nm579	32.8	105.8	1627	1992
nm580	34.97	108.18	-136	2004
nm581	36.533	106.02	1520	2003
nm582	36.617	105.98	1575	2003
nm583	36.35	106.52	1295	2007
nm584	36.283	106.62	644	2007

nm585	35.917	106.67	1568	2007
nm586	35.917	106.68	1298	2007
nm587	35.88	106.67	1304	2007
nv036	39.27	114.12	1567	1978
nv037	39.42	114.65	783	1976
nv040	39.33	114.75	1570	1976
nv048	40.15	115.53	1503	1978
nv049	39.82	114.62	1400	1982
nv052	39.1	115.8	1470	1982
nv053	40.4	114.22	1400	1982
nv055	38.68	117.23	1490	1982
nv056	41.05	114.58	1330	1982
nv060	41.3	118.43	1267	1984
nv061	41.9	115.42	1334	1984
nv506	36.67	115.17	1605	1977
nv507	39.38	114.92	1465	1976
nv509	39.37	114.72	1551	1976
nv510	36.27	115.7	800	1984
nv511	38.78	116.95	1300	1980
nv512	40.23	115.53	320	1985
nv513	38.9	114.32	825	1983
nv514	40.55	114.82	302	1985
nv516	38.93	114.23	0	1984
nv517	36.32	115.7	320	1984
nv518	41.3	118.43	975	1998
ny001	44.13	73.78	1608	1981
ny002	41.42	74.08	1648	1977
ny004	41.77	74.18	1636	1973
ny008	43.55	73.8	1595	1976

ny013	44.33	73.9	1632	1981
ny014	44.33	73.88	1696	1978
oh001	40.88	81.75	1626	1985
oh002	41.55	81.27	1612	1983
oh003	39.9	84.4	1662	1985
ok001	36.68	94.73	1675	1982
ok004	36.7	96.38	1737	1982
ok007	36.2	96.22	1611	1995
ok010	35.85	98.55	1772	1980
ok013	35.58	98.38	1680	1982
ok016	35.1	95.63	1745	1980
ok025	34.1	97.67	1691	1995
ok028	34.68	98.63	1686	1980
ok033	35.27	97.23	1755	1982
or001	45.15	120.12	1497	1975
or006	44.9	118.93	1405	1982
or009	43.98	118.8	1396	1982
or012	43.97	121.07	1281	1982
or015	43.58	120.45	1097	1982
or018	43.13	119.87	1377	1982
or021	42.67	118.92	1501	1982
or027	42.27	122.08	1495	1981
or029	45.97	117.68	1485	1991
or030	45.97	117.72	1502	1991
or031	45.47	118.2	1672	1990
or032	45.12	117.02	1550	1990
or033	45.28	118.57	1469	1990
or034	45.55	118.48	1761	1990
or035	45.83	117.8	1665	1990

or037	45.68	117.47	1760	1990
or038	45.78	117.92	1665	1990
or039	45	117.07	1585	1991
or040	45.77	117.97	1675	1991
or041	45.82	117.67	1714	1991
or046	43.75	121.65	1529	1995
or047	43.73	121.65	1493	1991
or048	43.7	121.62	1476	1993
or049	43.72	121.6	1334	1993
or050	43.62	121.3	1747	1995
or051	43.47	121.4	1574	1995
or052	43.32	121.75	1419	1995
or053	43.23	121.65	1639	1995
or054	43.08	121.95	1513	1995
or055	42.92	121.53	1423	1995
or056	42.93	121.62	1570	1995
or057	42.75	121.52	1442	1995
or058	42.78	122.07	1572	1990
or059	42.63	121.53	1653	1995
or060	43.58	120.45	870	1996
or061	43.97	121.07	830	1996
or062	43.18	120.9	530	1996
or082	44.7	118.55	1740	2002
or085	45.5	121.42	1602	1999
or089	44.57	121.27	1733	1996
pa001	40.67	77.7	1609	1981
pa002	40.88	77.32	1641	1981
pa003	41.22	74.92	1609	1981
pa004	41.33	77.72	1540	1981

pa005	39.83	79.7	1623	1981
pa006	41.32	79.22	1660	1981
pa007	40.23	77.65	1535	1981
pa008	41.33	79.2	1679	1981
pa009	39.88	76.4	1631	1981
pa010	41.37	76.3	1637	1981
pa011	41.87	75.88	1619	1981
pa012	39.83	78.52	1612	1981
pa013	41.75	78.97	1425	1978
sc003	34.7	82.87	1684	1973
sc005	33.18	80.42	1639	1992
sc006	33.8	79.87	550	1993
sd002	43.78	103.6	1600	1991
sd003	44.33	103.43	1753	1990
sd004	43.6	101.12	1646	1991
sd005	43.6	101.12	1691	1991
sd008	45.35	103.13	1651	1990
sd012	43.75	103.35	1703	1990
sd014	43.98	97.17	1740	1991
sd017	43.9	103.6	1281	1991
sd018	43.93	103.37	1717	1990
tn005	35.7	84.88	1651	1982
tn008	36.22	84.08	1633	1980
tn009	35.45	85.57	1610	1985
tn010	36.42	89.37	1677	1990
tn016	35.6	83.08	1736	1995
tn017	35.7	83.35	1735	1995
tn018	35.75	83.23	1765	1995
tn019	35.75	83.23	1793	1995

tn020	35.62	85.43	1743	1997
tn021	35.62	85.43	1750	1997
tn022	35.62	83.93	1683	1996
tn024	35.67	83.5	1685	1995
tn027	35.67	82.38	1698	1997
tx003	33.73	95.08	1694	1982
tx006	32.85	97.48	1737	1980
tx009	32.98	99.17	1681	1995
tx012	32.18	98.5	1730	1982
tx018	30.93	96.8	1668	1995
tx021	30.32	96.63	1658	1995
tx024	30.83	98.52	1735	1982
tx027	30.88	99.18	1677	1995
tx030	29.48	97.78	1712	1982
tx033	29.3	96.97	1668	1995
tx039	28.83	97.18	1682	1995
tx041	29.45	97.92	1695	1996
tx042	29.25	103.3	1473	1992
tx046	31.9	104.85	1537	1992
tx051	32.83	98.08	1793	2006
ut013	40.78	110	1433	1971
ut018	38.5	109.25	1489	1972
ut020	37.53	109.9	1445	1971
ut021	37.02	110.85	1565	1971
ut022	37.02	110.85	1469	1971
ut023	37.62	110.02	1347	1972
ut024	37.62	109.73	1276	1970
ut500	40.67	109.9	1730	1971
ut501	40.57	109.95	1635	1971

ut502	40.62	109.95	1423	1971
ut508	39.42	111.07	286	1985
ut509	37.65	112.67	0	1989
va006	38.63	77.3	1780	1978
va007	38.97	77.2	1742	1977
va008	38.3	79.35	1660	1978
va009	37.55	79.45	1587	1982
va010	37.5	79.52	1531	1982
va011	37.38	80.5	1552	1983
va012	36.67	81.67	1645	1982
va013	37.78	80.5	1694	1982
va014	38.5	78.35	1612	1981
va015	38.33	79.33	1595	1981
va017	37.92	79.8	1569	1982
va021	36.78	76.88	932	1985
va022	37.38	76.93	1662	1984
va023	37.62	76.67	1372	1984
va025	36.78	77.13	1171	1984
va027	37.55	79.07	1749	1998
vt001	44.32	72.9	1635	1971
vt002	44.03	72.83	1670	1981
wa003	48.83	118.3	1743	1975
wa005	48.83	117.55	1800	1975
wa007	48.25	118.75	1794	1975
wa008	48.12	118.78	1791	1975
wa009	48.42	120.4	1695	1975
wa010	48.5	118.8	1653	1975
wa011	48.57	119.15	1632	1975
wa013	46.22	117.7	1623	1975

wa014	45.32	118.8	1538	1975
wa015	47.65	120.43	1640	1975
wa016	46.67	120.93	1682	1975
wa017	46.67	121.53	1420	1975
wa019	48.9	121.8	1548	1976
wa020	47.95	123.25	1710	1976
wa021	48.65	121.83	1668	1976
wa025	48.73	121.05	1586	1976
wa027	45.97	121.98	1397	1976
wa029	46.17	122.2	1653	1976
wa030	47.38	121.5	1800	1976
wa031	47.82	123.15	1750	1976
wa032	47.98	123.47	1742	1976
wa033	45.88	122.03	1534	1976
wa034	48.13	121.63	1628	1976
wa035	47.85	123.28	1788	1976
wa036	47.97	123.47	1772	1976
wa037	48.28	120.23	1648	1975
wa039	48.83	120.65	1331	1976
wa041	48.35	121.75	1321	1976
wa046	48.73	120.9	1698	1989
wa047	48.05	121.4	1248	1980
wa048	46.88	121.62	1286	1979
wa049	48.07	121.33	1500	1980
wa050	47.02	121.7	1447	1980
wa051	48.63	121.37	1401	1980
wa052	47.3	120.55	1487	1980
wa053	47.6	123.58	1324	1980
wa054	47.6	123.23	1574	1980

wa055	47.98	123.05	1499	1980
wa056	47.42	121.47	1259	1979
wa057	47.53	121.05	1430	1980
wa058	47.48	123.58	1417	1980
wa059	47.35	120.55	1433	1980
wa060	48	120.6	1649	1980
wa061	48.47	120.5	1316	1980
wa062	47.07	121.57	1601	1980
wa064	48.17	120.37	1487	1982
wa065	47.5	120.8	1542	1982
wa066	46.62	121.42	1520	1982
wa067	48.68	120.63	1471	1991
wa074	48.73	120.65	1590	1990
wa077	48.75	120.63	1679	1991
wa078	48.75	120.63	1636	1990
wa085	47.37	121.33	1515	1987
wa086	47.83	123.03	1288	1987
wa087	48.33	121.72	1502	1987
wa088	48	124	1394	1987
wa089	46.63	121.83	1539	1987
wa090	47.88	121.33	1326	1987
wa091	46.8	122.88	1410	1987
wa129	46.45	123.97	991	1986
wi002	46.03	89.67	1750	1972
wi004	45.1	88.88	1595	1983
wi005	43.42	89.72	1642	1982
wv002	38.85	79.37	1476	1981
wy001	43.8	110.47	1400	1971
wy002	43.08	110.07	1492	1972

wy005	44.58	109.08	1580	1971
wy006	43.7	110.52	1400	1971
wy008	43.63	110.5	1462	1971
wy019	41.13	106.05	1412	1990
wy020	41.4	106.28	1421	1990
wy026	41.87	110.8	1480	1998
wy027	44.98	110.67	1168	1999
wy031	41.15	106.78	1380	2001
wy032	41.15	105.37	1511	2001
wy033	44.75	110.25	1390	2005

References

Alley, W.M., 1984: The Palmer Drought Severity Index: limitations and assumptions. *Journal of Climate and Applied Meteorology*, **23**, 1100-1109.

Anderson, L., 2011: Holocene record of precipitation seasonality from lake calcite $\delta^{18}O$ in the central Rocky Mountains, United States. *Geology*, **39**, 211-214.

Anderson, L., 2011: Rocky Mountain hydroclimate: Holocene variability and the role of insolation, ENSO, and the North American Monsoon. *Global and Planetary Change*, **92-93**, 198-208.

Asmerom, Y., V. Polyaka, J. Rasmussen, S. Burns, and M. Lachniet, 2013: Multidecadal to multicentury scale collapses of Northern Hemisphere monsoons over the past millennium. *Proceedings of the National Academy of Sciences*, **110**, 9651-9656.

Becker, A., P. Finger, A. Meyer-Christoffer, B. Rudolf, K. Schamm, U. Schneider, and M. Ziese, 2013: A description of the global land-surface precipitation data products of the Global Precipitation Climatology Centre with sample applications including centennial (trend) analysis from 1901-present. *Earth System Science Data*, **5**, 71-99.

Benson, L.V., M. Kashgarian, R.O. Rye, S.P. Lund, F.L. Paillet, J. Smoot, C. Kester, S. Mensing, D. Meko, and S. Lindstrom, 2002: Holocene multidecadal and multicentennial droughts affecting northern California and Nevada. *Quaternary Science Reviews*, **21**, 659-682.

Benson, L., B. Linsley, J. Smoot, S. Mensing, S. Lund, S. Stine, and A. Sarna-Wojcicki, 2003: Influence of the Pacific Decadal Oscillation on the climate of the Sierra Nevada, California and Nevada. *Quaternary Research*, **59**, 151-159.

Bradley, R.S., 1999: Paleoclimatology: Reconstructing climates of the Quaternary. Academic Press, 610 pp.

Briffa, K., P.D. Jones, and F.H. Schweingruber, 1988: Summer temperature patterns over Europe: a reconstruction from 1750 AD based on maximum latewood density indices of conifers. *Quaternary Research,* **30**, 36-52.

Briffa, K.R., P.D. Jones, and F.H. Schweingruber, 1994: Summer temperatures across northern North-America – regional reconstructions from 1760 using tree-ring densities. *Journal of Geophysical Research-Atmospheres*, **99(25)**, 835-844.

Brush, G.S., 2001: Natural and anthropogenic changes in Chesapeake Bay during the last 1000 yeas. *International Journal of Human and Ecological Risk Assessment*, **7.5**, 1283-1296.

Bunn, G., M.K. Hughes, and M.W. Salzer, 2011: Topographically modified tree-ring chronologies as a potential means to improve paleoclimate inference. *Climate Change*, **105**, 627-634.

Bussieres, N., and W. Hogg, 1989: The objective analysis of daily rainfall by distance weighting schemes on a mesoscale grid. *Atmosphere-Ocean*, **27**, 521-541.

Chen, M., P. Xie, J.E. Janowiak, and P.A. Arkin, 2002: Global land precipitation: a 50-year monthly analysis based on gauge observations. *Journal of Hydrometeorology*, **3**, 249-266.

Chivas, A.R., P. DeDeckker, and J.M.G. Shelley, 1986: Magnesium content of non-marine ostracod shells: a new palaeosalinometer and palaeothermometer. *Palaeogeography, Palaeoclimatology, and Palaeoecology*, **54**, 43-61.

Cook, B.I., J.E. Smerdon, R. Seager, and E.R. Cook, 2014: Pan-continental droughts in North America over the last millennium. *Journal of Climate*, **27**, 383-397.

Cook, E.R., 1985: A time series analysis approach to tree ring standardization. Ph.D. dissertation. School of Renewable Natural Resources, University of Arizona, 183 pp.

Cook, E.R., K.R. Briffa, and P.D. Jones, 1994: Spatial regression methods in dendroclimatology: A review and comparison of two techniques. *International Journal of Climatology*, **14**, 379-402.

Cook, E.R., D.M. Meko, D.W. Stahle, and M.K. Cleaveland, 1996: Tree-ring reconstructions of past drought across the coterminous United States: Tests of a regression method and calibration/verification results. *Tree Rings, Environment, and Humanity*, J.S. Dean, D.M. Meko, and T.W. Swetnam, Eds., Radiocarbon, 155-169.

Cook, E.R., D.M. Meko, D.W. Stahle, and M.K. Cleaveland, 1999: Drought reconstructions for the continental United States. *Journal of Climate*, **12**, 1145-1162.

Cook, E.R., C.A. Woodhouse, C.M. Eakin, D.M. Meko, and D.W. Stahle, 2004: Long-term aridity changes in the western United States. *Science*, **306**, 1015-1018.

Cook, E.R., R. Seager, M.A. Cane, and D.W. Stahle, 2007: North American drought: reconstructions, causes and consequences. *Earth-Science Reviews*, **81**, 93-134.

Cook, E.R., K.J. Anchukaitis, B.M. Buckley, R.D. D'Arrigo, G.C. Jacoby, and W.E. Wright, 2010: Asian monsoon failure and megadrought during the last millennium. *Science*, **328**, 486-489.

Cronin, T., S. Colman, D. Willard, R. Kerhin, C. Holmes, A. Karlsen, S. Ishman, and J. Bratton, 1999: Interdisciplinary project probes Chesapeake Bay down to the core. *Eos (Transcations of the American Geophysical Union)*, **80**, 240-241.

Cronin, T., D. Willard, A. Karlsen, S. Ishman, S. Verardo, J. McGeehin, R. Kerhin, C. Holmes, S. Colman, A. Zimmerman, 2000: Climatic variability in the eastern United States over the past millennium from Chesapeake Bay sediments. *Geology*, **28(1)**, 3-6.

Cronin, T.M., G.S. Dwyer, T. Kamiya, S. Schwede, and D.A. Willard, 2003: Medieval Warm Period, Little Ice Age and 20th century temperature variability from Chesapeake Bay. *Global and Planetary Age*, **36**, 17-29.

Curtis, J.H., D.A. Hodell, and M. Brenner, 1996: Climate variability on the Yucatan Peninsula (Mexico) during the past 3500 years, and implications for Maya Cultural Evolution. *Quaternary Research*, **46**, 37-47.

Dempster, A.P., N.M. Laird, and D.B. Rubin, 1977: Maximum likelihood estimation from incomplete data via the EM algorithm (with discussion). *Journal of the Royal Statistical Society – Series B*, **39**, 1-38.

Esper, J., E.R. Cook, and F.H. Schweingruber, 2002: Low-frequency signals in long tree-ring chronologies for reconstructing past temperature variability. *Science*, **295**, 2250-2253.

Fang, K., N. Davi, X. Gou, F. Chen, E. Cook, J. Li, and R. D'Arrigo, 2010: Spatial drought reconstructions for central High Asia based on tree rings. *Climate Dynamics*, **35**, 941-951.

Fang, K., X. Gou, F. Chen, E. Cook, J. Li, B. Buckley, and R. D'Arrigo, 2011: Large-scale precipitation variability over Northwest China inferred from tree rings. *Journal of Climate*, **24**, 3457-3468.

Feng, S., Q. Hu, Q. Wu, and M.E. Mann, 2013: A gridded reconstruction of warm season precipitation for Asia spanning the past half millennium. *Journal of Climate*, **26**, 2192-2204.

Fierro, R.D., G.H. Golub, P.C. Hansen, and D.P. O'Leary, 1997: Regularization by truncated total least squares. *SIAM Journal of Computation*, **18**, 1223-1241.

Fritts, H.C., D.G. Smith, J.W. Cardis, and C.A. Budelsky, 1965: Tree-ring characteristics along a vegetation gradient in northern Arizona. *Ecology*, **46**, 394-401.

Fritts, H.C., 1971: Dendroclimatology and dendroecology. *Quaternary Research*, **1**, 419-449.

Fritts, H.C., 1976: *Tree rings and climate*. Academic Press, 567 pp.

Fritts, H.C., 1991: *Reconstructing large-scale climatic patterns from tree-ring data.* University of Arizona press, 286 pp.

Giegengack, R.F., 1962: Recent volcanism near Dotsero, Colorado. M.S. Thesis, University of Colorado, 69 pp.

Golub, G.H., M.T. Heath, and G. Wahba, 1979: Generalized cross-validation as a method for choosing a good ridge parameter. *Technometrics*, **21**, 215-223.

Golub, G.H., P.C. Hansen, and D.P. O'Leary, 2000: Tikhonov regularization and total least-squares. *SIAM Journal of Matrix Analysis and Applications*, **21**, 185-194.

Graham, N.E., and Co-authors, 2007: Tropical Pacific – mid-latitude teleconnections in medieval times. *Climatic Change*, **83**, 241-285.

Graham, N.E., C.M. Ammann, D. Fleitman, K.M. Cobb, and J. Luterbacher, 2010: Support for global climate reorganization during the Medieval Climate Anomaly. *Climate Dynamics*, **37**, 1217-1245.

Grissino-Mayer, H.D., and H.C. Fritts, 1997: The International Tree-Ring Data Bank: an enhanced global database serving the global scientific community. *The Holocene*, **7**, 235-238.

Guiot, J., 1985: The extrapolation of recent climatological series with spectral canonical regression. *International Journal of Climatology*, **5**, 325-335.

Guttman, N., 1991: Sensitivity of the Palmer hydrological drought index to temperature and precipitation departures from average conditions. *Water Resources Bulletin*, **27**, 797-807.

Harmon, R.S., D.C. Ford, and H.P. Schwarcz, 1977: Interglacial chronology of the Rocky and Mackenzie mountains based on ^{230}Th and ^{234}U dating of calcite speleothems. *Canadian Journal of Earth Sciences*, **14**, 2543-2552.

Hijmans, R.J., S.E. Cameron, J.L. Parra, P.G. Jones, and A. Jarvis, 2005: Very high resolution interpolated climate surfaces for global land areas. *International Journal of Climatology*, **25**, 1965-1978.

Hill, C., and P. Forti, 1997: *Cave minerals of the world*. National Speleological Society, 463 pp.

Hoerling, M., X.W. Quan, and J. Eischeid, 2009: Distinct causes for two principal U.S. droughts of the 20th century. *Geophysical Research Letters*, **36**, L19708, doi:10.1029/2009GL039860.

Hughes, M.K., and G. Funkhouser, 2003: Frequency-dependent climate signal in upper and lower forest border trees in the mountains of the Great Basin. *Climatic Change*, **59**, 233-244.

Jäger, L., 1976: Monatskarten des Niederschlags für die ganze Erde. *Berichte des Deutschen Wetterdienstes*, **139**, 1-38.

Jones, P.D., K.R. Briffa, T.P. Barnett, and S.F.B. Tett, 1998: High-resolution paleoclimatic records for the last millennium: Interpretation, integration and comparison with circulation model control-run temperatures. *The Holocene*, **8**, 455-471.

Jones, P.D., and Co-authors, 2009: High-resolution palaeoclimatology of the last millennium: a review of current status and future prospects. *The Holocene*, **19(1)**, 3-49.

Jones, T.L., and A. Schwaitalla, 2008: Archaeological perspectives on the effects of medieval drought in California. *Quaternary International*, **188**, 41-58.

La Marche, V.C., 1974: Frequency-dependent relationships between tree-ring series along an ecological gradient and some dendroclimatic implications. *Tree-Ring Bulletin*, **34**, 1-20.

Lauritzen, S.-E., and J. Lundberg, 1999: Speleothems and climate: a special issue of *The Holocene*. *The Holocene*, **9**, 643-647.

Leathers, D.J., M.L. Malin, D.B. Kluver, G.R. Henderson, and T.A. Bogart, 2008: Hydroclimatic variability across the Susquehanna River Basin, USA, since the 17th century. *International Journal of Climatology*, **28**, 1615-1626.

Leavitt, S.W., and A. Long, 1989: Drought indicated in carbon-13/carbon-12 ratios of Southwestern tree rings. *Journal of the American Water Resources Association*, **25**, 341-347.

Lee, T.C.K., F.W. Zwiers, and M. Tsao, 2008: Evaluation of proxy-based millennial reconstruction methods. *Climate Dynamics*, **31**, 263-281.

Legates, D.R., 1987: A climatology of global precipitation. *Publications in Climatology*, **40(1)**, 1-85.

Little, R.J.A., and D.B. Rubin, 1987: *Statistical analysis with missing data*. Series in Probability and Mathematical Statistics, Wiley, 278 pp.

Lorenz, E.N., 1956: Empirical orthogonal functions and statistical weather prediction. Massachusetts Institute of Technology, Cambridge, Mass., 49 pp.

Luterbacher, J., and eight co-authors, 2002a: Reconstruction of sea level pressure fields over the Eastern North Atlantic and Europe back to 1500. *Climate Dynamics*, **18**, 545–561.

Luterbacher, J., and 10 co-authors, 2002b: Extending North Atlantic Oscillation reconstructions back to 1500. *Atmospheric Science Letters*, **2**, doi:10.1006/asle.2001.0044.

Karl, T.R., and R.W. Knight, 1985: *Atlas of monthly Palmer Hydrological Drought Indices (1931-1983) for the Contiguous United States*. Historical Climatology Series 3-7, National Climatic Data Center, Asheville, N.C.

Karl, T.R., C.N. Williams, Jr., F.T. Quinlan, and T.A. Boden, 1990: United States Historical Climatology Network (HCN) serial temperature and precipitation. Oak Ridge National Laboratory, Oak Ridge, Tenn., 83 pp.

Kennett, D.J., and J.P. Kennett, 2000: Competitive and cooperative response to climatic instability in southern California. *American Antiquity*, **65**, 379-395.

Mann, M.E., R.S. Bradley, and M.K. Hughes, 1998: Global-scale temperature patterns and climate forcing over the past six centuries. *Nature*, **392**, 779-787.

Mann, M.E., 2002: The value of multiple proxies. *Science*, **297**, 1481-1482.

Mann, M.E., and M.K. Hughes, 2002: Tree-ring chronologies and climate variability. *Science*, **296**, 848.

Mann, M.E., and S. Rutherford, 2002: Climate reconstruction using 'Pseudoproxies'. *Geophysical Research Letters*, **29**(10), 1501.

Mann, M.E., S. Rutherford, E. Wahl, and C. Ammann, 2005: Testing the fidelity of methods used in proxy-based reconstructions of Past Climate. *Journal of Climate*, **18**, 4097-4107.

Mann, M.E., S. Rutherford, E. Wahl, and C. Ammann, 2007a: Robustness of proxy-based climate field reconstruction methods. *Journal of Geophysical Research*, **112**, D12109.

Mann, M.E., S. Rutherford, E. Wahl, and C. Ammann, 2007b: Reply to "Comments on 'Testing the fidelity of methods used in proxy-based reconstructions of past climate'". *Journal of Climate*, **20**, 5671-5674.

Mann, M.E., Z. Zhang, M.K. Hughes, R.S. Bradley, S.K. Miller, S. Rutherford, and F. Ni, 2008: Proxy-based reconstructions of hemispheric and global surface temperature variations over the past two millennia. *Proceedings of the National Academy of Science*, **105**(36), 13252-13257.

Mann, M.E., Z. Zhang, S. Rutherford, R.S. Bradley, M.K. Hughes, D. Shindell, C. Ammann, G. Faluvegi, and F. Ni, 2009: Global signatures and dynamical origins of the Little Ice Age and Medieval Climate Anomaly. *Science*, **326**, 1256-1260.

Mardia, K.V., J.T. Kent, and J.M. Bibby, 1979: *Multivariate Analysis*. Series in Probability and Mathematical Statistics, Academic Press, 518 pp.

Matsuura, K., and C.J. Willmott, 2009: Terrestrial precipitation: 1900-2008 gridded monthly time series. [Available online at: <http://climate.geog.udel.edu>.].

McCabe, G.J., M.A. Palecki, and J.L. Betancourt, 2004: Pacific and Atlantic Ocean influences on multidecadal drought frequency in the United States. *Proceedings of the National Academy of Sciences*, **101**, 4136-4141.

McCabe, G.J., J.L. Betancourt, S.T. Gray, M.A. Palecki, and H.G. Hidalgo, 2008: Associations of multi-decadal sea-surface temperature variability with U.S. drought. *Quaternary International*, **188**, 31-40.

Meko, D.M., E.R. Cook, D.W. Stahle, C.W. Stockton, and M.K. Hughes, 1993: Spatial patterns of tree-growth anomalies in the United States and southeastern Canada. *Journal of Climate*, **6**, 1773-1786.

Mitchell, T.D., T.R. Carter, P.D. Jones, M. Hulme, and M. New, cited 2004: A comprehensive set of high-resolution grids of monthly climate for Europe and the globe: the observed record (1901-2000) and 16 scenarios (2001-2100). Tyndall Centre, Working Paper No. 55. [Available online at: <http://www.ipcc-data.org/docs/tyndall_working_papers_wp55.pdf>.].

Muhs, D.R., 1985: Age and paleo-climatic significance of Holocene sand dunes in Northeastern Colorado. *Annals of the Association of American Geographers*, **75**, 566-682.

Najjar, R.G., 1999: The water balance of the Susquehanna River Basin and its response to climate change. *Journal of Hydrology*, **219**, 7-19.

Nash, J.E., and J.V. Sutcliffe, 1970: River flow forecasting through conceptual models: Part I – A discussion of principles. *Journal of Hydrology*, **10**, 282-290.

National Climatic Data Center, Paleoclimatology Branch, cited 2008: Tree ring data description. [Available online at: <http://www.ncdc.noaa.gov/paleo/treeinfo.html>.].

Nelson, D.B., and Co-authors, 2011: Drought variability in the Pacific Northwest from a 6,000-yr lake sediment record. *Proceedings of the National Academy of Science*, **108**, 3870-3875.

Neukom, R., J. Luterbacher, R. Villalba, M. Küttel, D. Frank, P.D. Jones, M. Grosjean, J. Esper, L. Lopez, and H. Wanner, 2010: Multi-centennial summer and winter precipitation variability in southern South America. *Geophysical Research Letters*, **37**, L14708.

New, M., D. Lister, D. Hulume, and I. Makin, 2002: A high-resolution data set of surface climate over global areas. *Climate Research*, **21**, 1-25.

Ning, L., and R.S. Bradley, 2014: Winter precipitation variability and corresponding teleconnections over the northeastern United States. *Journal of Geophysical Research: Atmospheres*, **119**, 7931-7945.

Osborn, T.J., and K.R. Briffa, 2000: Revisiting timescale-dependent reconstruction of climate from tree-ring chronologies. *Dendrochronologia*, **18**, 9-26.

Overpeck, J.E., 1996: Varved sediment records of recent seasonal to millennial-scale environmental variability. *Climate variations and forcing mechanisms of the last 2000 years*, P.D. Jones, R.S. Bradley, and J. Jouzel, Eds., Springer-Verlag, 453-478.

Palmer, W.C., 1965: Meteorological Drought. Weather Bureau Res. Paper 45, U.S. Department of Commerce, Washington, DC, 58 pp.

Pederson, N., and Co-authors, 2012: A long-term perspective on a modern drought in the American Southeast. *Environmental Research Letters*, **7**, 014034, doi:10.1088/1748-9326/7/1/014034.

Peterson, T.C., and R.S. Vose, 1997: An overview of the Global Historical Climatology Network temperature database. *Bulletin of the American Meteorological Society*, **78**, 2837-2849.

Peterson, T.C., R.S. Vose, R. Schmoyer, and V. Razuvaev, 1998: Global Historical Climatology Network (GHCN) quality control of monthly temperature data. *International Journal of Climatology*, **18**, 1169-1179.

Pompeani, D.P., B.A. Steinman, M.B. Abbott, J.D. Ortiz, N. Stansell, and J.P. Cwiklik, 2013: A 7600-year high-resolution record of hydroclimate variability from oxygen isotopes in authigenic carbonate lake sediment: Cleland Lake, southeastern British Columbia. *Fall Meeting 2013*, San Francisco, American Geophysical Union, abstract no. PP23C-1981.

Rudolf, B., H. Hauschild, M. Reiss, and U. Schneider, 1992: Berechnung der Gebietsniederschläge im 2,5°-Raster durch ein objektives Analyseverfahren. *Meteorologische Zeitschrift*, **1**, 32-50.

Rudolf, B., H. Hauschild, W. Rueth, and U. Schneider, 1994: Terrestrial precipitation analysis: Operational method and required density of point measurements. *Global Precipitation and Climate Change*, M. Desbois and F. Desalmand, Eds., Springer, 173-186.

Rutherford, S., M.E. Mann, T.L. Delworth, and R.J. Stouffer, 2003: Climate Field Reconstruction under Stationary and Nonstationary Forcing. *Journal of Climate*, **16**, 462-479.

Rutherford, S., M.E. Mann, T.J. Osborn, R.S. Bradley, K.R. Briffa, M.K. Hughes, and P.D. Jones, 2005: Proxy-based Northern Hemisphere surface temperature reconstructions: sensitivity to method, predictor network, target season, and target domain. *Journal of Climate*, **18**, 2308-2329.

Rutherford, S.D., M.E. Mann, C.M. Ammann, and E.R. Wahl, 2010: Comments on "A surrogate ensemble study of climate reconstruction methods: stochasticity and robustness". *Journal of Climate*, **23**, 2832-2838.

St. George, S., D.M. Meko, and E.R. Cook, 2010: The seasonality of precipitation signals embedded within the North American Drought Atlas. *The Holocene*, **20(6)**, 983-988.

St. George, S., and T.R. Ault, 2014: The imprint of climate within Northern Hemisphere trees. *Quaternary Science Reviews*, **89**, 1-4.

Schneider, T., 2001: Analysis of incomplete climate data: estimation of mean values and covariance matrices and imputation of missing values. *Journal of Climate*, **14**, 853-871.

Schneider, U., A. Becker, P. Finger, A. Meyer-Christoffer, B. Rudolf, and M. Ziese, 2011: *GPCC full data reanalysis version 6.0 at 0.5°: monthly land-surface precipitation from rain-gauges built on GTS-based and historic data.* Global Precipitation Climatology Centre, doi:10.5676/DWD_GPCC/FD_M_V6_050.

Schneider, U., A. Becker, P. Finger, A. Meyer-Christoffer, M. Ziese, and B. Rudolf, 2014: GPCC's new land surface precipitation climatology based on quality-controlled in situ data and its role in quantifying the global water cycle. *Theoretical and Applied Climatology*, **115**, 15-40.

Schubert, S.D., M.J. Suarez, P.J. Pegion, R.D. Koster, and J.T. Bacmeister, 2004a: Causes of long-term drought in the U.S. Great Plains. *Journal of Climate*, **17**, 485-503.

Schubert, S.D., M.J. Suarez, P.J. Pegion, R.D. Koster, and J.T. Bacmeister, 2004b: On the cause of the 1930s Dust Bowl. *Science*, **303**, 1855-1859.

Schweingruber, F.H., K.R. Briffa, and P.D. Jones, 1991: Yearly maps of summer temperatures in Western-Europe from AD 1750 to 1975 and western North America from 1600 to 1982 – results of a radiodensitometrical study on tree rings. *Vegetatio*, **92**, 5-71.

Seager, R., A. Tzanova, and J. Nakamura, 2009: Drought in the southeastern United States: Causes, variability over the last millennium, and the potential for future hydroclimate change. *Journal of Climate*, **22**, 5021-5045.

Shepard, D., 1968: A two-dimensional interpolation function for irregularly spaced data. *23rd ACM National Conference*, New York City, Association for Computing Machinery, 517-524.

Smerdon, J.E., and A. Kaplan, 2007: Comments on "Testing the fidelity of methods used in proxy-based reconstructions of past climate": The role of the standardization interval. *Journal of Climate*, **20**, 5666-5670.

Steinman, B.A., M.F. Rosenmeier, M.B. Abbott, and D.J. Bain, 2010a: The isotopic and hydrologic response of small, closed-basin lakes to climate forcing from predictive models: Application to paleoclimate studies in the upper Columbia River basin. *Limnology and Oceanography*, **55**, 2231-2245.

Steinman, B.A., M.F. Rosenmeier, and M.B. Abbott, 2010b: The isotopic and hydrologic response of small, closed-basin lakes to climate forcing from predictive models: Simulations of stochastic and mean state precipitation variations. *Limnology and Oceanography*, **55**, 2246-2261.

Steinman, B.A., M.B. Abbott, M.E. Mann, N.D. Stansell, and B.P. Finney, 2012: 1,500 year quantitative reconstruction of winter precipitation in the Pacific Northwest. *Proceedings of the National Academy of Science*, **109**(29), 11619-11623.

Steinman, B.A., and Co-authors, 2014: Ocean-atmosphere forcing of centennial hydroclimate variability in the Pacific Northwest. *Geophysical Research Letters*, **41**, 2553-2560.

Stevens, L.R., J.R. Stone, J. Campbell, and S.C. Fritz, 2006: A 2200-yr record of hydrologic variability from Foy Lake, Montana, USA, inferred from diatom and geochemical data. *Quaternary Research*, **65**, 264-274.

Stevens, L.R., and W.E. Dean, 2008: Geochemical evidence for hydroclimatic variability over the last 2460 years from Crevice Lake in Yellowstone National Park, USA. *Quaternary International*, **188**, 139-148.

Stine, S., 1994: Extreme and persistent drought in California and Patagonia during medieval time. *Nature*, **369**, 546-549.

Swetnam, T.W., 1993: Fire history and climate change in Giant Sequoia Groves. *Science*, **262**, 885-889.

Tikhonov, A.N., and V.Y. Arsenin, 1977: *Solution of ill-posed problems*. Scripta Series in Mathematics, V.H. Winston and Sons, 258 pp.

Tingley, M.P., P.F. Craigmile, M. Haran, B. Li, E. Mannshardt, and B. Rajaratnam, 2012: Piecing together the past: statistical insights into paleoclimatic reconstructions. *Quaternary Science Reviews*, **35**, 1-22.

Wilks, D.S., 2011: *Statistical Methods in the Atmospheric Sciences*. Academic Press, 676 pp.

Willard, D.A., T.M. Cronin, S. Verardo, 2003: Late Holocene climate and ecosystem variability from Chesapeake Bay sediment cores. *The Holocene*, **13**, 201-214.

Willard, D.A., C.E. Bernhardt, D.A. Korejwo, S.R. Meyers, 2005: Eastern North American terrestrial ecosystem response to millennial-scale Holocene climate variability: pollen-based climatic reconstruction. *Global and Planetary Change*, **47**, 17-35.

Willmott, C.J., C.M. Rowe, and W.D. Philpot, 1985: Small-scale climate maps: A sensitivity analysis of some common assumptions associated with grid-point interpolation and contouring. *American Cartographer*, **12**, 5-16.

Woodhouse, C.A., D.M. Meko, G.M. MacDonald, D.W. Stahle, and E.R. Cook, 2010: A 1,200-year perspective of 21st century drought in southwestern North America. *Proceedings of the National Academy of Sciences*, **107**, 21 283 – 21 288.

Yuan, F., B.K. Linsley, S.P. Lund, and J.P. McGeehin, 2004: A 1200-year record of hydrologic variability in the Sierra Nevada from sediments in Walker Lake, Nevada. *Geochemistry Geophysics Geosystems*, **5**, Q03007.

Zhang, Z., M.E. Mann, and E.R. Cook, 2004: Alternative methods of proxy-based climate field reconstruction: application to summer drought over the conterminous United States back to AD 1700 from tree-ring data. *The Holocene*, **14**(4), 502-516.